

I. Kristen Buck, Shannon Burns, Salvatore Caprara, Casey Nickel, Ethan Goddard, Zachary Atlas

Nutrients (phosphate, nitrate, nitrite, silicic acid)	Water
Sulfate (discharge tracer)	Water
Trace metals (Fe, Cu, Co, Cd, Ni, Mn, Zn, Pb)	Water+Suspended Particles
Nutrient isotopes (POC, 13C-POC, PON, 15N-PON)	Suspended Particles

Total budget: \$50,816

Activities during this period:

1. *Trace metal concentrations: surface waters and suspended particles*

The concentrations of aluminum (Al), phosphorus (P), vanadium (V), manganese (Mn), iron (Fe), cobalt (Co), nickel (Ni), copper (Cu), zinc (Zn), cadmium (Cd), and lead (Pb) were determined in surface waters and surface waters containing suspended particles by high resolution inductively coupled plasma mass spectrometry (HR-ICP-MS) analyses of samples that had been collected from Tampa Bay between April 7 and June 22, 2021 and archived at the University of South Florida. Surface water concentrations of trace metals were determined in the archived dissolved (<0.2 μm filtered, acidified with 0.024 M ultrapure hydrochloric acid, stored room temperature) samples. The trace metal concentrations in in surface waters including suspended particles were determined from archived dissolvable (unfiltered, acidified with 0.024 M ultrapure hydrochloric acid, stored room temperature; <0.4 μm filtered immediately prior to analysis) samples collected. For both types of samples, concentrations of most trace metals were much higher than neighboring Gulf of Mexico waters, and all samples were first diluted 20x with the exception of three pond samples, which were diluted 50x, prior to analysis to allow detection of the trace metals within the calibration curve range. Sample dilutions were done in 2% nitric acid (HNO_3 , Optima Grade) containing a 1 ppb Indium (In) internal standard. Calibration curves were optimized to cover the full range of aluminum (Al), phosphorus (P), vanadium (V), manganese (Mn), iron (Fe), cobalt (Co), nickel (Ni), copper (Cu), zinc (Zn), cadmium (Cd), and lead (Pb) found in the samples using natural abundance metal standards. Counts for each element were normalized to the In internal standard to account for any drift in the instrument sensitivity during analyses. All analyses were conducted on an Element XR HR-ICP-MS at the University of South Florida Tampa Bay Plasma Facility by direct injection. The reference materials NASS-7 and CASS-6 were analyzed along with the samples to ensure accuracy. Dilution acid blanks were subtracted from the sample concentrations prior to dilution factor correction and finalization of trace metal concentration results.

We also analyzed a series of archived samples from a mixing experiment conducted between the pond water and open ocean Gulf of Mexico seawater. Dissolved trace metal samples from these experiments were analyzed following the same approach outlined above for field samples. The filters used to filter the dissolved samples from the mixing experiment were analyzed using the “Berger leach” method for quantifying labile trace metal concentrations in particles captured on the filter (Berger et al. 2008). Trace metals leached from the filters were dissolved in 2% HNO_3 (Optima Grade) that contained a 1 ppb Indium (In) internal standard. Trace metal concentrations in the leaches were measured on the Element XR HR-ICP-MS at the University of South Florida by direct injection, as described above. We also applied the same leach procedure to filter blanks (filters that were exposed only to ultrapure water) and subtracted the resulting filter blank

concentrations from trace metal concentrations from the sample filters, and then corrected the values for the sample volume passed through the filter to finalize results.

2. *Particulate Organic Carbon (POC) and Nitrogen (PON), nutrient isotope analyses*

Particulate organic nitrogen (N) and carbon (C) isotope ($\delta^{15}\text{N}$ -PON, $\delta^{13}\text{C}$ -POC) and bulk (PON, POC) composition were measured for archived suspended particle field samples by CF-EA-IRMS (Continuous Flow Elemental Analyzer Isotope Ratio Mass Spectrometry) at the University of South Florida College of Marine Science Marine Environmental Chemistry Laboratory using commonly accepted procedures (Werner et al 1999). Isotope compositions were measured on a ThermoFinnigan Delta+XL IRMS, are reported in per mil (‰) notation and are scaled to VPDB ($\delta^{13}\text{C}$) and AT-Air ($\delta^{15}\text{N}$). Secondary reference materials (NIST 8574 $\delta^{13}\text{C} = +37.63 \pm 0.10$ ‰, $\delta^{15}\text{N} = +47.57 \pm 0.22$ ‰, N = 9.52%, C = 40.81%, C:N (molar) = 5.0; NIST 8573 $\delta^{13}\text{C} = -26.39 \pm 0.09$ ‰, $\delta^{15}\text{N} = -4.52 \pm 0.12$ ‰ N = 9.52%, C = 40.81%, C:N (molar) = 5.0) were used to normalize raw measurements to the VPDB ($\delta^{13}\text{C}$) and AT-Air ($\delta^{15}\text{N}$) scales (Werner et al 2002, Qi et al 2002, Coplen et al 2006) and to calibrate elemental N, C and C:N. Measurement uncertainties, expressed as ± 1 standard deviation of $n=65$ measurements of a laboratory reference material (NIST1577b $\delta^{13}\text{C} = -21.69 \pm 0.14$ ‰, $\delta^{15}\text{N} = 7.83 \pm 0.16$ ‰, N = $9.95 \pm .48$, C = $48.04 \pm .71$ %, C:N (molar) = 5.63 ± 0.27) were ± 0.19 ‰ for $\delta^{13}\text{C} \pm 0.14$ ‰ for $\delta^{15}\text{N}$, ± 2.99 %RSD for N concentration (mg/L), ± 3.47 %RSD for C concentration (mg/L), and ± 0.04 for C:N.

3. *Sulfate and major ion analyses*

Dissolved ($<0.2 \mu\text{m}$) sulfate and major ion (fluoride, chloride, nitrite, bromide, nitrate, and phosphate) concentrations were measured in archived water samples from the field and from the mixing experiment. Samples were diluted 100x with ultrapure water (Milli-Q, $18.2 \text{ M}\Omega \cdot \text{cm}$) prior to analysis. Larger volumes were dispensed by a Hamilton Microlab 500 series auto dispenser calibrated by weight to a precision less than 0.5%. Smaller volumes were pipetted by hand with precision of 1% or better. Calibration standards were made to 10 ppm from single ion stocks and mixed just before analysis. All runs were performed on a Thermo-Dionex Integriion High Pressure Ion Chromatography (HPIC) System with a Dionex IonPac AS19 column in isocratic mode with potassium hydroxide (KOH) eluent set at 20 mM run at 1 mL/min for 40 minutes duration. Accuracy on the IC-1 was better than 10% in the first run (phosphate was at 9% maximally at the end of the first run), and generally better than or about 5% for all other anions over the three runs. Single anion standards were made primarily for peak identification and secondarily for additional quality control were used in each of the three separate runs. These were also mixed to 10 ppm and were generally better than 5% on all three runs.

4. *Inorganic macronutrients (phosphate, nitrate, nitrite, silicic acid)*

Archived dissolved ($<0.2 \mu\text{m}$ filtered) water samples were analyzed for the inorganic macronutrients nitrate, phosphate, silicic acid, and nitrite at the University of South Florida College of Marine Science Nutrient Lab following established techniques (Parsons et al. 1984). A Seal Analytical Quattro instrument was used for all macronutrient analyses using standard curves made daily for each analytical run. Accuracy of the method was confirmed by analysis for reference standards obtained from Konso in Japan, and quality control checks were performed at regular intervals during the runs.

Deliverables produced:

A breakdown of samples analyzed for each analyte are provided in **Table Buck-1**; discrete samples were analyzed multiple times as needed to accomplish final results. All data generated from these analyses are included in the accompanying Excel spreadsheet, 2022 Piney Point Results_Buck nutrients trace metals major ions nutrient isotopes.xlsx.

Table Buck-1. Summary measurements for Piney Point April-June 2021.

	Analyst: Ethan Goddard; USF MECA Lab	Analysts: Casey Nickel, Dr. Salvatore Caprara; Instrument: Seal Quattro	Analyst: Dr. Zachary Atlas; USF Center for Geochemistry Analysis	Analyst: Shannon Burns; USF Tampa Bay Plasma Facility, Element XR HR-ICP-MS							
				Analytes	PON, POC, d ¹⁵ N- PON, d ¹³ C- POC, C:N	Phosphate, Nitrate+Nitrite, Silicic Acid, Nitrite	Fluoride, Chloride, Nitrite (IC), Bromide, Nitrate (IC), Sulfate, Phosphate (IC)	dAl, dP, dV, dMn, dFe, dCo, dNi, dCu, dZn, dCd, dPb	TD-Al, TD-P, TD-V, TD-Mn, TD-Fe, TD-Co, TD-Ni, TD-Cu, TD-Zn, TD-Cd, TD-Pb	LP-Al_0.4µm, LP-P_0.4µm, LP-V_0.4µm, LP- Mn_0.4µm, LP-Fe_0.4µm, LP-Co_0.4µm, LP-Ni_0.4µm, LP-Cu_0.4µm, LP-Zn_0.4µm, LP-Cd_0.4µm, LP-Pb_0.4µm	LP-Al_3µm, LP-P_3µm, LP-V_3µm, LP-Mn_3µm, LP-Fe_3µm, LP-Co_3µm, LP-Ni_3µm, LP-Cu_3µm, LP-Zn_3µm, LP-Cd_3µm, LP-Pb_3µm
								# of sample analytes	5	4	7
Date collected	Number of discrete locations or experiments sampled for each analyte										
Field Sampling	4/7/2021	0	12	12	12	12	0	0			
	4/8/2021	19	18	18	11	10	0	0			
	4/9/2021	14	16	16	12	14	0	0			
	4/12/2021	19	20	20	13	13	0	0			
	4/13/2021	1	3	3	2	3	0	0			
	4/16/2021	0	1	1	0	0	1	1			
	4/21/2021	5	5	5	5	5	0	0			
	4/29/2021	25	25	25	15	15	0	0			
	5/27/2021	25	25	25	0	15	0	0			
6/22/2021	13	25	25	15	15	0	0				
Mixing Experiment	5/25/2021	0	5	5	5	0	5	5			
Total number of discrete locations or experiments sampled for each analyte		121	155	155	90	102	6	6			
Total samples (# analytes x # discrete locations/experiments)		605	620	1085	990	1122	66	66			

Discussion of findings:

1. Field samples

Our analyses of field samples focused on samples collected between April 7 and June 22, 2021, from the *R/V Weatherbird II*, the *R/V Weatherbird II* tender, the *R/V W. T. Hogarth*, and a Florida Fish and Wildlife Conservation Commission (FWC) small boat (**Fig. Buck-1**).

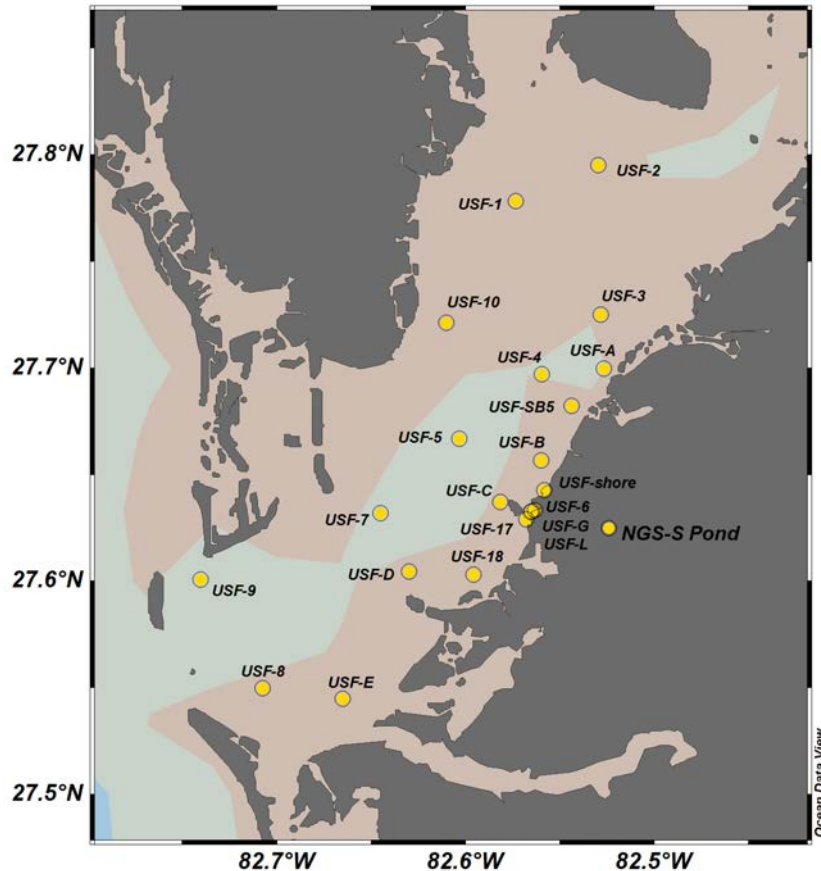
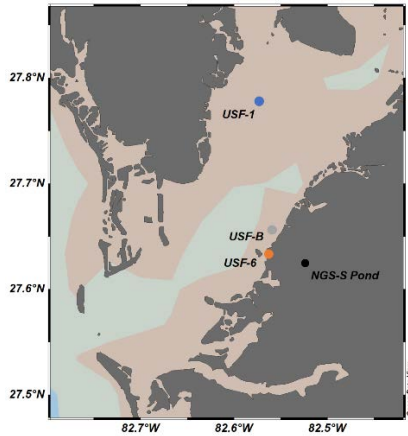


Figure Buck-1. Map of discrete field stations sampled April-June of 2021.

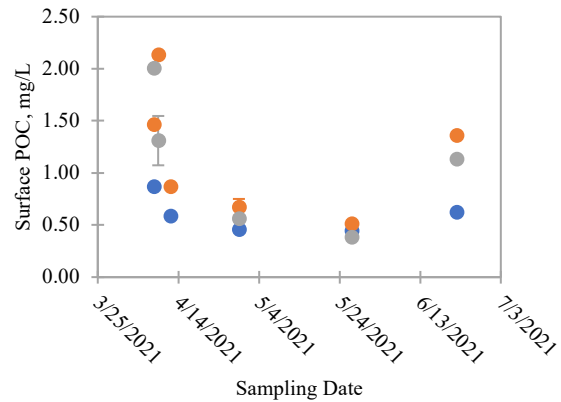
Particulate Organic Carbon, Phosphate/Phosphorus, Sulfate, and Nutrient isotopes

We selected three stations to compare surface (~ 1 m) conditions over time: USF-1, located northeast of Bayboro Harbor, across the Bay from the Piney spill; USF-B, just north of Port Manatee; and USF-6, located in Port Manatee (**Fig. Buck-2a**). The highest concentrations of particulate organic carbon (POC), phosphate, dissolved phosphorus (dP), and total dissolvable phosphorus (TD-P) were observed in Port Manatee immediately following the spill (**Fig. Buck-2**), this was also the case for particulate organic nitrogen (PON; **Fig. Buck-3a**). Phosphate results from the QuAAtro aligned well with dP results from the Element XR (**Fig. Buck-2c-d**). Surface concentrations of these parameters in Port Manatee declined rapidly in the weeks following the spill, and were similar to the concentrations at USF-1 in early May. Surface sulfate remained elevated at USF-6 through May, even increasing at USF-6 and USF-B between early and late May before declining again in June. In general, surface sulfate was higher in Port Manatee compared to USF-B and USF-1 post-spill, until they all reached similar concentrations in June of 2021 between 1100-1300 $\mu\text{g}/\text{mL}$. POC concentrations increased between our two last samples, likely reflecting the onset of the June *Karenia brevis* bloom in the Bay. Results for the same parameters at all stations are shown in daily surface maps (**Fig. Buck-4**).

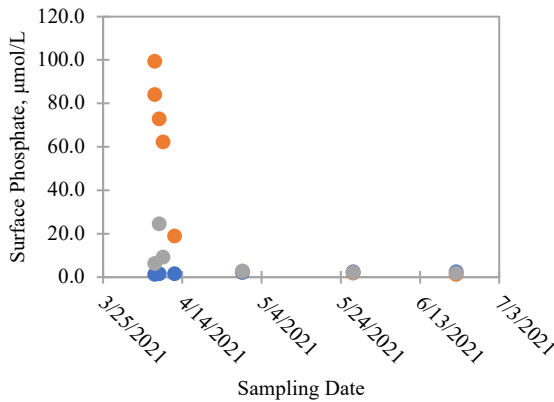
a) Map



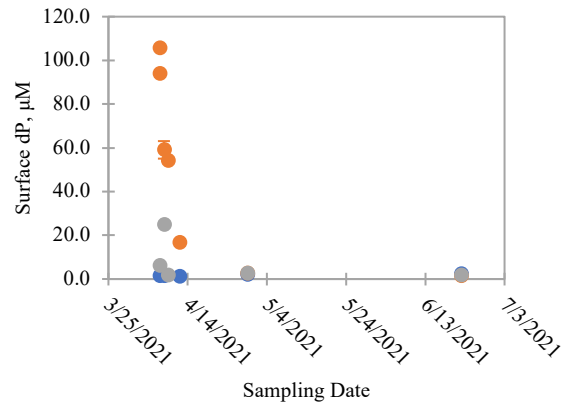
b) Particulate Organic Carbon



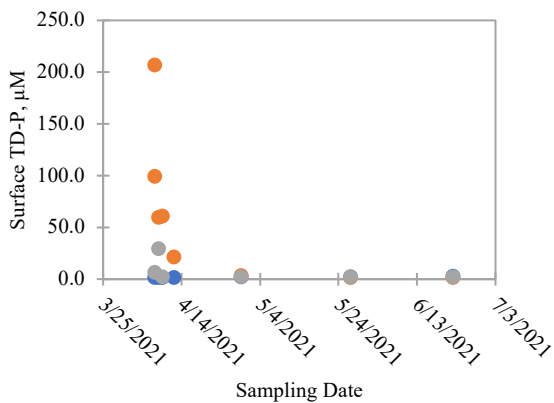
c) Phosphate



d) Dissolved phosphorus



e) Total dissolvable phosphorus



f) Sulfate

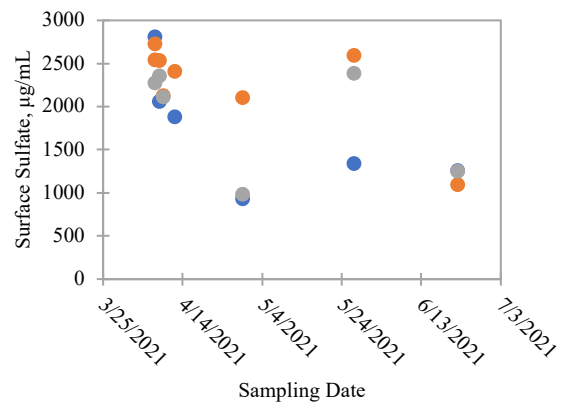
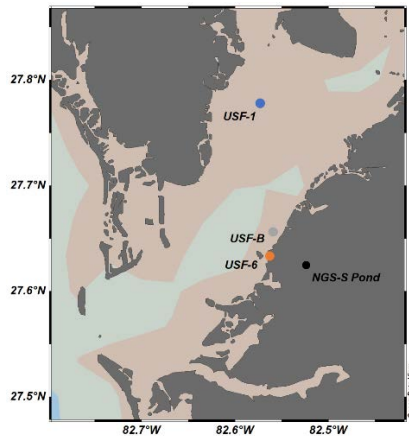


Figure Buck-2. (a) Map of three stations, USF-1 (27.78°N, -82.57°E), USF-6 (27.63°N, -82.56°E), and USF-B (27.66°N, -82.56°E), in relation to the NGS-S Pond of Piney Point. (b) Surface (~1 m) Particulate Organic Carbon (POC), (c) phosphate, (d) dissolved (<0.2 µm) and (e) total dissolvable (unfiltered, acidified) phosphorus, and (f) sulfate concentrations plotted over time at each of the three stations. Blue symbols are for USF-1, orange symbols are for USF-6, and grey symbols are for USF-B.

a) Map



b) Particulate Organic Nitrogen

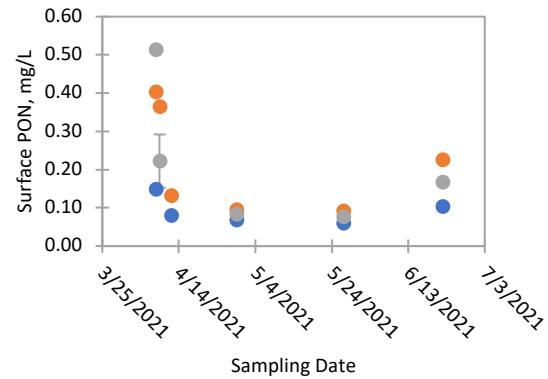
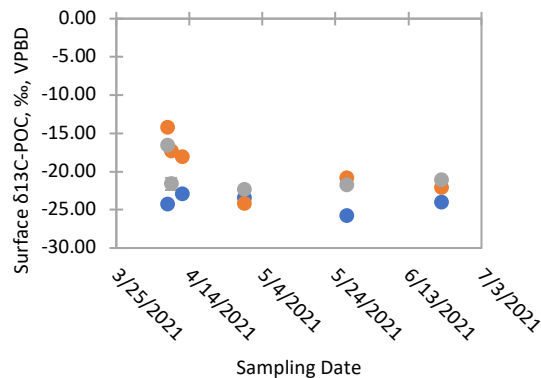
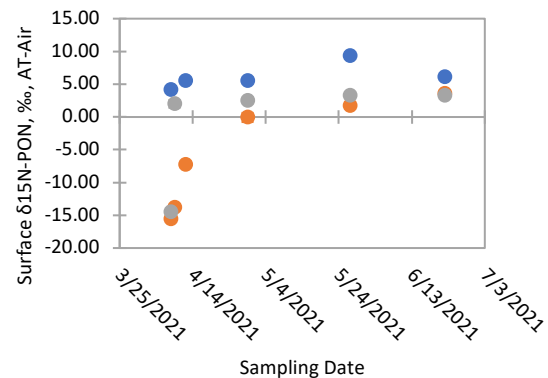
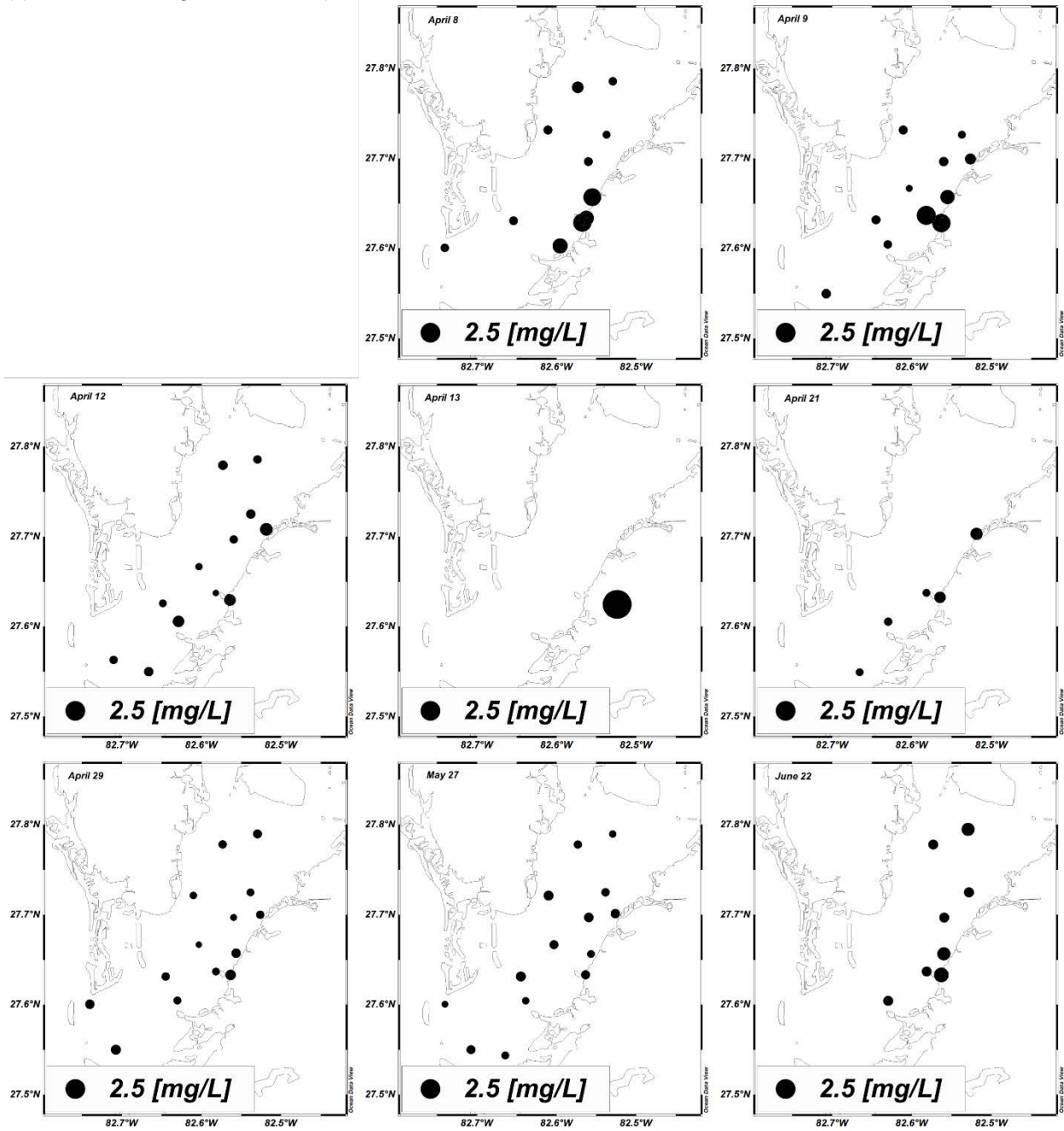
c) $\delta^{13}\text{C-POC}$ d) $\delta^{15}\text{N-PON}$ 

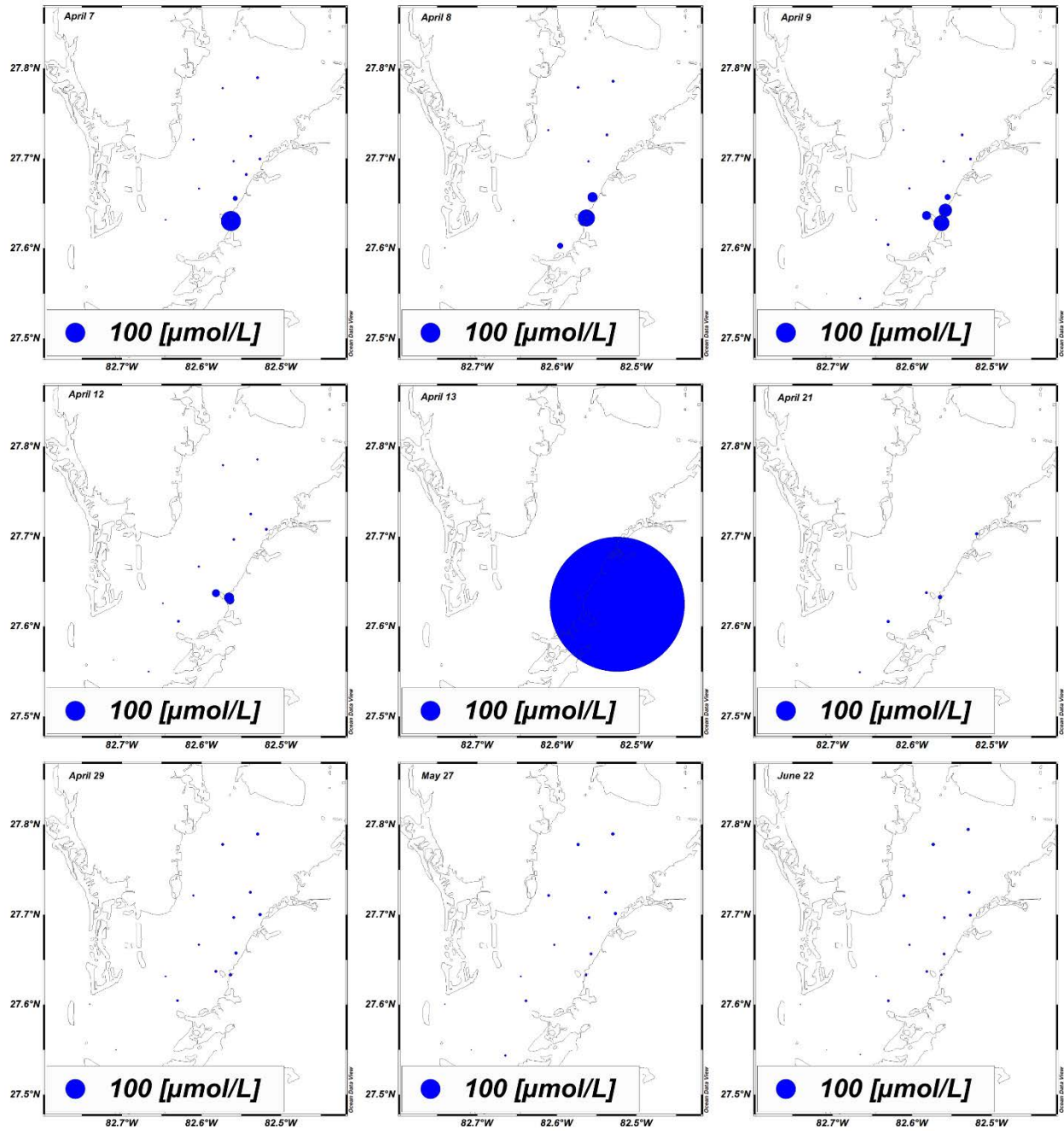
Figure Buck-3. (a) Map of three stations, USF-1 (27.78°N, -82.57°E), USF-6 (27.63°N, -82.56°E), and USF-B (27.66°N, -82.56°E), in relation to the NGS-S Pond of Piney Point. (b) Surface (~1 m) Particulate Organic Nitrogen (PON) concentrations, (c) $\delta^{13}\text{C-POC}$ (‰, relative to Vienna Pee Dee Belemnite (VPDB)), and (d) $\delta^{15}\text{N-PON}$ (‰, relative to atmospheric air (AT-Air)) values plotted over time at each of the three stations. Blue symbols are for USF-1, orange symbols are for USF-6, and grey symbols are for USF-B.

For the nutrient isotopes measured in archived samples ($\delta^{13}\text{C-POC}$, $\delta^{15}\text{N-PON}$), there were distinct spatial and temporal trends in values (**Figs. Buck-3,5**). In the days immediately following the Piney Point spill, $\delta^{13}\text{C-POC}$ values were higher in the Port Manatee samples than in surface water samples collected on the other side of the bay (USF-1), which stayed relative constant over the sampling period (**Fig. Buck-3c**). By early May, $\delta^{13}\text{C-POC}$ were roughly equivalent spatially across the Bay (**Figs. Buck-3,5**). The initial samples collected in and around Port Manatee had very negative $\delta^{15}\text{N-PON}$ values, which became positive over time and approached the same values as in the samples collected at USF-1 on the opposite side of the Bay by June 2022. The samples with elevated PON and POC in the early samples near Port Manatee were thus associated with strongly negative $\delta^{15}\text{N-PON}$ and less negative $\delta^{13}\text{C-POC}$, respectively, while the increased PON and POC at the end of the sampling period in June was characterized by positive $\delta^{15}\text{N-PON}$ and more negative $\delta^{13}\text{C-POC}$ (**Fig. Buck-3**).

(a) Particulate Organic Carbon (POC)



(b) Phosphate



(c) Sulfate

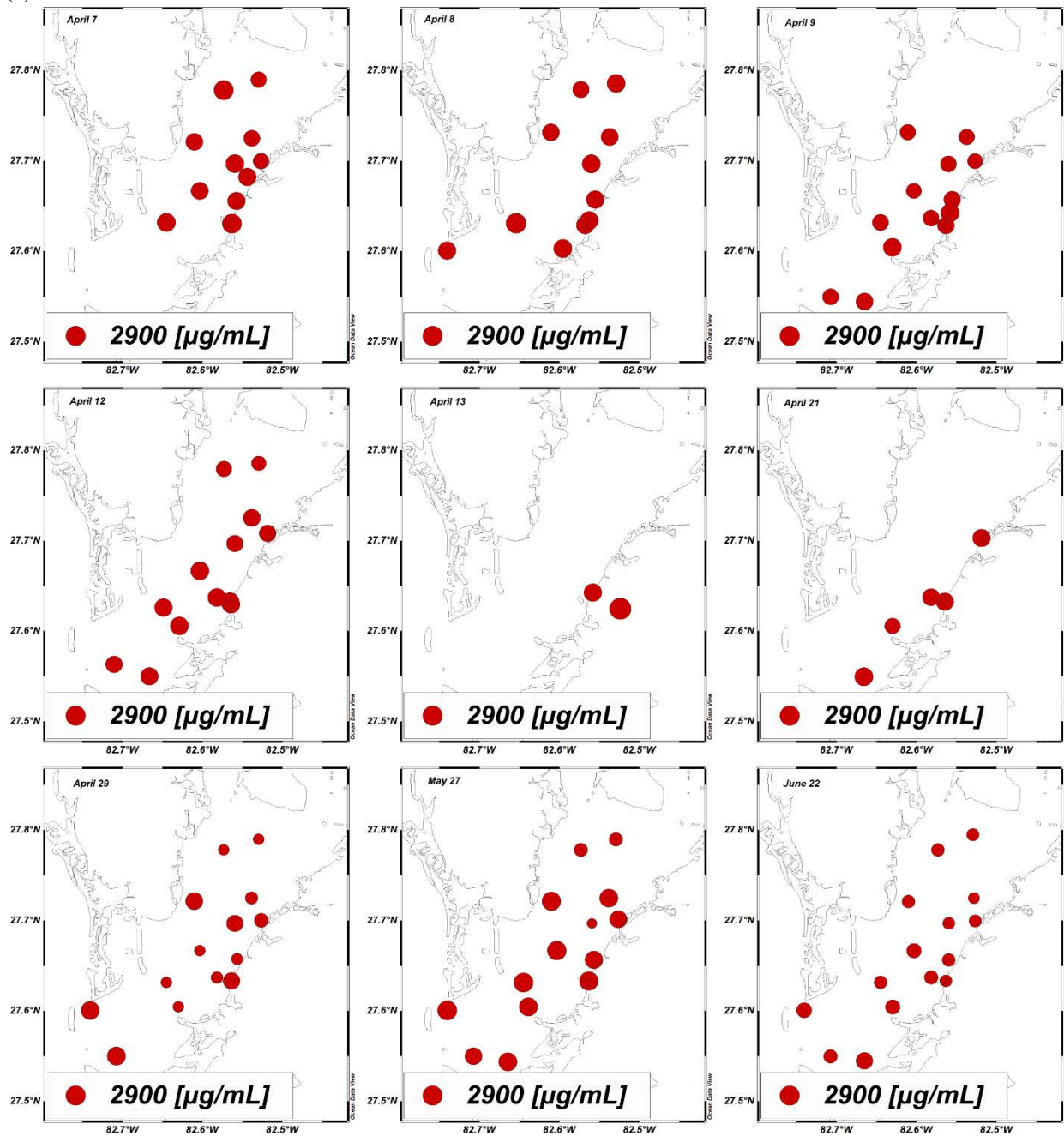
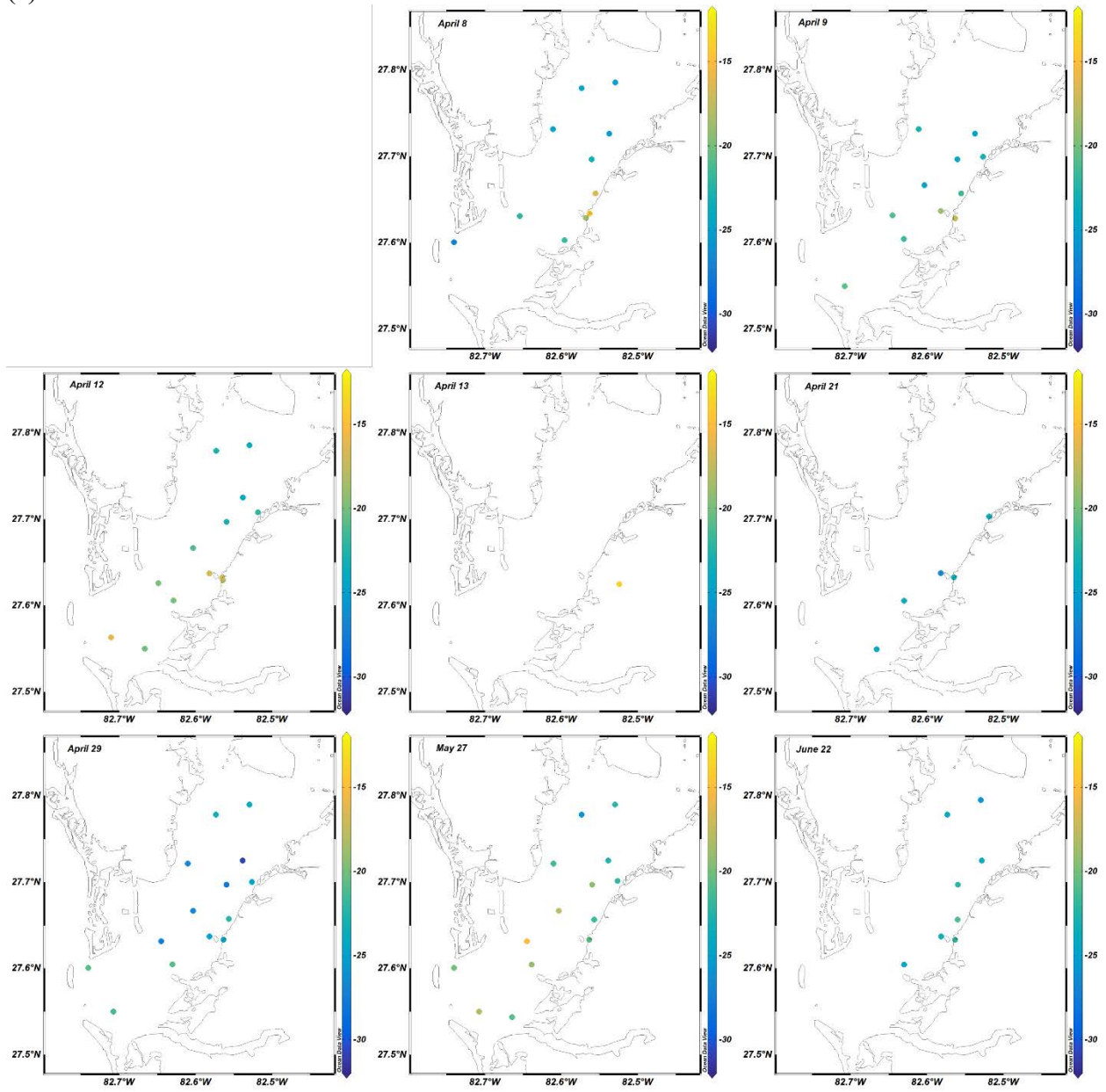


Figure Buck-4. Surface (~1 m) (a) Particulate Organic Carbon (POC), (b) phosphate, and (c) sulfate concentrations at all stations sampled for every day in 2021. Dot sizes are scaled to analyte concentrations at each station, using the same concentrations scale for each analyte.

(a) $\delta^{13}\text{C}$ -POC



(b) $\delta^{15}\text{N-PON}$

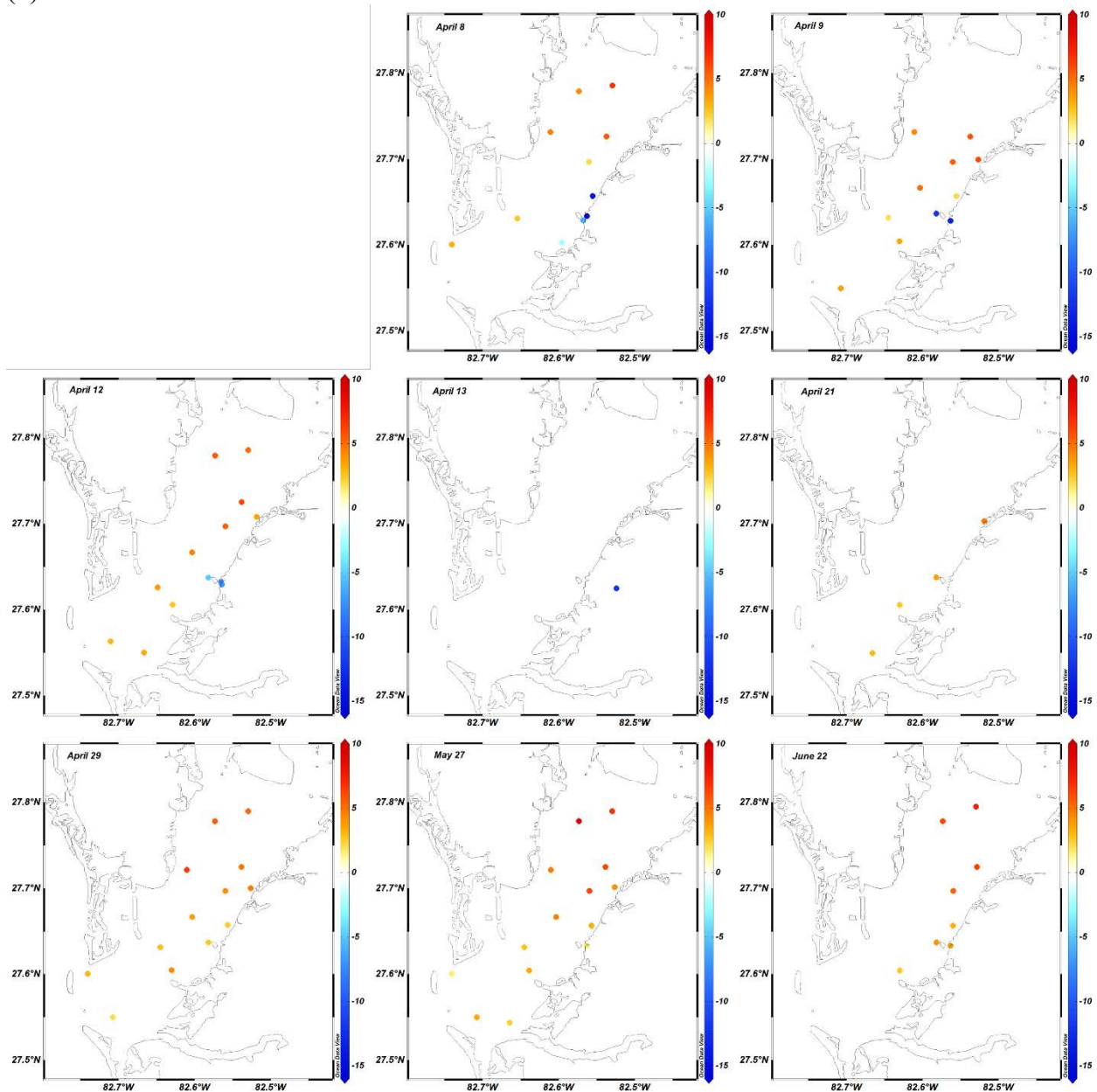


Figure Buck-5. Surface (~1 m) values of (a) $\delta^{13}\text{C-POC}$ (‰, relative to Vienna Pee Dee Belemnite (VPDB)) and (b) $\delta^{15}\text{N-PON}$ (‰, relative to atmospheric air (AT-Air)) at each station every day sampled in 2021. Color bar scales are the same for every panel in (a) and (b). For (b), red colors are positive values and blue colors are negative values.

Trace Metals

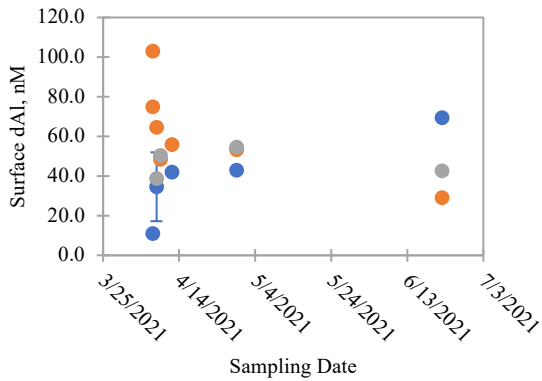
Surface concentrations of dissolved (d, **Fig. Buck-6**) and total dissolvable (TD, **Fig. Buck-7**) trace metals (Al, P, V, Mn, Fe, Co, Ni, Cu, Zn, Cd, Pb) were measured in archived field samples.

In the initial samples collected in the days following the Piney Point spill, the concentrations of most dissolved trace elements were elevated at the Port Manatee stations USF-6, USF-B) compared USF-1 on the other side of the Bay (**Fig. Buck-6**). A single sample from USF-B was especially elevated in dAl, dFe, dNi, dCu, dZn, dCd, dPb (see accompanying Excel file), and was flagged as a possible outlier in the dataset. In the remaining samples, dAl, dMn, dCo, and dNi most clearly tracked with dissolved phosphate concentrations, declining rapidly in the first week of sampling. Notably, dAl concentrations at USF-1 on the other side of the Bay showed an opposing trend, with low concentrations at USF-1 increasing as dAl concentrations at Port Manatee decreased. This may reflect mixing of dAl across the Bay in the days and weeks following the spill. These opposing trends were observed to a lesser extent for the other trace metals, perhaps because, unlike dAl, many of the other trace metals measured are more bioactive and may have been taken up by phytoplankton that bloomed in the Bay following the spill.

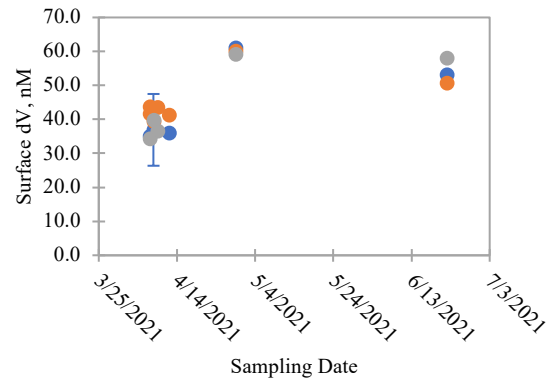
Spatial and temporal trends in the concentrations of total dissolvable (TD) trace metals, which include both dissolved concentrations and the concentrations of metals leached from suspended particles in the unfiltered acidified samples during storage, were generally more variable than was observed in the dissolved metal concentrations (**Fig. Buck-7**). A few surface TD trace metal concentration trends over time were observed. At USF-1, TD-V had an upwards trend in concentration after April 12th, whereas TD-V at the other two stations stayed relatively constant (**Fig. Buck-7b**). Surface TD-Cu at USF-1 showed the same pattern as the dCu data over time, except the peak in concentration occurred May 27th (**Fig. Buck-6g, 7g**). No dissolved samples were collected on May 27th, so it is not possible to determine if the dissolved concentrations peaked on this day, too. In contrast, TD-Cu at USF-B remained relatively constant after April 12th. For USF-6, TD-Cu increased on April 29th back to the initial concentration observed on April 7th and then plateaued (**Fig. Buck-7g**). Surface TD-Co, TD-Ni, TD-Zn, TD-Cd, and TD-Pb all exhibited the same temporal concentration pattern as surface TD-Cu at USF-1: an increase to near-April 7th concentrations on May 27th, followed by a decline in June (**Fig. Buck-7**). The only metals that had similar trends and concentrations across all three stations over time after April 12th were TD-Mn and TD-Co (**Fig. Buck-7c, e**).

Daily surface maps of dCo and TD-Co concentrations for all stations are provided (**Fig. Buck-8**).

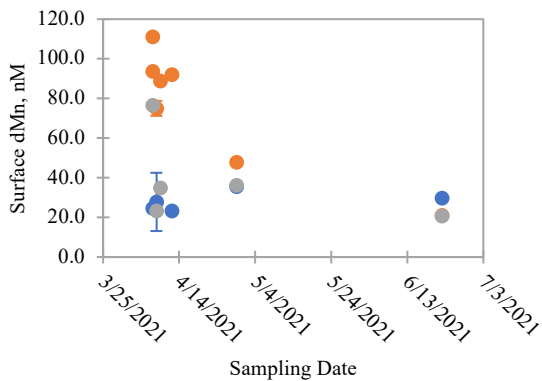
a) Aluminum (dAl)



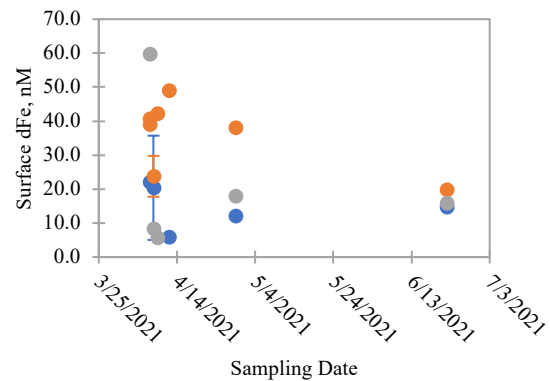
b) Vanadium (dV)



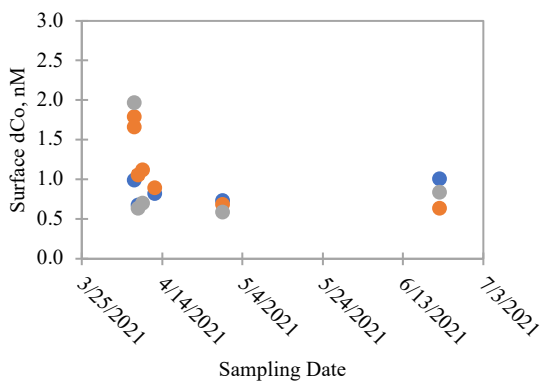
c) Manganese (dMn)



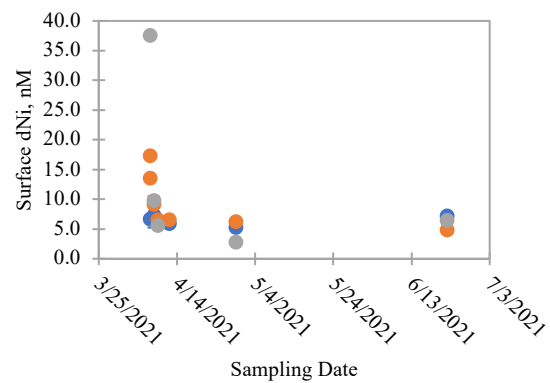
d) Iron (dFe)



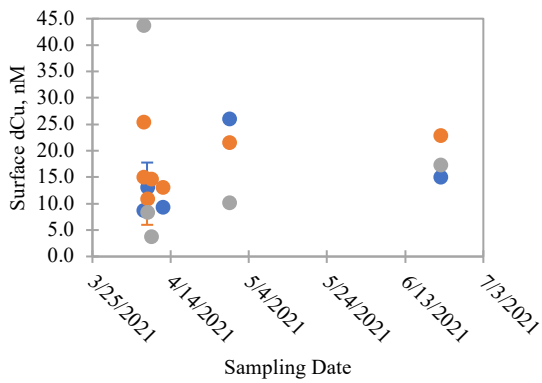
e) Cobalt (dCo)



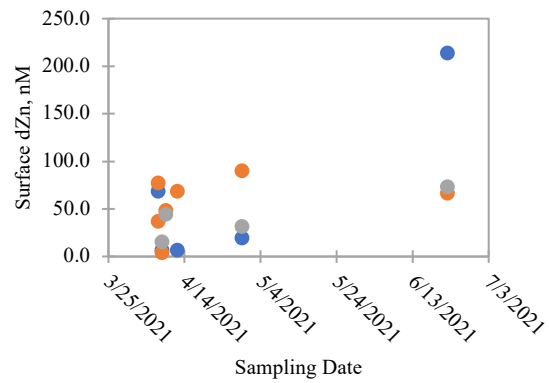
f) Nickel (dNi)



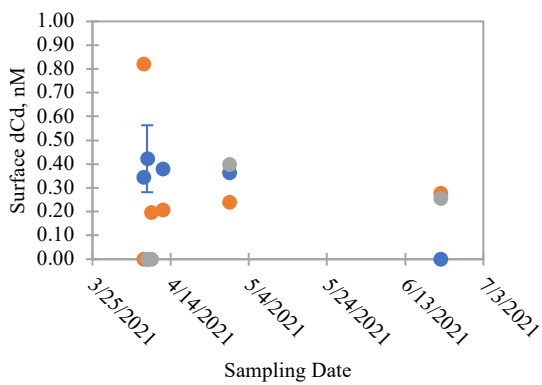
g) Copper (dCu)



h) Zinc (dZn)



i) Cadmium (dCd)



j) Lead (dPb)

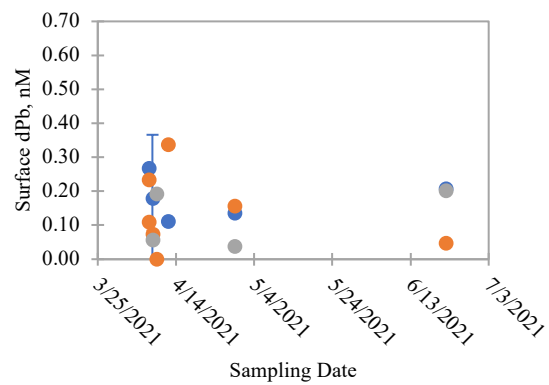
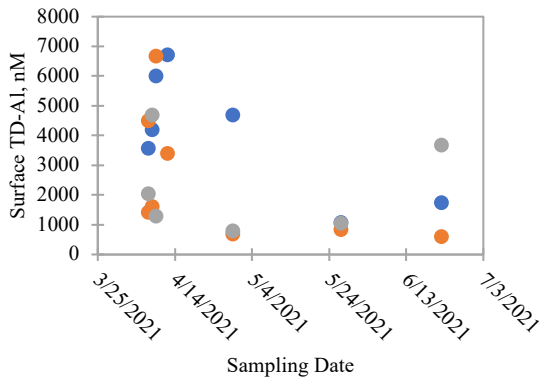
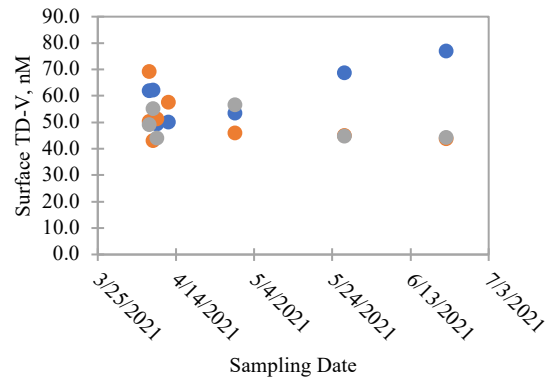


Figure Buck-6. Dissolved (<math><0.4 \mu\text{m}</math>) surface (~1 m) trace metal (Al, V, Mn, Fe, Co, Ni, Cu, Zn, Cd, and Pb) concentrations over time from three stations (see Fig. 3a for map): USF-1 (blue symbols), USF-6 (orange symbols) and USF-B (grey symbols).

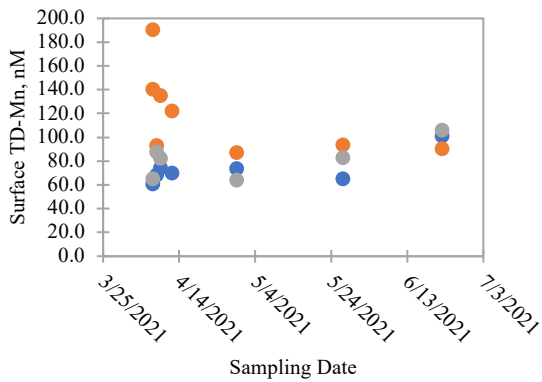
a) Aluminum (TD-Al)



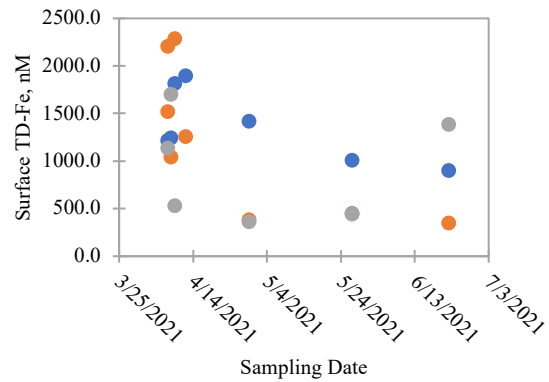
b) Vanadium (TD-V)



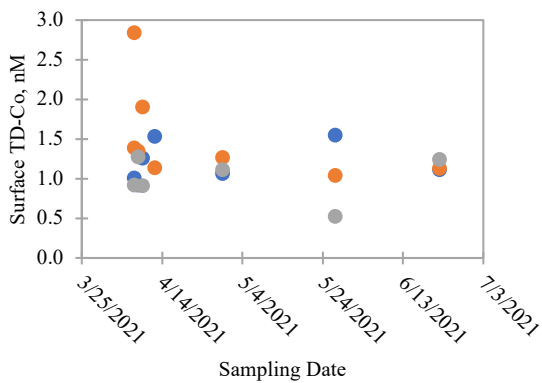
c) Manganese (TD-Mn)



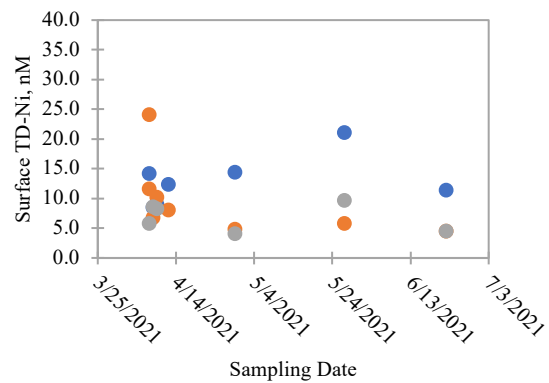
d) Iron (TD-Fe)



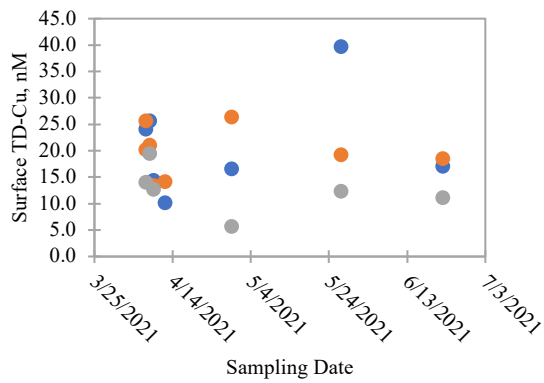
e) Cobalt (TD-Co)



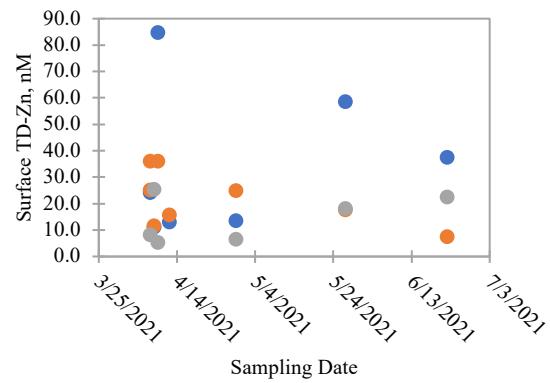
f) Nickel (TD-Ni)



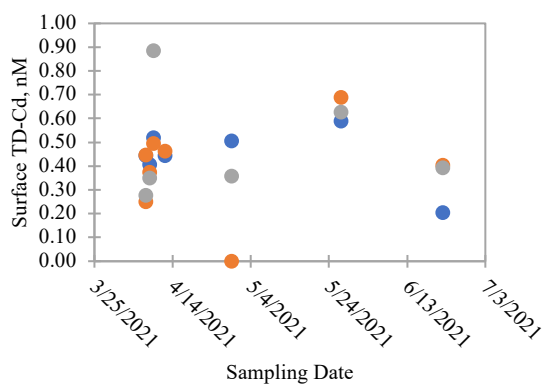
g) Copper (TD-Cu)



h) Zinc (TD-Zn)



i) Cadmium (TD-Cd)



j) Lead (TD-Pb)

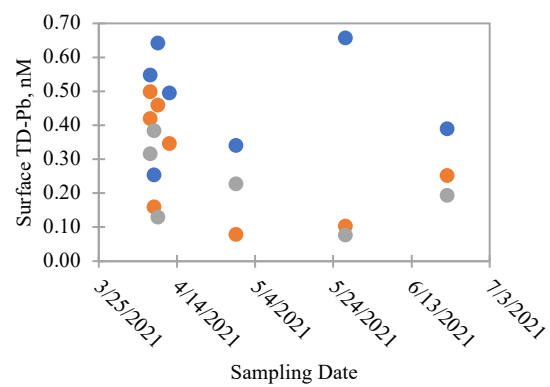
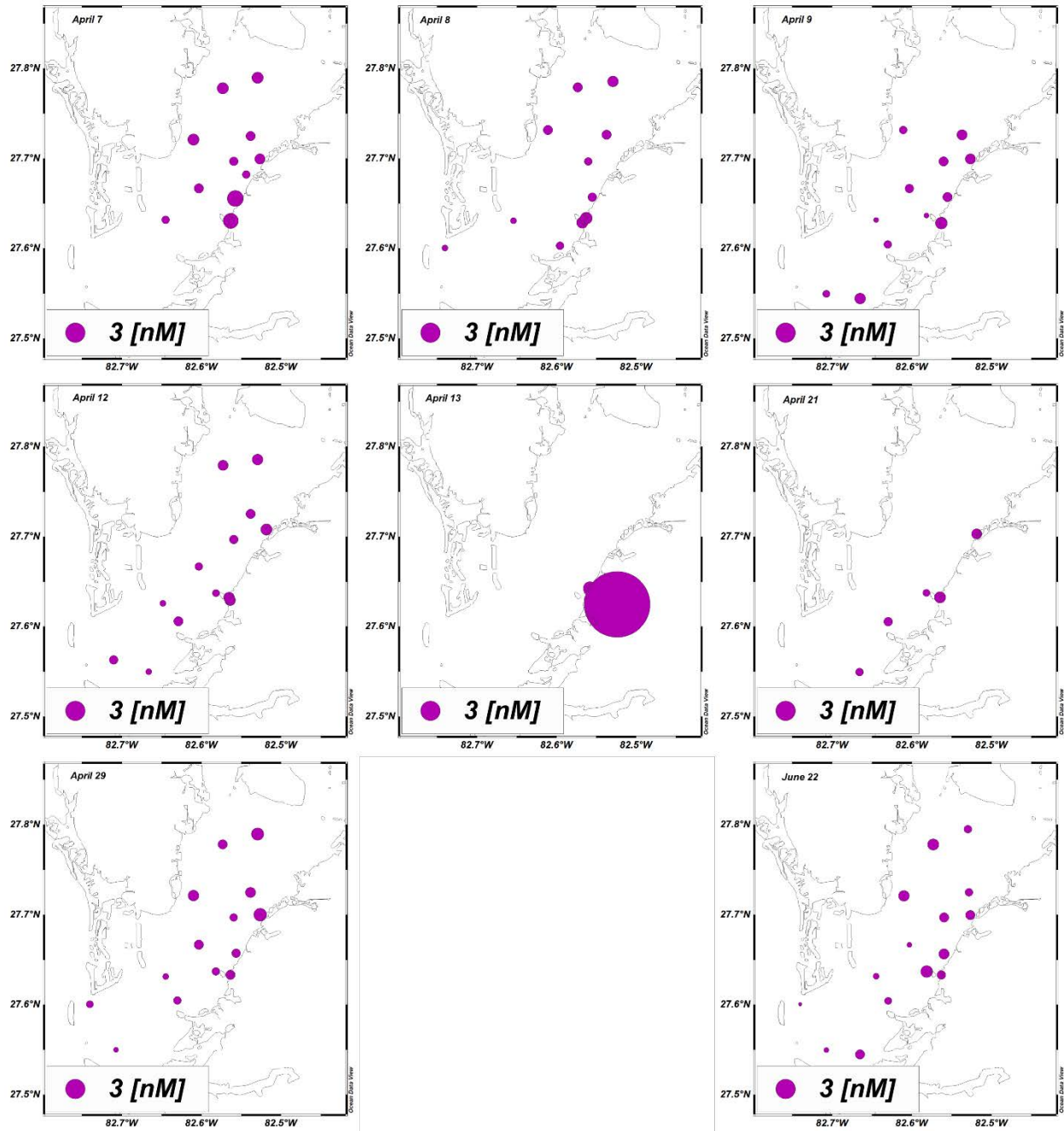


Figure Buck-7. Total dissolvable (unfiltered acidified) surface (~1 m) trace metal (Al, V, Mn, Fe, Co, Ni, Cu, Zn, Cd, and Pb) concentrations over time from three stations (see Fig. 3a for map): USF-1 (blue symbols), USF-6 (orange symbols) and USF-B (grey symbols).

(a) Dissolved Co



(b) Total dissolvable Co

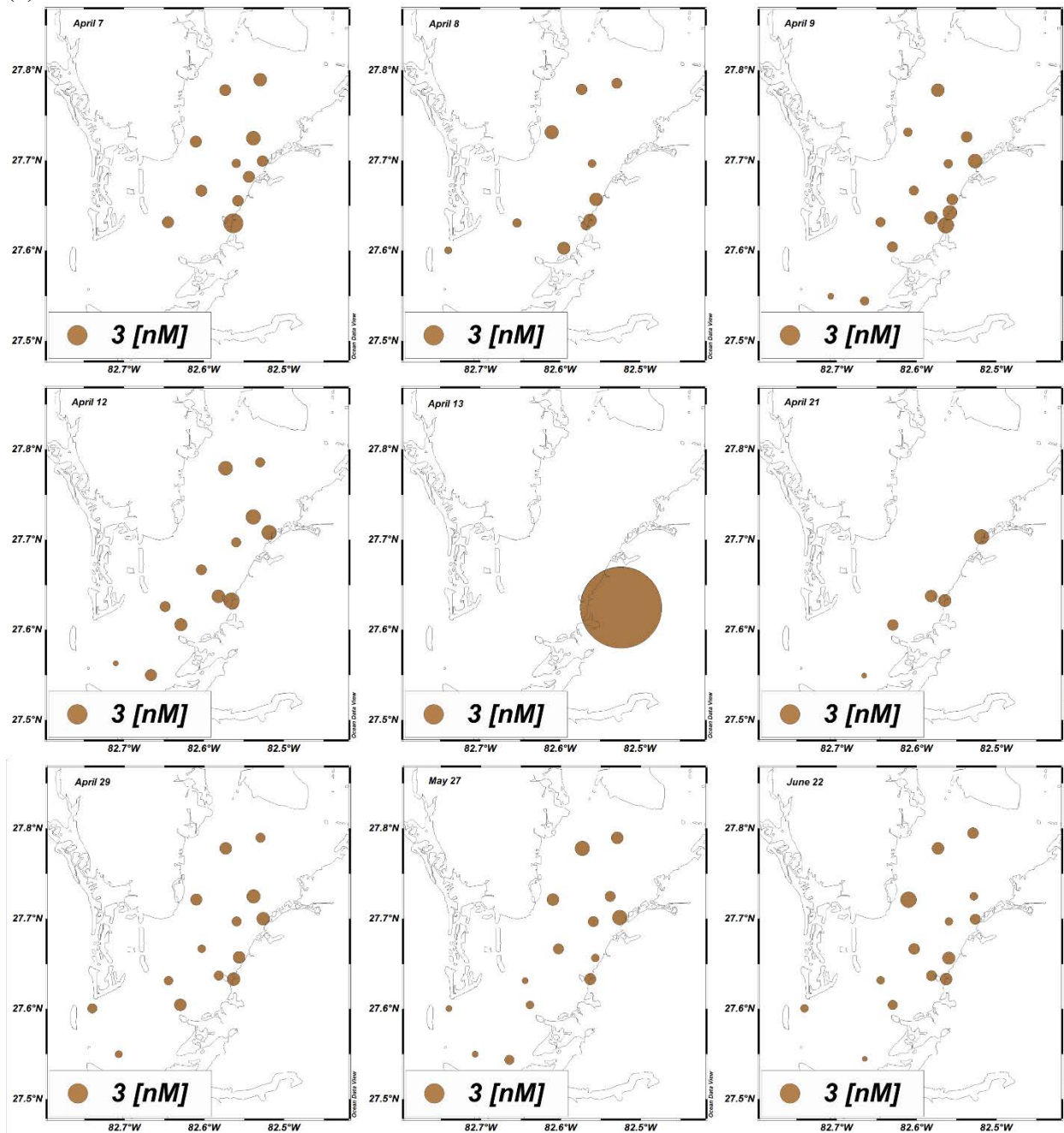


Figure Buck-8. Surface (~1 m) (a) dissolved ($d; < 0.4 \mu\text{m}$) Co and (b) total dissolvable (TD; unfiltered acidified) Co concentrations at each station for every day sampled in 2021. Dot sizes are scaled to concentrations at each station, and the same scale was used for both dissolved and total dissolvable Co concentrations.

2. Mixing Experiments

In addition to the field samples collected in the days and weeks following the Piney Point spill, we had also archived samples from mixing experiments conducted between source waters for the Piney Point spill and offshore Gulf of Mexico seawater (GOM) to approximate previous studies

of trace metal behavior during estuarine mixing (Sholkovitz 1976; Boyle et al. 1977) and evaluate abiotic drivers of changes in analyte concentrations. The pond water used for the mixing experiments was collected on April 13, 2021 at the NGS-S pond (27.625°N, -82.524°E) in Piney Point (**Fig. Buck-7a**). The pond water was filtered (<0.4 μm) using a Teflon dual-stage filter rig (Saville) connected to a custom-made trace-metal-clean vacuum filtration system. The GOM endmember had been previously collected using trace metal clean techniques from a small boat about 20 miles offshore (27.194°N, -82.962°E), and filtered (<0.2 μm, Pall Acropak) prior to storage in an acid-cleaned carboy since January 2017. Five target salinities were selected based on the measured salinities of the pond (S = 10.33) and GOM (S = 35.72) water: S = pond, S = 14, S = 20, S = 28, S = GOM). The three intermediate solutions were made by mixing the pre-filtered pond and GOM water in 1-L acid-cleaned polycarbonate bottles. Salinity was measured using an Autosal Guildline Salinometer. The actual salinities of the three mixed solutions were S = 14.91, S = 20.82, and S = 28.71. The intermediate solutions were left to equilibrate for one hour after mixing prior to sampling. The pre-filtered endmembers were treated similarly, left at room temperature for one hour prior to sampling (**Fig. Buck-7b**).

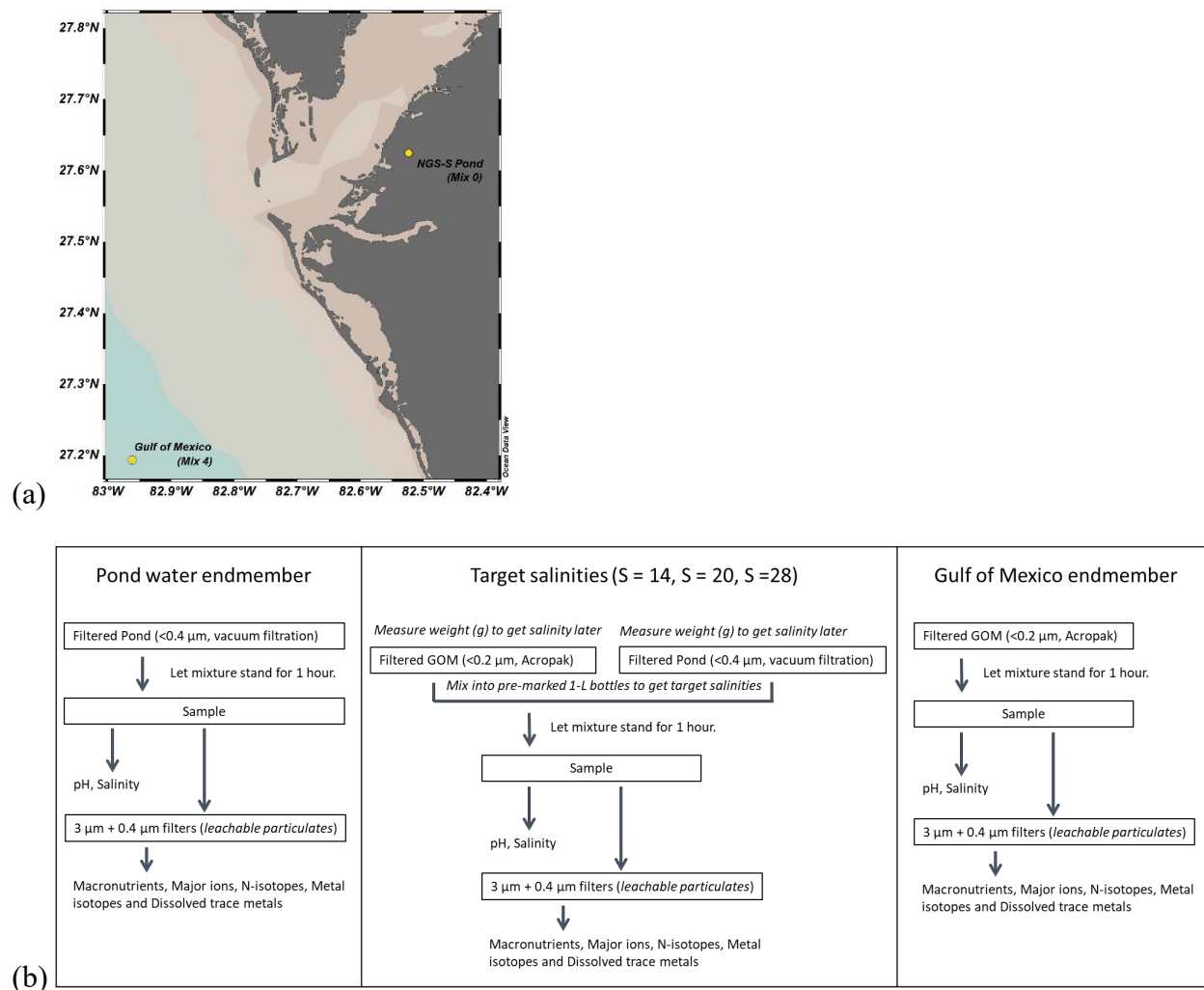


Figure Buck-7. Mixing experiment (a) endmember collection locations and (b) sampling setup.

Phosphate and Sulfate

Dissolved phosphate concentrations were low in the GOM endmember (0.12 μM), and extremely high (5,030 μM) in the pond water. Phosphate concentrations declined linearly with increasing salinity, reflecting conservative mixing between the endmembers (**Fig. Buck-8a**); no abiotic losses of phosphate were observed during mixing. Sulfate concentrations, on the other hand, declined non-conservatively with increasing salinity (**Fig. Buck-8b**).

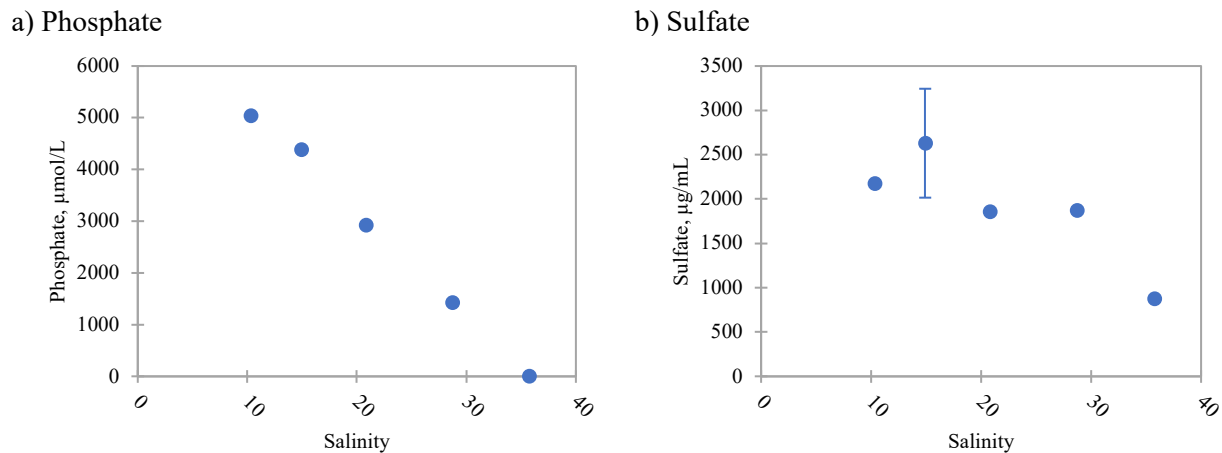
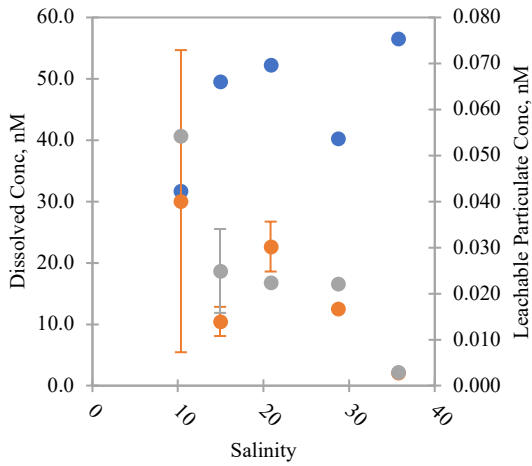


Figure 8. Phosphate and sulfate from the mixing experiments, plotted against salinity.

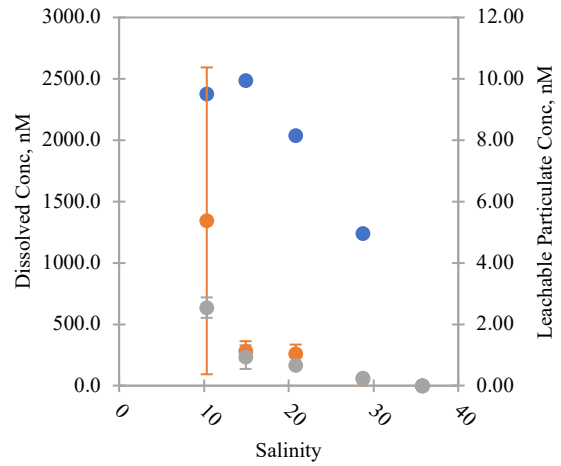
Trace Metals

The concentrations of dissolved ($<0.4 \mu\text{m}$ filtered) and leachable particulate (determined from a weak acid leach of the particles on the two filter pore sizes used, see *Activities* above) trace metals (Al, P, V, Mn, Fe, Co, Ni, Cu, Zn, Cd, Pb) were measured in the mixing experiment samples. Dissolved Mn, Co, Ni, Zn, and Cd showed an overall decline with increasing salinity. The same was true for the small ($0.4\text{--}3 \mu\text{m}$) and large ($>3 \mu\text{m}$) leachable particulate size fractions of these metals (**Fig. Buck-9b-d, f, g**). In each of these cases, minimal exchange between dissolved and particulate phases was observed in the mixing experiment samples, and indicate that abiotic concentration changes in the experiments primarily reflect dilution with the lower concentrations in the offshore water used for the mixing rather than precipitation. For V on the other hand, leachable particulate V and dissolved V concentrations followed opposing trends with increasing salinity (**Fig. Buck-9a**), suggesting exchange of V between the dissolved and particulate fractions. Dissolved Cu and Pb also showed some evidence of dissolved-particulate exchange, although not in the same way: dissolved Cu (**Fig. Buck-9e**) concentrations peaked in the middle of the salinity range ($S = 20.82$), whereas dissolved Pb concentrations were at a minimum (**Fig. Buck-9h**). The small and large leachable particulate size fractions for Cu and Pb showed declining concentrations with increasing salinity and only in the case of Pb was the loss of dissolved metal picked up in the leachable particulate fraction. Leachable particulate copper showed the greatest concentration difference between large and small size fractions in the pond water, the large size fraction having more Cu than the small size fraction (**Fig. Buck-9e**). As salinity increased, the concentrations of Cu in the large and small size fractions converged.

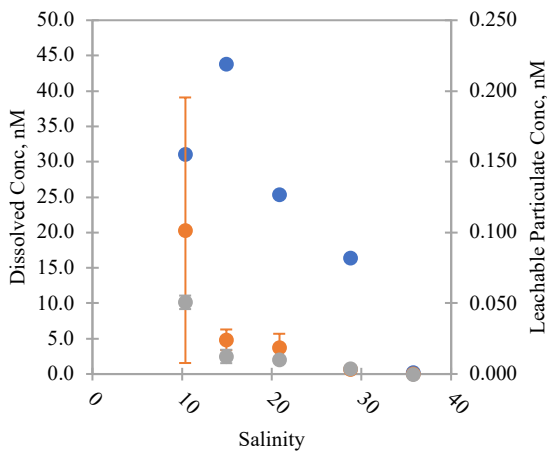
a) Vanadium (V)



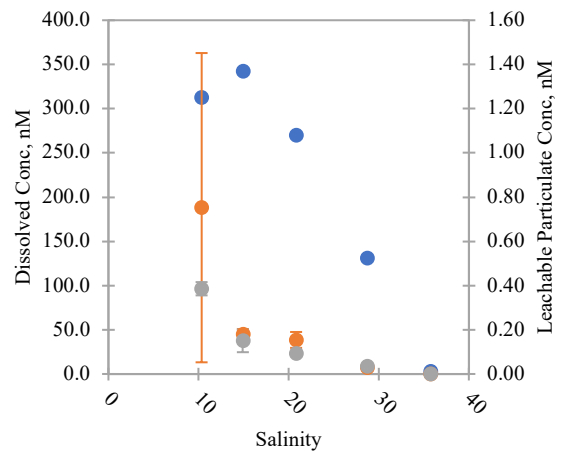
b) Manganese (Mn)



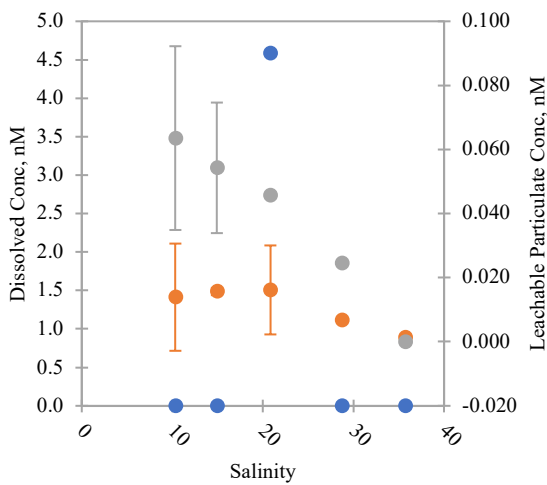
c) Cobalt (Co)



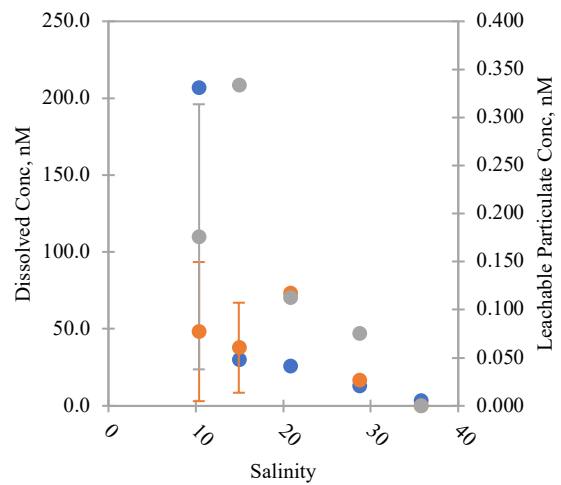
d) Nickel (Ni)



e) Copper (Cu)



f) Zinc (Zn)



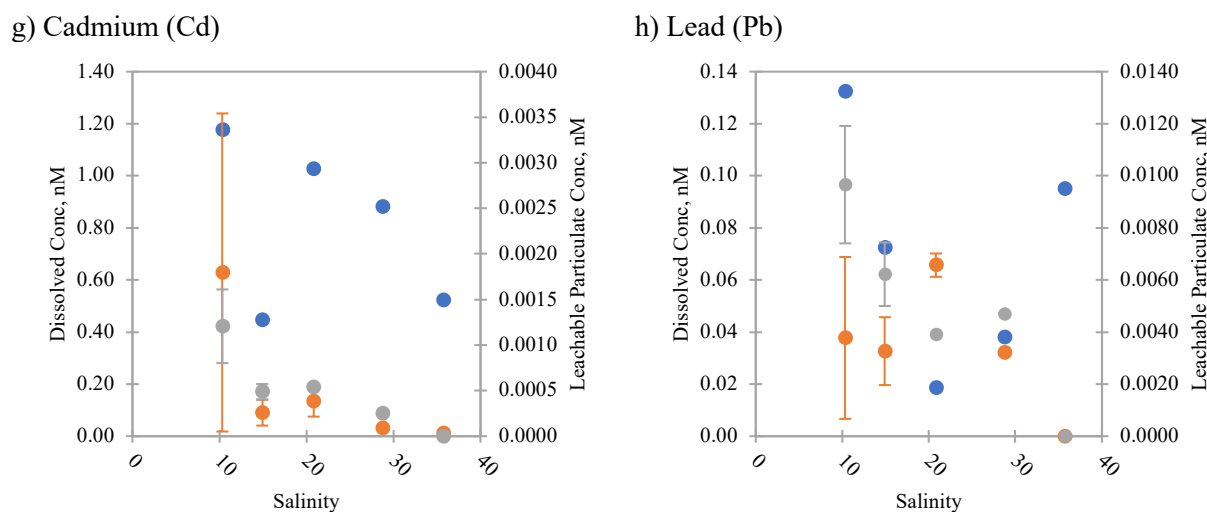


Figure Buck-9. Concentrations of trace metals (V, Mn, Co, Ni, Cu, Zn, Cd, and Pb) from the mixing experiments plotted against salinity. Dissolved (<math><0.4\ \mu\text{m}</math>) trace metal concentrations are represented by the blue symbols, small leachable particulate (0.4-3 μm) trace metal concentrations by the orange symbols, and large leachable particulate trace metal concentrations by the grey symbols. Data for aluminum (Al), phosphorus (P), and iron (Fe) concentrations are also available, but the “HIGH” results could not be plotted for the leachable particulate samples; see accompanying spreadsheet for these results.

References

- Berger, C. J. M., S. M. Lippiatt, M. G. Lawrence, and K. W. Bruland. 2008. Application of a chemical leach technique for estimating labile particulate aluminum, iron, and manganese in the Columbia River plume and coastal waters off Oregon and Washington. *Journal of Geophys. Res.* 113. 10.1029/2007jc004703
- Boyle, E. A., J. M. Edmond, and E. R. Sholkovitz. 1977. The mechanism of iron removal in estuaries. *Geochimica et Cosmochimica Acta* 41: 1313-1324. doi: 10.1016/0016-7037(77)90075-8
- Coplen, T.B., Brand, W.A., Gehre, M., Gröning, M., Meijer, H.A.J., Toman, B. and Verkouteren, R.M. (2006), New Guidelines for $\delta^{13}\text{C}$ Measurements. *Analytical Chemistry* 2006 78 (7), 2439-2441 DOI: 10.1021/ac052027c
- Parsons, T. R., Y. Maita, and C. M. Lalli. 1984. A manual of chemical and biological methods for seawater analysis. Pergamon Press.
- Qi, H., Coplen, T. B., Geilmann, H., Brand, W. A. and Böhlke, J. K. (2003), Two new organic reference materials for $\delta^{13}\text{C}$ and $\delta^{15}\text{N}$ measurements and a new value for the $\delta^{13}\text{C}$ of NBS 22 oil. *Rapid Commun. Mass Spectrom.*, 17: 2483–2487. Doi:10.1002/rcm.1219
- Werner, R. A., Bruch, B. A. and Brand, W. A. (1999), ConFlo III – an interface for high precision $\delta^{13}\text{C}$ and $\delta^{15}\text{N}$ analysis with an extended dynamic range. *Rapid Commun. Mass Spectrom.*, 13: 1237–1241.
- Werner, R. A. and Brand, W. A. (2001), Referencing strategies and techniques in stable isotope ratio analysis. *Rapid Commun. Mass Spectrom.*, 15: 501–519. Doi:10.1002/rcm.258
- Sholkovitz, E. R. 1976. Flocculation of dissolved organic and inorganic matter during the mixing of river water and seawater. *Geochimica et Cosmochimica Acta* 40: 831-845. doi: 10.1016/0016-7037(76)90035-1

II. Mya Breitbart, Natalie Sawaya, Makenzie Kerr, Grace Koziol

Bacteria and phytoplankton community composition
(16S rRNA, 18S rRNA)

Suspended Particles

Total budget: \$88,730

Activities during this period:

A total of 250 samples were collected for analysis of microbial communities in the vicinity of Piney Point to assess the impact of the discharge into Tampa Bay. Samples were collected on April 7, April 8, April 9, April 12, April 13, April 16, April 29, May 27, and June 22. Samples were collected from 13 unique sites (sites USF1-13) aboard the R/V Weatherbird II and 5 unique sites in shallower water via a small boat (sites USF A-E). In addition, we analyzed two source water samples (primary discharge waters) and two nearshore samples collected during a visible phytoplankton bloom.

At each collection station, approximately 1 Liter of water was pumped through a 0.22 μm Sterivex filter using a peristaltic pump. Often the collected waters were thick with organisms and debris, causing the filter to build pressure and pop off the tubing. In these cases, less water was pumped through the filter and that amount was noted. Once the filter clogged or 1 Liter was pumped through, the excess liquid in the filter was removed by pushing air through the tubing. The Sterivex filter was wrapped with Parafilm, then aluminum foil, then labeled for storage in a -20°C freezer until return to the dock (within 8 hours). Upon return to the laboratory, samples were transferred to a -80°C Ultra Freezer for storage until processing.

DNA was extracted from each Sterivex filter using methods previously developed for environmental DNA analyses (Djurhuus et al. 2017, Djurhuus et al. 2020). Screwcap tubes (1.7 mL) with O rings (Genesee Cat. 21262 and 223421) were filled with 0.2 g of 0.5 mm and 0.2 g of 0.1 mm autoclaved glass beads. The outer casing of the Sterivex filters was cracked open using bleach sterilized crab crackers & pliers. The filter inside was removed from the casing using sterile razor blades and folded using sterile forceps to place in the 1.7 mL screwcap tube. Using products from the Qiagen DNeasy Blood & Tissue Kit (Qiagen Cat. 69504), 800 μL of ATL buffer was added to each tube and bead beat at max speed (5 m/s) for 1 min using a Bead Mill 4. Tubes were incubated for 30 minutes at 56°C. The bead beating step was repeated and incubated again for 30 minutes at 56°C. 100 μL of Proteinase K was added to each tube and vortexed for 10 seconds. The tubes were incubated for 2 hours, while shaking, at 56°C, then vortexed for 15 seconds. Tubes were spun down at 4000 g for 1 minute and 650-900 μL of supernatant were transferred to clean 2 mL tubes. The 2 mL tubes were spun down for 1 minute at 13000 g and 650 μL of bead-free supernatant was transferred to a new tube. Then 650 μL of Buffer AL was added to each tube and vortexed to mix. Samples were incubated at 56°C for 10 minutes, then 650 μL of 96-100% Ethanol was added to each tube and mixed by vortexing. Each sample was transferred to a DNeasy mini spin column within a 2 mL collection tube and centrifuged for 1 minute at ≥ 6000 g. Flow through was discarded and this process was repeated for the entire sample volume. The procedure in the Qiagen kit was followed for the remainder of the process (steps 4-8) and final DNA was eluted from the column with 50 μL of water. DNA was quantified using the Qubit 2.0 in ng/ μL . DNA samples were sent off for next generation sequencing of 16S rRNA genes (bacteria and archaea) and 18S rRNA genes (eukaryotes) using a 500 cycle MiSeq at Iowa State University (<https://dna.biotech.iastate.edu/nextgen-metagenomics.html>). The V4 hypervariable region of the 16S rRNA gene was amplified using primers 515F and 806R and the V8 region of the 18S rRNA gene was amplified using primers V8F and EukBR. Processing and analysis of sequence data were conducted using R (R Core

Team 2013). First, adapters and primers were trimmed with Trimmomatic v 0.36.0 (Bolger et al. 2014). Amplicon sequence variants (ASVs) were generated by the Divisive Amplicon Denoising Algorithm (DADA2) package v 1.21.0 (Callahan et al. 2016). For taxonomic assignment, ASVs were compared against the SILVA v 138.1 rRNA database for 16S rRNA genes and SILVA v 132 for 18S rRNA genes, using a default bootstrapping value of 50 (Quast et al. 2012). The data were normalized based on library size using the R package metagenomeSeq v 1.36.0 (Paulson et al. 2013), which uses cumulative sum scaling to correct for differences in sampling depth. NMDS plots based on a Bray-Curtis dissimilarity of the relative abundance of normalized ASVs were constructed using the metaMDS function in vegan v 2.5-7 and ggplot2 v 3.3.5 (Wickham and Wickham 2007, Oksanen et al. 2013). Compositional bar plots depicted the top 25 families (if available) or higher level taxonomic classifications across all samples and their percent abundance per sample were constructed using phyloseq v 1.38 (McMurdie and Holmes 2013) and microViz 0.9.0 (Barnett et al. 2021). For 16S rRNA gene compositional bar plots analysis, sequences assigned as mitochondria and chloroplasts were removed.

Deliverables produced:

We produced high quality 16S rDNA sequences from a total of 126 unique samples and 18S rDNA sequences from 123 unique samples, which are provided in the accompanying Excel file 2022 Piney Point Results_Breitbart community composition. All samples (with the exception of S100 for the 16S rRNA gene) are included in the barplots showing the top 25 families across all samples (**Figures Breitbart-1 and 2**) and for the 18S rRNA gene NMDS (**Figure Breitbart-3**), while four samples (samples S50, S51, S100, S127) needed to be excluded from the 16S rRNA gene NMDS (**Figure Breitbart-4**) because of their high divergence from other samples.

Discussion of findings:

18S rRNA gene composition (Figure Breitbart-1): Dominant groups within the Tampa Bay water samples included copepods (Copepoda), diatoms (Mediophyceae, Rhizosolenids), dinoflagellates (Peridinales, Syndiniales, Gymnodinophycidae, Thoracosphaeraceae, Kareniaceae, Gonyaulacales), green algae (Trebouxiophyceae, Chlorophyta, Mamiellales, Chlorodendrales), ciliated protozoa (Hypotrichia, Oligotrichia, Peniculia, Choreotrichia), tunicates (Copelata), brachiopods (Lingulata), heterokonts (Ochrophyta), molluscs (Gastropoda), and Ellobiopsidae. *Karenia brevis* was only observed in samples from May 27th and June 22nd, 2021, slightly preceding but consistent with other reports (Beck et al. 2022).

The Piney Point source water was dominated by Hypotrichia, a group of ciliated protozoa, with additional large contributions from the order Chlorophyta (green algae) and Peniculia (ciliates). These taxa were not observed within the Tampa Bay water samples, despite the input of a significant amount of source water into the Bay. Shore-based samples collected on April 9, 2021 and April 13, 2021 in visibly discolored water near the Piney Point discharge site were dominated by sequences most similar to *Kryptoperidinium foliaceum*, a binucleate dinoflagellate belonging to the Peridinales (Figuerola et al. 2009). However, this taxon was not widely observed in Tampa Bay.

16S rRNA gene composition (Figure Breitbart-2): The major contributors to the bacterial communities based on 16S rRNA gene sequences were Cyanobiaceae, Rhodobacteraceae, Flavobacteriaceae, Actinomarinaceae, Halieaceae, and SAR86. The community composition patterns at each site over time remained fairly stable at the family level,

although a notable exception was the increased contribution of Vibrionaceae in some sites on June 22, 2021 compared with earlier in the time series.

Overall trends: With the exceptions of the shore and the source water, the Tampa Bay microbial community ASVs grouped together and displayed shifts over time (**Figures Breitbart-3 and 4**). The 18S rDNA eukaryotic community composition at the Family level was more variable over the sampled sites and time-series than the bacterial community, which was quite stable at the Family level (**Figures Breitbart-1 and 2**). Since we do not have data from prior to the Piney Point discharge, or from these sites collected in another year, we are limited in our ability to identify changes driven by this discharge.

References:

- Barnett, D. J., I. C. Arts and J. Penders (2021). "microViz: an R package for microbiome data visualization and statistics." *Journal of Open Source Software* **6**(63): 3201.
- Beck, M. W., A. Altieri, C. Angelini, M. C. Burke, J. Chen, D. W. Chin, J. Gardiner, C. Hu, K. A. Hubbard and Y. Liu (2022). "Initial estuarine response to inorganic nutrient inputs from a legacy mining facility adjacent to Tampa Bay, Florida." *Marine Pollution Bulletin* **178**: 113598.
- Bolger, A. M., M. Lohse and B. Usadel (2014). "Trimmomatic: a flexible trimmer for Illumina sequence data." *Bioinformatics* **30**(15): 2114-2120.
- Callahan, B. J., P. J. McMurdie, M. J. Rosen, A. W. Han, A. J. A. Johnson and S. P. Holmes (2016). "DADA2: High-resolution sample inference from Illumina amplicon data." *Nature methods* **13**(7): 581-583.
- Djurhuus, A., C. J. Closek, R. P. Kelly, K. J. Pitz, R. P. Michisaki, H. A. Starks, K. R. Walz, E. A. Andruszkiewicz, E. Olesin and K. Hubbard (2020). "Environmental DNA reveals seasonal shifts and potential interactions in a marine community." *Nature Communications* **11**(1): 1-9.
- Djurhuus, A., J. Port, C. J. Closek, K. M. Yamahara, O. Romero-Maraccini, K. R. Walz, D. B. Goldsmith, R. Michisaki, M. Breitbart and A. B. Boehm (2017). "Evaluation of filtration and DNA extraction methods for environmental DNA biodiversity assessments across multiple trophic levels." *Frontiers in Marine Science* **4**: 314.
- Figueroa, R. I., I. Bravo, S. Fraga, E. Garcés and G. Llaveria (2009). "The life history and cell cycle of *Kryptoperidinium foliaceum*, a dinoflagellate with two eukaryotic nuclei." *Protist* **160**(2): 285-300.
- McMurdie, P. J. and S. Holmes (2013). "phyloseq: an R package for reproducible interactive analysis and graphics of microbiome census data." *PLoS One* **8**(4): e61217.
- Oksanen, J., F. G. Blanchet, R. Kindt, P. Legendre, P. R. Minchin, R. O'hara, G. L. Simpson, P. Solymos, M. H. H. Stevens and H. Wagner (2013). "Package 'vegan'." *Community ecology package, version 2*(9): 1-295.
- Paulson, J. N., M. Pop and H. C. Bravo (2013). "metagenomeSeq: Statistical analysis for sparse high-throughput sequencing." *Bioconductor package* **1**(0): 191.
- Quast, C., E. Pruesse, P. Yilmaz, J. Gerken, T. Schweer, P. Yarza, J. Peplies and F. O. Glöckner (2012). "The SILVA ribosomal RNA gene database project: improved data processing and web-based tools." *Nucleic Acids Research* **41**(D1): D590-D596.
- R Core Team (2013). *R: a language and environment for statistical computing*. Vienna, Austria, R Foundation.

Wickham, H. and M. H. Wickham (2007). "The ggplot package." URL: <https://cran.r-project.org/web/packages/ggplot2/index.html>.

Figure Breitbart-1: 18S rRNA Gene Composition

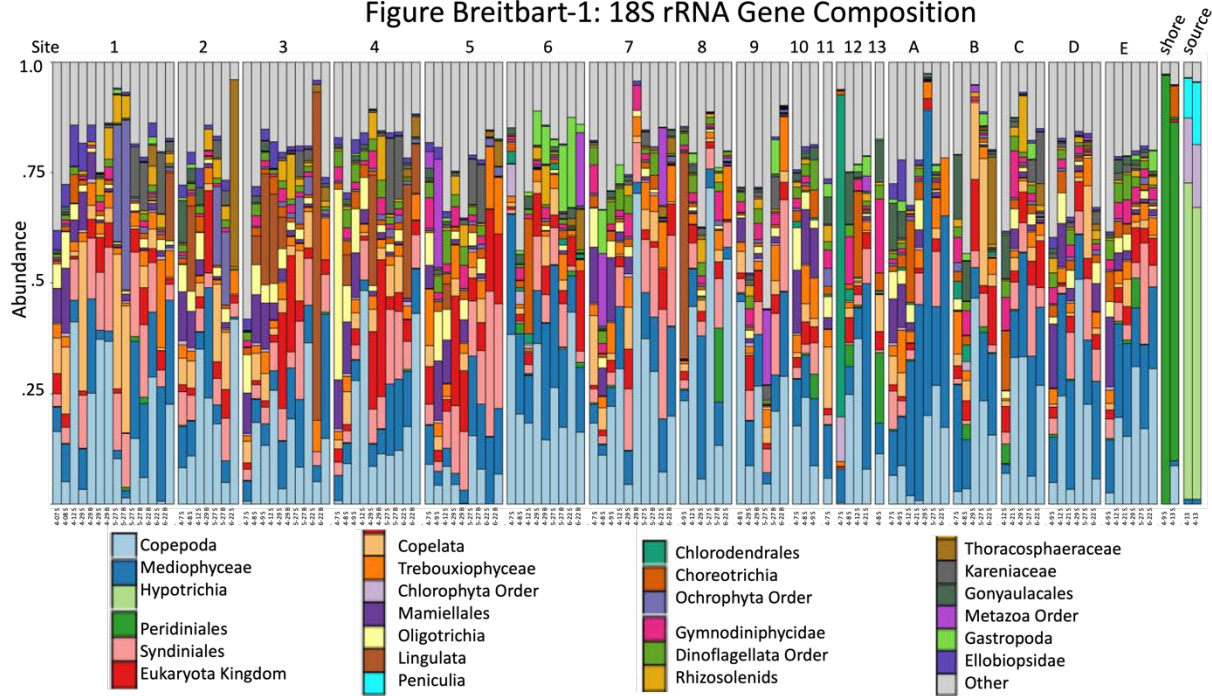


Figure Breitbart-2: 16S rRNA Gene Composition

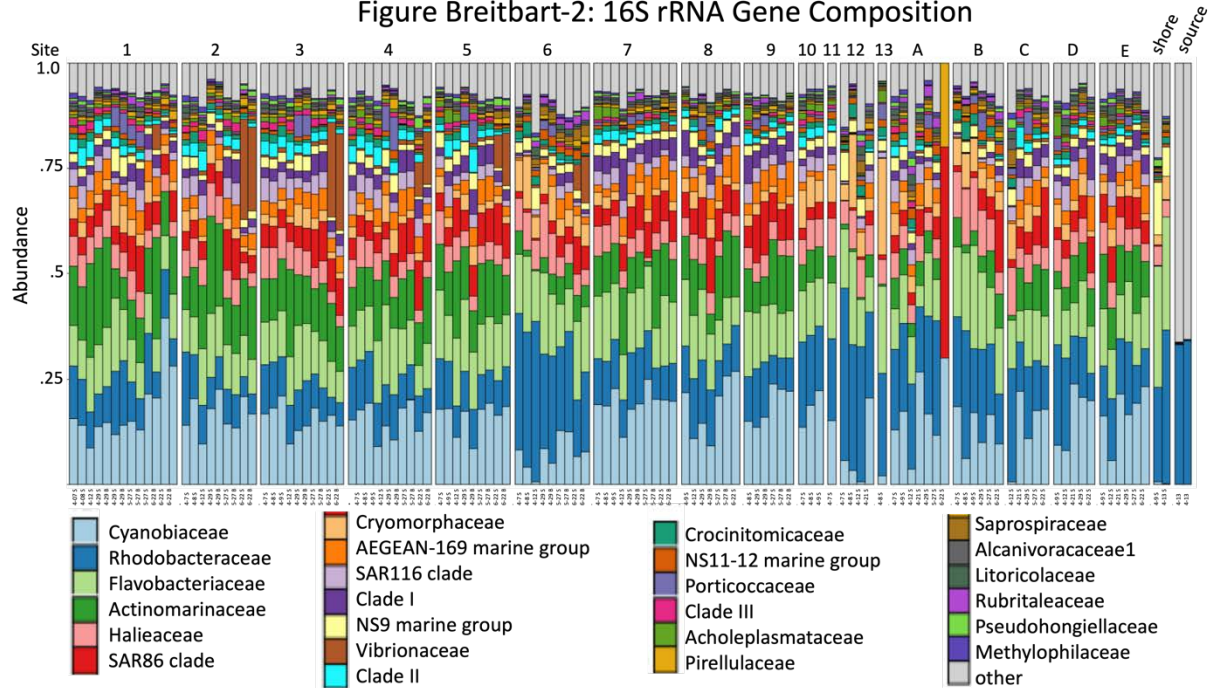


Figure
Breitbart-3:
18S rRNA
Gene NMDS

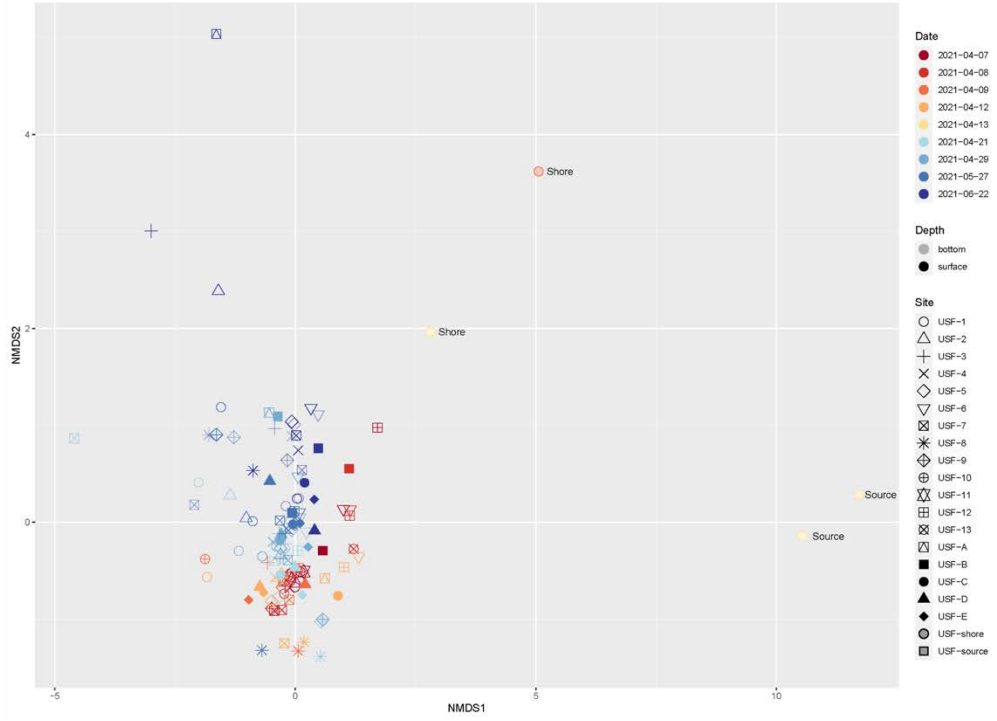
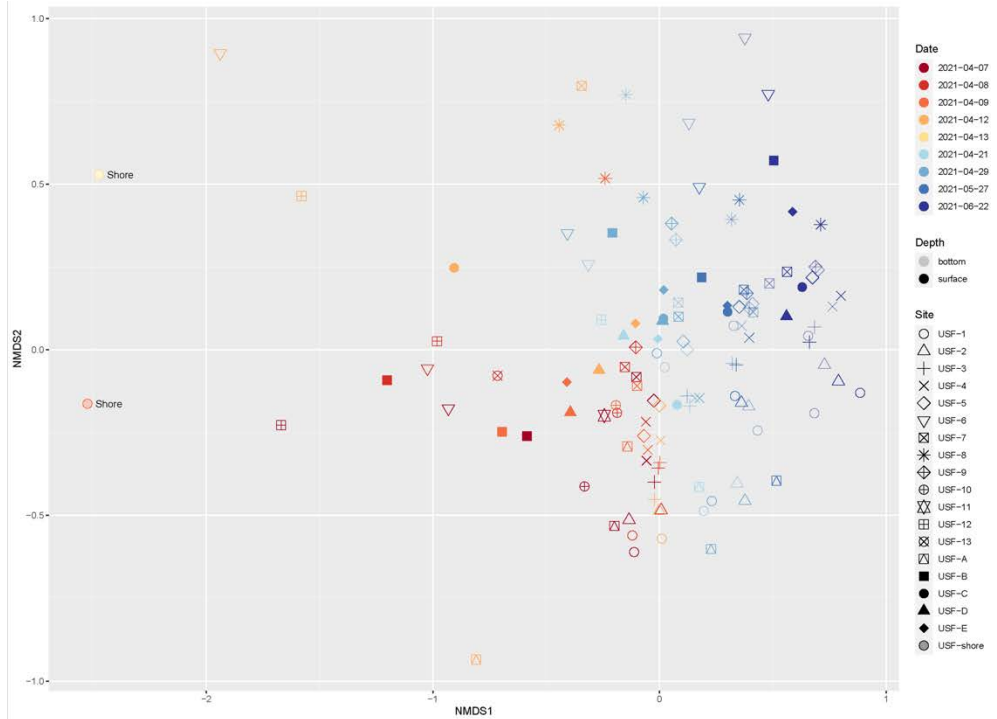


Figure
Breitbart-4:
16S rRNA
Gene NMDS



III. Robert Byrne, Sherwood Liu, Juan Millan-Otoya

Inorganic carbon system (pH, DIC, TA)	Water
Total budget: \$4,380	

Activities during this period:

The CO₂ chemistry lab of USF responded to the Piney point leak by analyzing water column CO₂ samples collected from April 7 to June 22. In the early part of the response, pH samples were collected directly in 10 cm cylindrical cells and analyzed right after they were brought back to the lab. A_T and C_T samples were collected in 500 ml of borosilicate glass bottles. 200 μl of saturated HgCl₂ solution were added to sample to stabilize the solution. The bottles were capped with greased stoppers. For the latter sampling when no pH samples were collected, pH were measured first from A_T sample bottles.

Table Byrne-1 summarized the sampling effort of the CO₂ parameters.

Measurement procedures

pH

pH sample cells were first rinsed and dried with Kimwipes, and put in thermostated cell warmer which was kept at 25°C. pH were measured using Agilent 8453 spectrophotometer with custom 10 cm thermostated cell holder. After reference was taken, 10 μl of 10 mM purified mCP dye were added using Gilmont pipette, then absorbances at 434, 578 and 730 were taken. Then second 10 μl mCP dye were added and absorbances were taken. The unperturbed R0 ratio ($R = A_{578}/A_{434}$) was calculated using

$$R_0 = 2R_1 - R_2 \quad (1)$$

The pH was calculated using the purified mCP quantification (Liu et al 2011). The measurement precision was about 0.001 pH.

C_T

CT was measured using automated multisample C_T instrument with Picarro CRD as detector. Sample bottles were thermostated in a 20°C waterbath. For stations that pH samples were not collected separately, pH samples were collected first by gravity from bottles using PEEK tubing with fitted cap just before C_T analysis. After initial discharge of previous sample in the PEEK tubing, 3 volumes samples were allowed to fill up the cylindrical cell. For C_T analysis, sample was drawn into a fixed volume glass bulb with peristaltic pump, then acid was added, the acidified samples were delivered to a purging chamber by N₂ carrier gas. The evolved CO₂ was carried to Picarro instrument for detection. Picarro instrument with integration addon established baseline with N₂ carrier gas. When CO₂ signal was detected over the baseline level, it would trigger the integration software, until all CO₂ were purged and CO₂ signal returned to the baseline level, the peak area of the CO₂ signal was integrated.

The DIC of the sample was calculated as

$$DIC = \text{Count}(s)/\text{Count}(crm)/(d(s)/d(crm))*DIC(CRM) \quad (2)$$

Where Count are the integration of the signal, d(s) and d(crm) are the density of sample and CRM. DIC(crm) is the certified value of the CRM.

A_T

A_T was analyzed using the spectrophotometric titration system (Liu et al., 2015). Left over samples from C_T analysis were weighed into another clean 300 ml BOD bottle. The sample bottle was inserted into the sample holder. After reference was taken, 0.1 ml of 10 mM BCP dye was added, the sample was titrated to R (A589/A432) of 0.067, then sample was purged using CO_2 free air to constant R ratio. The A_T was calculated by

$$A_T = (C_{HCl} * V_{HCl} - [H^+] * (M_a + M_{sw})) / M_{sw} \quad (3)$$

where C_{HCl} is the concentration of HCl, V_{HCl} is Dosimat volume, H^+ is proton concentration at end of the titration. M_a is the weight of the acid and M_{sw} is weight of the sample. The C_{HCl} is calibrated using CRM obtained from Dr. Andrew Dickson's lab.

Deliverables produced:

Totally 128 pH samples and 110 A_T and C_T samples were collected. On April 29, only pH samples were collected.

Table Byrne-1. Samples analyzed by CO_2 group during Piney Point project

Date	pH	A_T	C_T
7-Apr	11	11	11
8-Apr	16	16	16
9-Apr	17	18	18
12-Apr	18	18	18
21-Apr	5	5	5
29-Apr	19	0	0
27-May	20	20	20
22-Jun	22	22	22
Total	128	110	110

The data are summarized in Excel file, 2022 Piney Point Results_Byrne_inorganic carbon system.xlsx.

Discussion of findings:

Salinity distribution

Salinities at sampling sites were measured using a YSI sensor at early part of the sampling efforts (until April 13). After April 13, no salinities were sampled.

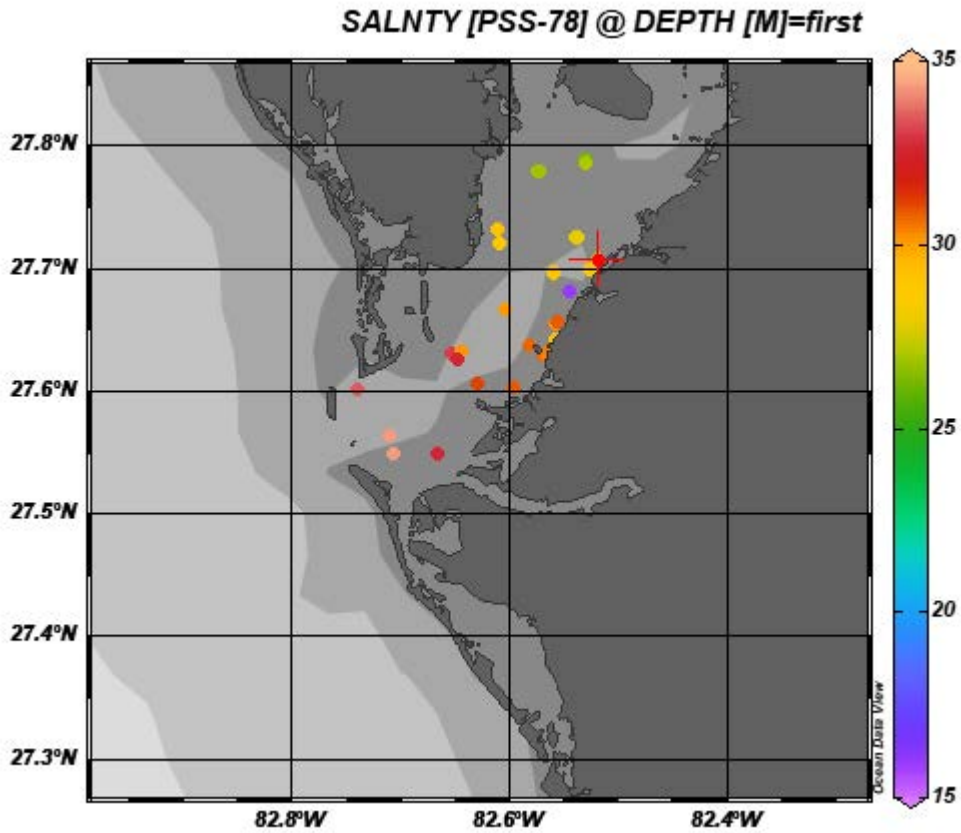


Figure Byrne-1. Salinity collected from April 7 to April 12.

The Piney point storage pond has a salinity around 10. The upper Tampa Bay salinity was around 26. At Sunshine Skyway, the salinity was about 35. Other than a few readings of salinity 15 which were marked as not reliable, the salinity increased from upper Tampa Bay to sunshine sky way.

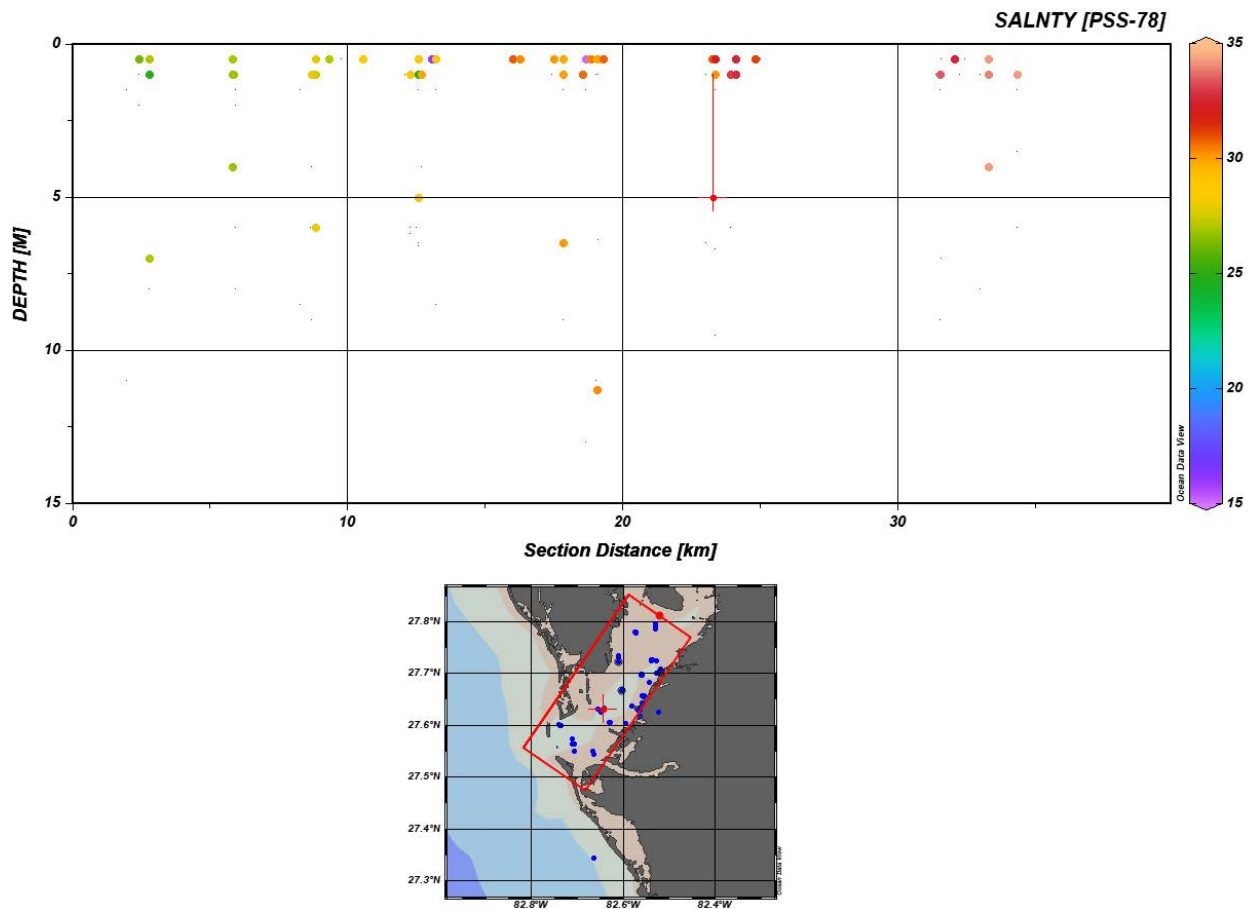


Figure Byrne-2. Cross view of salinity changes across Tampa Bay starting from upper Tampa Bay (0 section distance).

Since there were no salinity measurements in the later part of the cruise, salinities (from April 12) were estimated from the previous sample locations based on the proximity of sample locations. Such estimates may affect the quality of A_T and C_T data around $5 \mu\text{M}/\text{kg}$. **Table Byrne-2** summarizes the assigned salinity for selected samples when no salinities were available. As salinities were measured before the leak was stopped, it is possible that some of the estimates were lower than the actual salinities after the leak was stopped.

Table Byrne-2. Salinity assignment for samples missing salinity values.

Sample	Lat	Long	Reference Station	assigned S
USF-1	27.7783	-82.5733	33	26.8
USF-2	27.795	-82.5295	34	26.97
USF-3	27.725	-82.5283	35	27.8
USF-4	27.697	-82.5595	36	29.08
USF-5	27.6667	-82.6033	37	29.81
USF-6	27.6333	-82.5633	20	30.63
USF-7	27.6317	-82.645	30	30.12

USF-8	27.5499	-82.7073	31	34.23
USF-9	27.6008	-82.7402	22	33.42
USF-10	27.7213	-82.61	23	28.62
USF-A	27.69958	-82.52676	4	28.4
USF-B	27.65652	-82.5599	6	30.2
USF-C	27.63714	-82.58157	H	30.73
USF-D	27.60455	-82.62989	I	31.1
USF-E	27.5447	-82.66511	J	32.52

pH

The range of the pH measured from April to June is 7.71 to 8.51. The single high value of 8.51 from a shore collected sample was unexpected, the sample also has unusual high A_T of 2776. The low pH of 7.7 was not collected at Piney Point leak area but up north in Apollo beach area. The north Tampa Bay area has pH around 7.9, and outside the Tampa Bay the pH is generally higher, around 8.05.

Table Byrne-3 summarized the observation of Tampa Bay water close to Piney Point. pH change observed at this location almost reflect the range of the pH across the Tampa Bay water. The slightly lower pH of 7.98 may be the result of Piney point pond input. But the difference is so small, it is hard to give definitive answer. Similar pH was observed on April 29, after the pumping effort stopped. One possible reason for the scattering of the data may be the highly diurnal change of pH value once the wastewater discharged into Tampa Bay. Increased load of nutrients could further increase the dynamic range of the pH signal, which may not reflect the pH of the Piney point reservoir.

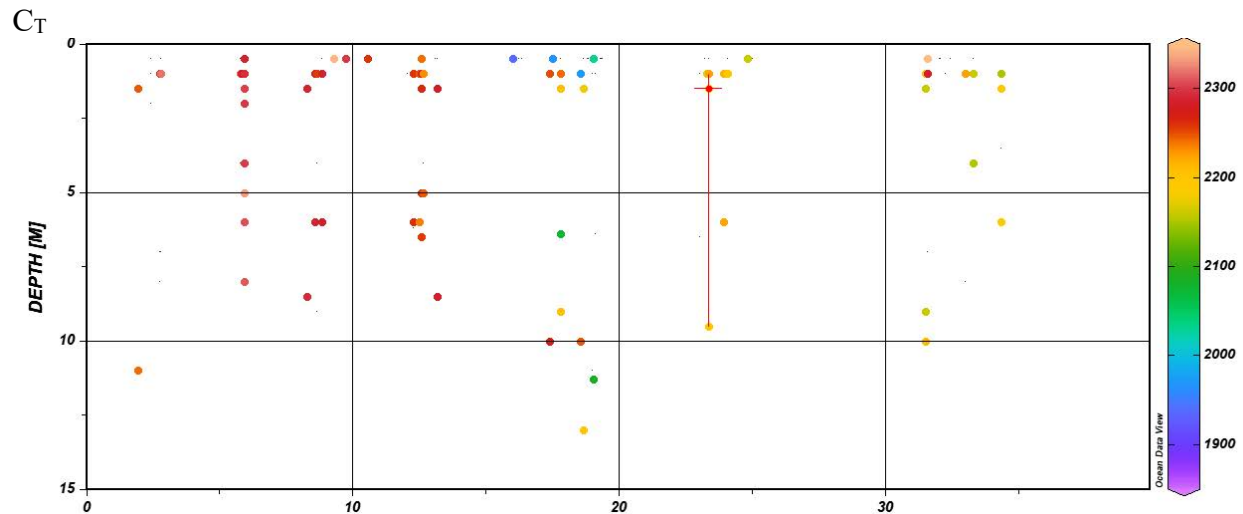
Table Byrne-3. CO₂ parameters at Piney Point from April 7 to June 22, 2022.

Date	sample ID	Type	Sample Depth	Latitude	Longitude	S	pH	AT	CT
4/7/2021	10	Bucket	0.5	27.6283	-82.5633	29.8	7.967	2364.1	1869.1
4/8/2021	20	Towfish	1	27.634	-82.5628	30.63	8.128	2394.3	1971.3
4/9/2021	30	Towfish	1	27.6317	-82.645	30.12	7.978	2479.0	2221.8
4/9/2021	29	CTD	1	27.6283	-82.5633		8.05	2495.3	2223.0
4/12/2021	38	Bucket	0.5	27.6295	-82.5642	29.74	8.149	2380.2	2030.5
4/29/2021	USF-6	CTD	1	27.6301	-82.5643		7.986		
5/27/2021	USF-7	CTD	1	27.6170 3	-82.5639		8.042	2489.6	2240.5
6/22/2021	USF-6	CTD	1.5	27.6333	-82.5633		8.146	2449.7	2177.0

A_T

Relative to pH, A_T is more subjected to the influence by freshwater input. **Table Byrne-3** showed that A_T was lowered by 100 $\mu\text{M}/\text{kg}$. It is complicated by the fact that the upstream of Tampa Bay water received Hillsborough River input which has high A_T content. The A_T was

generally higher than 2450 $\mu\text{M}/\text{kg}$. The A_T outside Sunshine skyway was about 2450 $\mu\text{M}/\text{kg}$, while the salinity changed from 29 to 34 in the short distance.



C_T at Piney point ranged 1850 to 2240 $\mu\text{M}/\text{kg}$, with lower value observed at early sampling effort when wastewater pumping was underway. From the section view of Tampa Bay water, the CO_2 content in freshwater is generally higher than the open ocean. Seawater outside Sunshine skyway has C_T around 2150, while in upper Tampa Bay, 2300 $\mu\text{M}/\text{kg}$ were observed.

In summary, when active pumping of Piney Point wastewater was underway, the fresh water with pH 5 and very low C_T content mixed with seawater, dropped C_T and A_T around 100 to 200 $\mu\text{M}/\text{kg}$. The high A_T and C_T water from upper Tampa Bay buffered the impact of the acidified water to the Tampa Bay water.

References

Xuewu Liu, Mark C. Patsavas, and Robert H. Byrne, 2011, Purification and Characterization of meta-Cresol Purple for Spectrophotometric Seawater pH Measurements, *Environ. Sci. Technol.* 45, 4862–4868.

Xuewu Liu, Robert H. Byrne, Michael Lindemuth, Regina Easley, Jeremy T. Mathis, 2015, An automated procedure for laboratory and shipboard spectrophotometric measurements of seawater alkalinity: Continuously monitored single-step acid additions, *Marine Chemistry*, 174, 141-146, <https://doi.org/10.1016/j.marchem.2015.06.008>.

IV. Tim M. Conway, Hannah R. Hunt, Shannon M. Burns, and Matthias Sieber

Trace metal isotopes ($\delta^{56}\text{Fe}$, $\delta^{66}\text{Zn}$, $\delta^{114}\text{Cd}$)	Water
Total budget: \$13,472	

Activities during this period: The USF MARine Metal Isotope & Trace Element laboratory at the College of Marine Science (<https://tconway.co.uk/>) received a total of 24 filtered (0.4 μm) water samples from lead PI Kristen Buck from the Piney Point Response Cruises during 4/8/21-4/12/21 (these included 2 NGS-S pondwater samples, 18 surface bay seawater samples, 4 mixing experiment samples). Dissolved Fe, Zn and Cd concentrations and isotopic measurements were made in these samples using multi-collector ICPMS (following established methods in Conway *et al.*, 2013). Data quality was high for all samples, with external precision of 0.05‰ on $\delta^{56}\text{Fe}$, 0.03‰ on $\delta^{66}\text{Zn}$, 0.06‰ on $\delta^{114}\text{Zn}$ and 2% on concentrations. This is based on routine analysis of isotope standards (Conway *et al.*, 2013; Sieber *et al.*, 2021). Data were examined to investigate the impact of the Piney Point release on bay metal distributions; specifically, the dissolved isotopic composition of the metals (expressed as $\delta^{56}\text{Fe}$, $\delta^{66}\text{Zn}$ and $\delta^{114}\text{Cd}$) was used to fingerprint the Piney Point source vs other sources of these metals (e.g., local sediments, Gulf of Mexico Seawater).

Deliverables produced: All samples were analyzed for dissolved Fe, Zn, Cd, $\delta^{56}\text{Fe}$, $\delta^{66}\text{Zn}$ and $\delta^{114}\text{Cd}$.

- Dissolved Fe, Zn and Cd concentrations (24 of each, 72 in total)
- Dissolved $\delta^{56}\text{Fe}$, $\delta^{66}\text{Zn}$ and $\delta^{114}\text{Cd}$ (24 of each, 72 in total).

Discussion of findings: Tampa Bay data are presented in Figs 1-3, plotted using Ocean Data View. Discussion of results are described here subdivided by element.

Fe. The Piney Point (PP) NGS-S Pond endmember for Fe was distinctly isotopically light with some variability in two pond samples ($\delta^{56}\text{Fe}$ of $-0.74 \pm 0.05\%$ and $-1.15 \pm 0.05\%$), with extremely elevated Fe concentrations (0.5-0.9 $\mu\text{mol kg}^{-1}$), compared to coastal Gulf of Mexico waters (~5-10 nmol kg^{-1} ; Mellett and Buck, 2020). There is a clear indication of PP-derived Fe in the proximal sample (USF6; labelled in **Fig. Conway-1**), where $\delta^{56}\text{Fe}$ was $-0.84 \pm 0.05\%$ and Fe was 34 nmol kg^{-1} . Beyond this sample, no clear influence of PP is seen in the surface distribution $\delta^{56}\text{Fe}$ of the bay, with samples ranging from 0 to -0.7% , consistent with an isotope signature of Fe generally released from local sources such as Fe(III) reduction and/or marine sediments (-3 to 0‰; Severmann *et al.*, 2006). The bay also shows elevated Fe away from PP (e.g., near Saint Petersburg; 24 nmol kg^{-1} , -0.5%), suggesting that the distal $\delta^{56}\text{Fe}$ signature of PP release is not distinguishable from other local sources to the bay during the sampling interval (4/8-4/12).

Zn. The PP NGS-S Pond dissolved $\delta^{66}\text{Zn}$ endmember was $+0.22 \pm 0.01\%$ (SD, n=2) with ~70 nmol kg^{-1} Zn, which is resolvable from the mean Zn isotopic signature of Tampa Bay waters ($+0.40 \pm 0.06\%$; 1SD, n=19), meaning that any significant Zn addition to the Bay from Piney Point should be visible. As for Fe, the dissolved $\delta^{66}\text{Zn}$ in the canal near PP (USF-6) was equivalent to the Pond ($+0.22 \pm 0.03\%$), suggesting PP derived Zn did make it this far. However, the rest of the bay $\delta^{66}\text{Zn}$ range from $+0.34$ to $+0.45\%$, which is consistent with Zn being sourced largely from Gulf seawater. This finding is consistent with dissolved Zn, which varied from 1.5-9.5 nmol kg^{-1} , with more Zn in Upper Tampa Bay, and less Zn near the mouth and in the region expected to be influenced by PP. Dissolved Zn concentrations from the mouth of the bay (~1-2 nmol kg^{-1}) are

consistent with previous coastal values ($\sim 1 \text{ nmol kg}^{-1}$) for the region (Mellett and Buck, 2020), and $\delta^{66}\text{Zn}$ are consistent with coastal samples (+0.3 to +0.4‰; Conway and John, 2014; 2015). Overall, this suggests no clear Zn addition to Tampa Bay from PP during the sampling interval (4/8-4/12).

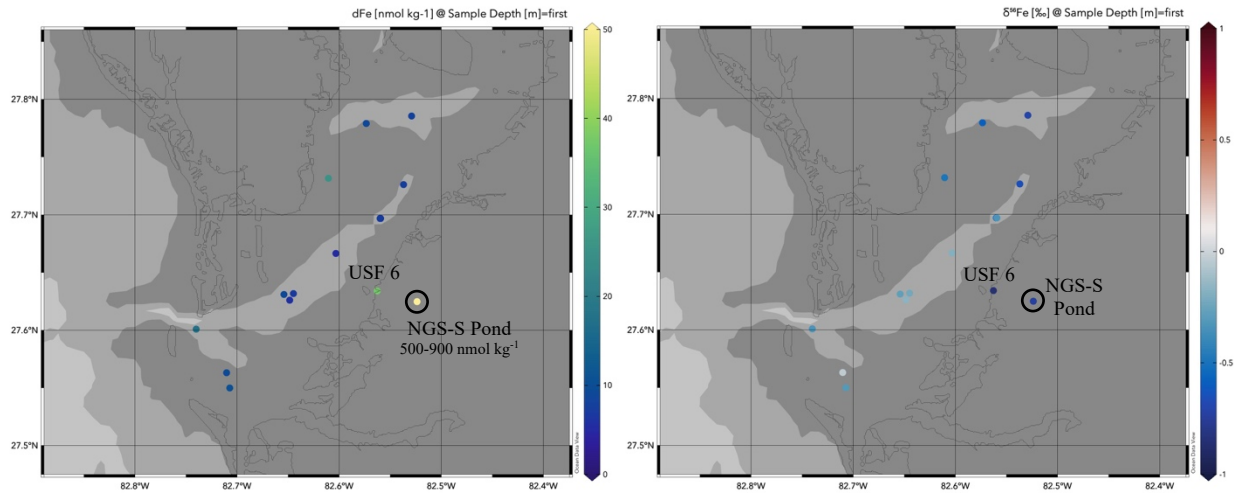


Figure Conway-1. Dissolved Fe concentrations and Fe isotopic composition ($\delta^{56}\text{Fe}$) in Piney Point Pond water (NGS-S Pond) and in Tampa Bay Surface waters (4/8-4/12/21). Isotopic scale is set so that white is equivalent to crustal composition. There is little variability at locations between sampling days, so averages are shown for repeat sampling.

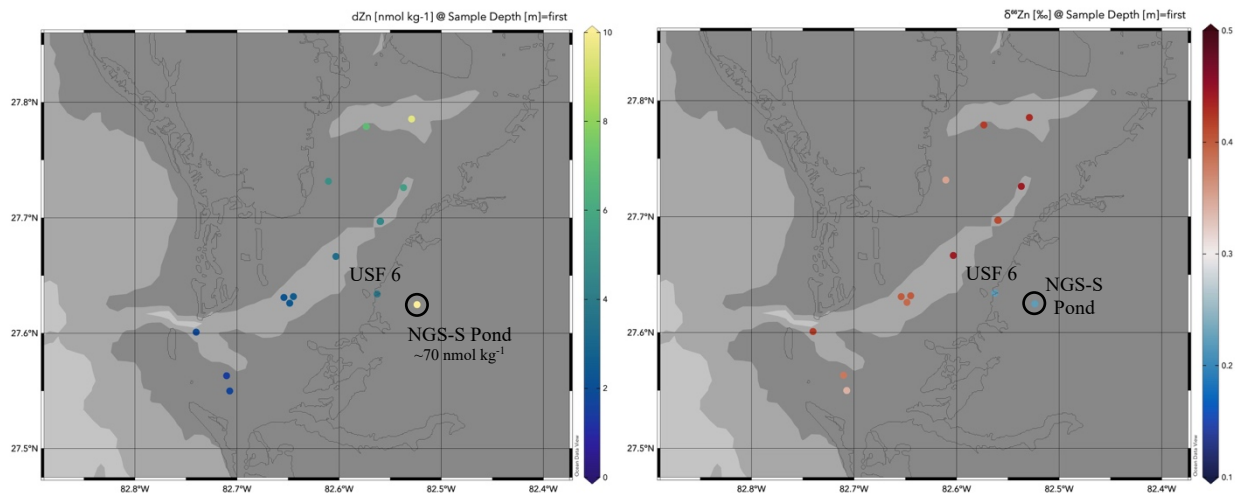


Figure Conway-2. Dissolved Zn concentrations and Zn isotopic composition ($\delta^{66}\text{Zn}$) in Piney Point Pond water (NGS-S Pond) and in Tampa Bay Surface waters (4/8-4/12/21). Isotopic scale is set so that white is equivalent to crustal composition. There is little variability at locations between sampling days, so averages are shown for repeat sampling.

Cd. The Piney Point NGS-S Pond dissolved $\delta^{114}\text{Cd}$ endmember was $+0.32 \pm 0.02\text{‰}$ (SD, $n=2$), indistinguishable from the average surface Cd isotopic composition of Tampa Bay ($+0.34 \pm 0.02\text{‰}$; SD, $n=19$), and global ocean seawater composition (+0.2 to +0.4‰; Horner *et al.*, 2021). As such, $\delta^{114}\text{Cd}$ cannot be used to distinguish Cd release by PP to the bay, consistent with pond waters being only slightly elevated in Cd (1 nmol kg^{-1} vs $0.1\text{-}0.3 \text{ nmol kg}^{-1}$). The loosely-inverse relationship between dissolved Cd and $\delta^{114}\text{Cd}$ in Bay waters (**Fig. Conway-3**) is also consistent with biological uptake of Cd dominating Cd isotopic systematics.

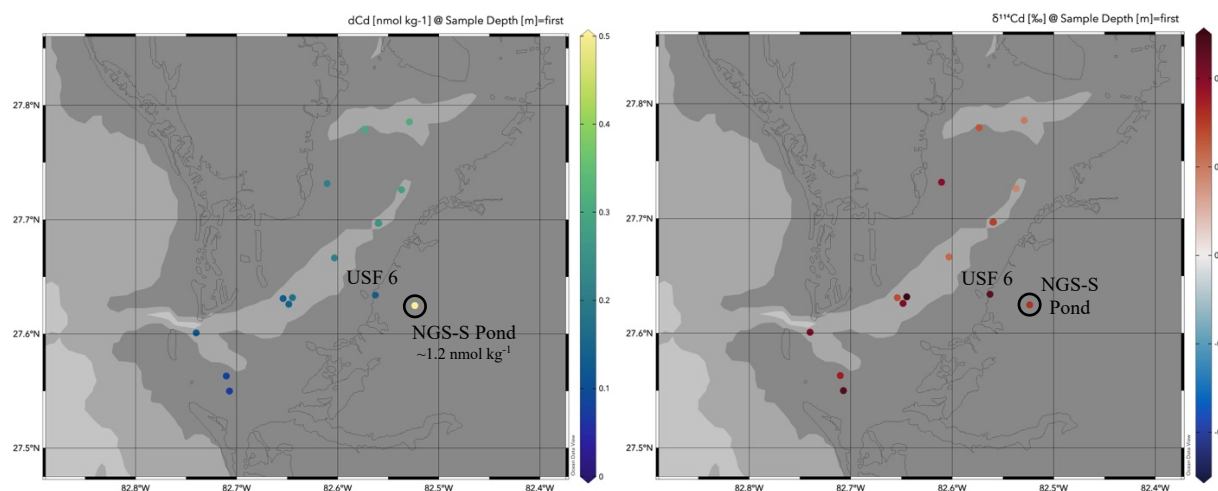


Figure Conway-3. Dissolved Cd concentrations and Cd isotopic composition ($\delta^{114}\text{Cd}$) in Piney Point Pond Water (NGS-S Pond) and in Tampa Bay Surface waters (4/8-4/12/21). Isotopic scale is set so that white is equivalent to crustal composition. There is little variability at locations between sampling days, so averages are shown for repeat sampling.

Pond and Gulf of Mexico Seawater Mixing Experiments. Results of mixing experiments carried out between Gulf of Mexico Seawater are shown in **Table Conway-1** and **Figure Conway-4**. These results provide insight into how the mixing of Piney Point NGS-S pond water with Tampa Bay seawater should affect $\delta^{56}\text{Fe}$, $\delta^{66}\text{Zn}$ and $\delta^{114}\text{Cd}$ signatures, as well as the chemical processes which may be occurring. For Cd (which behaved conservatively during the mixing experiments) and Zn (which was lost from solution during mixing experiments), the measured isotopic compositions of the mixture are equivalent to the calculated compositions, showing no fractionation of isotopic composition during mixing or during any loss of either metal from solution. **This means that $\delta^{66}\text{Zn}$ and $\delta^{114}\text{Cd}$ can be used as conservative source tracers for PP water into the bay/ocean.** However, Fe behaved conservatively in the low salinity (~ 14) mixture, but Fe was lost from solution at mixtures with target salinity of 20 and 28. This is consistent with expectations of rapid Fe loss as pH 4.7 (likely reducing) PP water mixes with oxic, high pH (7.93), high salinity seawater. Accompanied with this Fe loss from solution is an isotope fractionation, leaving the remnant dissolved Fe isotopically heavier (see isotope fractionation vs expected mixing line in **Fig. Conway-4**). At a loss of about 50%, the remnant dissolved Fe is $\sim 1\%$ lighter than expected (**Fig. Conway-4; Table Conway-1**). The direction of this fractionation factor is consistent with Fe(II)-Fe(III) equilibrium fractionation (Welch *et al.*, 2003; Severmann *et al.*, 2006), suggesting that oxidation of Fe^{2+} to Fe^{3+} followed by precipitation of Fe(III) is occurring during mixing events. This finding would suggest that any PP-derived Fe that makes it into the bay is likely to be significantly isotopically lighter ($< -2\%$) than the NGS-S Pond endmember; **this finding, together with data from the bay samples (Fig. Conway-1), suggests that it is even less likely that much of the Fe measured is sourced from PP during the locations and times sampled for $\delta^{56}\text{Fe}$ analysis during the cruises.**

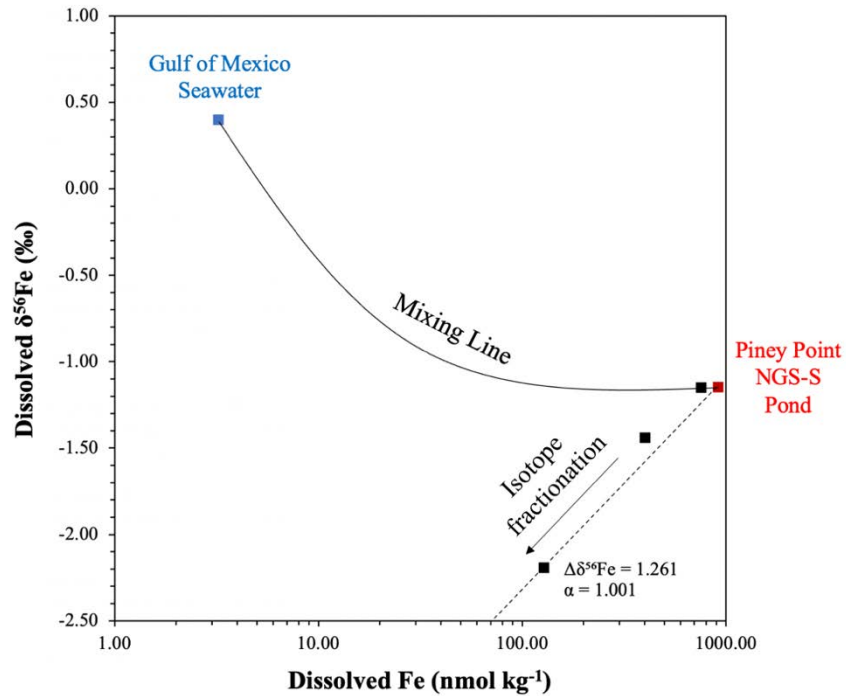


Figure Conway-4. Fe isotope systematics of Piney Point Mixing Experiments. Black curve shows predicted conservative mixing line between Piney Point NGS-S Pond water and Gulf of Mexico seawater, with deviations from this line indicating Fe isotopic fractionation. The dashed line indicates isotopic fractionation that is inferred from mixing experiments, attributed to the effects of fractionation during Fe(II)-Fe(III) exchange. Red square denotes the composition of an aliquot of NGS-S Pond water, and the blue square denotes the composition of Gulf of Mexico seawater, both used for mixing experiments on 5/25/21. Samples were acidified and filtered following mixing experiments. Black squares indicate the measured Fe and $\delta^{56}\text{Fe}$ of the mixtures (see **Table Conway-1** for more details).

Target Salinity	Approx. Mixing Ratio (sw:pond)	% Fe in Mixture (exp.-cal.)	Measured $\delta^{56}\text{Fe}$ (‰)	Calculated $\delta^{56}\text{Fe}$ (‰)
28	1:0.2	50%	-2.19 ± 0.05	-1.13 ± 0.07
20	1:1.5	74%	-1.44 ± 0.05	-1.15 ± 0.07
14	1:4.0	102%	-1.15 ± 0.05	-1.15 ± 0.07

Target Salinity	Approx. Mixing Ratio (sw:pond)	% Zn in Mixture (exp.-cal.)	Measured $\delta^{66}\text{Zn}$ (‰)	Calculated $\delta^{66}\text{Zn}$ (‰)
28	1:0.2	72%	+0.16 ± 0.05	+0.17 ± 0.04
20	1:1.5	95%	+0.14 ± 0.03	+0.19 ± 0.04
14	1:4.0	76%	+0.17 ± 0.03	+0.21 ± 0.04

Target Salinity	Approx. Mixing Ratio (sw:pond)	% Cd in Mixture (exp.-cal.)	Measured $\delta^{114}\text{Cd}$ (‰)	Calculated $\delta^{114}\text{Cd}$ (‰)
28	1:0.2	97%	+0.40 ± 0.13	+0.32 ± 0.15
20	1:1.5	96%	+0.17 ± 0.16	+0.33 ± 0.15
14	1:4.0	117%	+0.41 ± 0.11	+0.34 ± 0.15

Table Conway-1. Results of Mixing Experiments between open Gulf of Mexico Seawater (sw) and Piney Point NGS-S Pond water (pond). Approx. Mixing ratios are calculated from volume of seawater and pond water combined. %metal is based on measured concentration subtracted from predicted concentration assuming conservative mixing of endmembers. Calculated isotopic compositions are similarly based on conservative mixing of endmembers, with propagated error. Isotopic compositions shown in red deviate from expected conservative mixing.

References:

- Conway, T. M., Rosenberg, A. D., Adkins, J. F., and John, S. G. (2013). A new method for precise determination of iron, zinc and cadmium stable isotope ratios in seawater by double-spike mass spectrometry. *Analytica Chimica Acta*, 793, 44-52.
- Conway, T. M. and John, S. G. (2014). The biogeochemical cycling of zinc and zinc isotopes in the North Atlantic Ocean. *Global Biogeochemical Cycles*, 28(10). 1111-1128
- Horner, T. J., Little, S. H., Conway, T. M., Farmer, J. R., Hertzberg, J. E., Janssen, D. J., Lough, A. J. M., Mckay, J., Tessin, A., Galer, S. J. G., Jaccard, S. L., Lacan, F., Paytan, A., Wuttig, K., and GEOTRACES–PAGES Biological Productivity Working Group Members. (2021). Bioactive trace metals and their isotopes as paleoproductivity proxies: An assessment using GEOTRACES-era data. *Global Biogeochemical Cycles*. 35, 11, e2020GB006814.
- Mellett, T., and Buck, K. N. (2020). Spatial and temporal variability of trace metals (Fe, Cu, Mn, Zn, Co, Ni, Cd, Pb), iron and copper speciation, and electroactive Fe-binding humic substances in surface waters of the eastern Gulf of Mexico. *Marine Chemistry*. 227, 103891.
- Severmann, S., Johnson, C. M., Beard, B. L., and McManus, J. (2006). The effect of early diagenesis on the Fe isotope compositions of porewaters and authigenic minerals in continental margin sediments. *Geochimica Cosmochimica Acta*. 70, 2006–2022.
- Sieber, M., Conway, T. M., de Souza, G. F., Hassler, C.S., Ellwood, M.J., and Vance, D. (2021). Isotopic fingerprinting of biogeochemical processes and iron sources in the iron-limited surface Southern Ocean. *Earth and Planetary Science Letters*. 567, 116967.
- Welch S. A. , Beard, B. L., Johnson C. M., Braterman P. S. (2003). Kinetic and equilibrium Fe isotopic fractionation between aqueous Fe(II) and Fe(III). *Geochimica Et Cosmochimica Acta*. 67, 4231-50

V. Pamela Hallock Muller, Ana Coye Hoare, Natalia Lopez-Figueroa, Avion Stevenson

Foraminiferal assemblages, grain size analysis

Sediments

Total budget: \$5,008

Activities during this period:

Sediment texture was determined for samples collected in Tampa Bay between April 9 and June 22, 2021. Standard sieve methods were used for one sample from each site for each date. Total foraminiferal assemblages were also analyzed by examination under a stereomicroscope. Foraminiferal specimens were picked from a dried sediment sample and placed on micropaleontological faunal slides. Portions of the sub-sample were picked until a sample size of at least 150 specimens was reached or the entire subsample was analyzed. Each specimen was identified to lowest taxonomic level possible.

Deliverables produced:

The sites from which samples were collected for these analyses are shown in Figure 1. The resulting data are summarized in Table 1. Additional data generated from these analyses are included in the accompanying Excel spreadsheet, 2022 Piney Point Results_Hallock-Muller_foraminifera.xlsx.

Discussion of findings:

Most samples were very poorly sorted with varying amounts of shell fragments and fine quartz sands. Samples from Site 6 were predominantly fine organic mud.

Three major groups of foraminiferal taxa commonly occur in Tampa Bay (Poag, 2015). Those groups are evaluated based on their shell construction: agglutinated, porcelaneous high-Mg calcite miliolids, and hyaline, typically low-Mg calcite rotaliids. In Tampa Bay and around the Gulf of Mexico region, agglutinated taxa are most common in low salinity environments. As most of the samples collected were from near-normal marine salinities, agglutinated taxa only exceeded 10% of the specimens identified from two samples (6% of samples analyzed). The most common rotaliid genus found in estuarine environments worldwide is *Ammonia*, which typically includes 1 or 2 species that thrive on fresh, extremely labile organic matter and can tolerate intermittent hypoxia (e.g., Carnahan et al., 2009; Yanko et al., 2017). The most common miliolid genus is *Quinqueloculina*, for which as many as 10 species can be found in Tampa Bay, though three species tend to be most common. As a consequence, the relative abundances of these key genera are useful bioindicators of eutrophication and associated stress in bay and shelf benthic environments.

Hallock Muller Table 1 presents the samples analyzed and the relative abundances of these major groups, color-coded to reflect different proportions of key groups. Typical bay assemblages are about one-third *Ammonia* and one third *Quinqueloculina*, with about 15–20 additional species making up the other third (see green areas in Table 1). In samples taken in the early days of the onset of discharge into Tampa Bay (April 9, 2021), data from Sites 3, 4 and 10 exhibited this type of assemblage, and that assemblage persisted at Site 3 through the June 22. In contrast, at Site 10 the assemblage changed dramatically to *Ammonia* dominated at 68%. Interestingly, at Site 1, which was not sampled on April 9, a similar change was recorded between the May 27 and June 22 samplings. At sites 5 and 7, miliolids dominated samples collected on all three sampling dates (yellow highlight), while at Site 8, *Ammonia* dominated

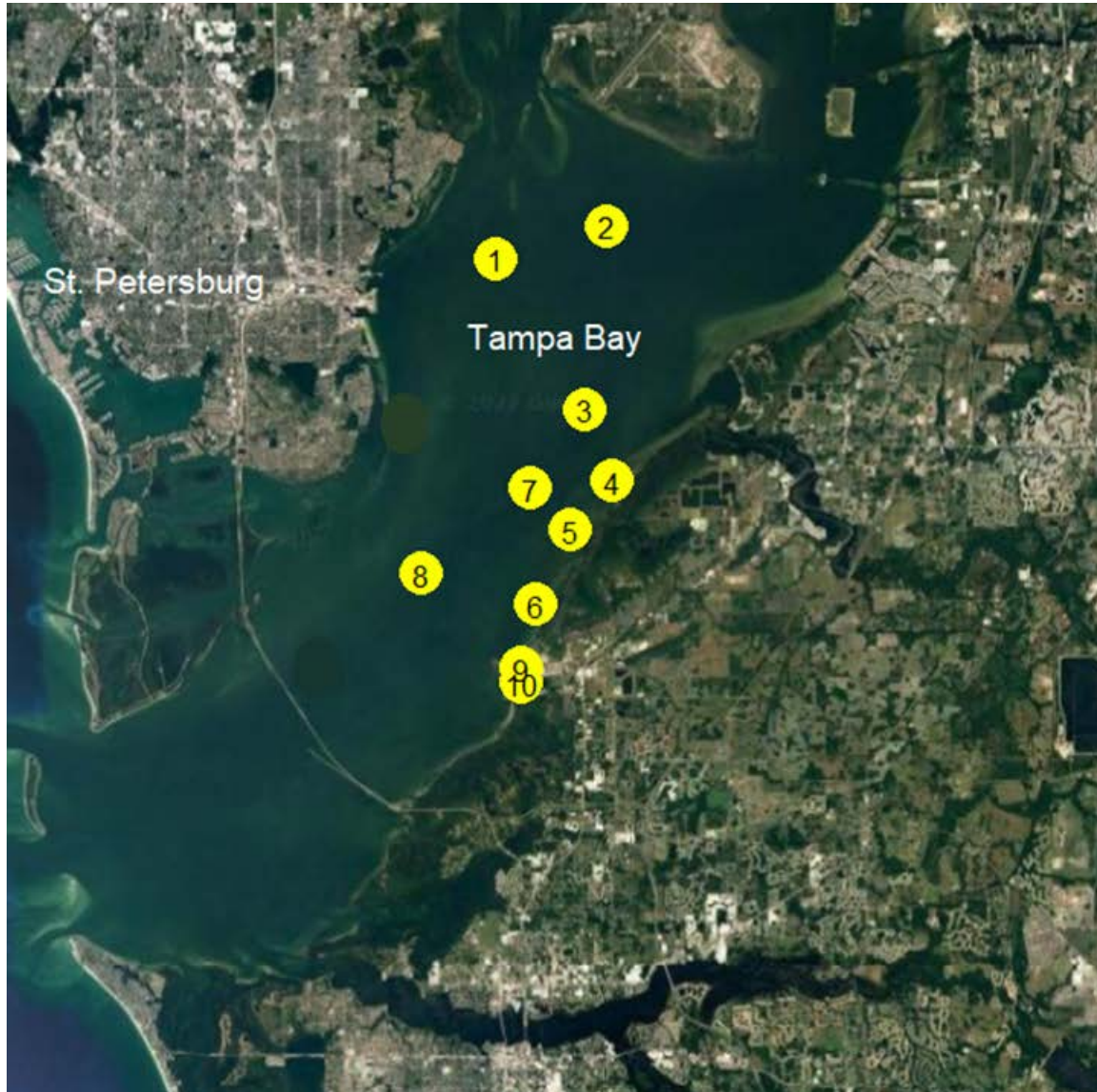
(blue highlight). Samples from Site 6 were mud dominated (orange highlight), other rotaliids were found more abundantly than either *Ammonia* or the miliolids.

An ancillary observation made during microscopic examination of the samples was the extreme abundances of centric diatom frustules. Additional analyses of the ostracod assemblages would also provide an interesting diversity of those microfossils.

In summary, the specific results of the analyses of sediment samples revealed some intriguing temporal differences at sites 1 and 10. However, the numbers of samples and the lack of samples from certain sites limited the conclusions that can be drawn from these analyses.

References cited:

- Carnahan, E.A., Hoare, A.M. , Hallock, P., Lidz, B.H. , Reich, C.D. 2009. Foraminiferal assemblages in Biscayne Bay, Florida, USA: Responses to urban and agricultural influence in a subtropical estuary. *Marine Pollution Bulletin* 59:221–233.
- Poag, C.W. 2013. *Benthic Foraminifera of the Gulf of Mexico Distribution, Ecology, Paleoecology*. Texas A&M University Press, 256 pp.
- Yanko, V., Kondariuk, T., Motnenko, I. 2017. Benthic foraminifera indicate environmental stress from river discharge to marine ecosystems: example from the Black Sea. *Journal Foraminiferal Research*, 47:70–92.



Hallock Muller- Figure 1. Tampa Bay, Florida, illustrating sampling sites. Note that sediment samples were not collected for foraminiferal assemblages from sites 11 and 12.

Hallock Muller Table 1. Data on foraminiferal assemblages from samples collected between April 9 and June 22, 2021 in Tampa Bay in response to the Piney Point discharge. Color coding is as follows: green indicates similar proportions of *Quinqueloculina* spp. and *Ammonia* spp., blue indicates dominance by stress-tolerant *Ammonia* spp., yellow indicates dominance by *Quinqueloculina* spp., orange indicates dominance by other rotaliid taxa, and pink indicates a sample with relatively few specimens found.

Date	Sample #	Site	Lat	Long	Texture	Abundance	Species Richness	Agglut	Quinqueloculina	Other Miliolids	Ammonia	Other Rot
5/27/2021	PP3	1	27.7783	-82.5733	Poor Sort	V abundant	21	3.9%	32.6%	4.4%	29.8%	29.3%
6/22/2021	PP3	1	27.7783	-82.5733	Poor Sort	V Abundant	13	4.5%	2.7%	0.0%	68.2%	24.5%
6/22/2021	PP6	2	27.795	-82.5295	Poor Sort	V Abundant	13	0.6%	0.6%	1.3%	70.9%	26.6%
04/09/21	PP1	3	27.7263	-82.5372	Poor Sort	Abundant	27	0.4%	38.1%	5.7%	37.2%	18.6%
04/09/21	PP2	3	27.7263	-82.5372	Poor Sort	Abundant	29	5.4%	29.7%	4.7%	32.2%	27.9%
04/09/21	PP3	3	27.7263	-82.5372	Poor Sort	Moderate	21	1.7%	39.3%	3.5%	34.1%	21.4%
5/27/2021	PP8	3	27.7268	-82.5370	Poor Sort	V abundant	23	4.2%	27.4%	4.8%	22.0%	41.7%
6/22/2021	PP8	3	27.725	-82.5283	Poor Sort	V Abundant	30	3.3%	39.1%	6.6%	32.5%	18.5%
04/09/21	PP4	4	27.6968	-82.5602	Poor Sort	Abundant	29	3.2%	35.9%	7.8%	31.8%	21.2%
04/09/21	PP5	4	27.6968	-82.5602	Poor Sort	Abundant	28	4.9%	32.3%	2.2%	36.3%	24.3%
04/09/21	PP6	4	27.6968	-82.5602	Poor Sort	Moderate	18	2.1%	51.6%	11.6%	16.8%	17.9%
04/09/21	PP7	5	27.6667	-82.6033	Poor Sort	Abundant	29	5.7%	37.6%	12.9%	16.2%	27.6%
04/09/21	PP8	5	27.6667	-82.6033	Poor Sort	Abundant	29	3.1%	47.4%	25.0%	15.1%	9.4%
04/09/21	PP9	5	27.6667	-82.6033	Poor Sort	Low	15	1.8%	52.7%	10.9%	21.8%	12.7%
5/27/2021	PP10	5	27.6696	-82.6010	Poor Sort	Abundant	22	8.4%	32.3%	13.5%	20.6%	25.2%
6/22/21	PP14	5	27.6667	-82.6033	Poor Sort	V Abundant	24	6.2%	46.3%	14.7%	23.2%	9.6%
04/09/21	PP10	6	27.6283	-82.5633	Muddy	Moderate	19	11.6%	23.2%	5.3%	8.4%	51.6%
04/09/21	PP11	6	27.6283	-82.5633	Muddy	Moderate	18	8.1%	14.5%	9.7%	15.3%	52.4%
04/09/21	PP12	6	27.6283	-82.5633	Muddy	Sparse	7	6.7%	0.0%	0.0%	33.3%	60.0%
04/09/21	PP13	7	27.6317	-82.645	Coarse	V abundant	27	1.7%	39.2%	14.3%	15.6%	29.1%
04/09/21	PP14	7	27.6317	-82.645	Coarse	V abundant	22	2.3%	70.2%	13.3%	5.5%	8.7%
04/09/21	PP15	7	27.6317	-82.6450	Coarse	V abundant	25	1.6%	31.9%	4.8%	27.4%	34.3%
5/27/2021	PP15	7	27.6319	-82.6443	Poor Sort	V Abundant	23	4.3%	39.0%	10.2%	16.6%	29.9%
6/22/21	PP19	7	27.6317	-82.645	Poor Sort	Abundant	19	6.6%	62.0%	4.4%	5.8%	21.2%
04/09/21	PP16	8	27.5499	-82.7073	Poor Sort	V abundant	19	4.3%	1.4%	0.7%	75.3%	18.3%
04/09/21	PP17	8	27.5499	-82.7073	Poor Sort	V abundant	23	0.6%	7.2%	5.3%	82.2%	4.7%
04/09/21	PP18	8	27.5499	-82.7073	Poor Sort	V abundant	24	0.7%	23.6%	6.9%	54.2%	14.6%
5/27/2021	PP17	8	27.5645	-82.7077	Poor Sort	V Abundant	27	2.4%	6.1%	4.3%	59.1%	28.0%
5/27/2021	PP18	9	27.5989	-82.7384	Poor Sort	V Abundant	8	0.0%	0.0%	0.7%	81.9%	17.4%
6/22/21	PP26	9	27.6008	-82.7402	Poor Sort	Abundant	29	10.2%	41.0%	7.2%	14.5%	27.1%
04/09/21	PP19	10	27.7318	-82.6107	Poor Sort	V abundant	26	6.0%	33.7%	4.6%	41.8%	13.8%
04/09/21	PP20	10	27.7318	-82.6107	Poor Sort	V abundant	25	5.1%	42.9%	5.1%	35.3%	11.6%
04/09/21	PP21	10	27.7318	-82.6107	Poor Sort	V abundant	18	2.0%	33.6%	1.3%	32.9%	30.2%
5/27/2021	PP21	10	27.5989	-82.7384	Poor Sort	Moderate	11	4.6%	1.3%	0.0%	68.4%	25.7%

VI. Jennifer Cannizzaro, David English, and Chuanmin Hu

Chl-a, CDOM fluorescence, phycoerythrin
fluorescence, satellite imagery compositesWater+Suspended
Particles

Total budget: \$32,299

Activities during this period: The Optical Oceanography Laboratory (<https://optics.marine.usf.edu/>) collected a total of 136 surface and bottom water samples for chlorophyll-a concentration (Chl-a; Method: 24hr, cold methanol extraction), 95 surface and bottom water samples for Chl-a (Method: 20 minute, hot methanol extraction), and 95 surface and bottom water samples for spectral absorption coefficients of phytoplankton ($a_{ph}(\lambda)$), non-algal detrital material ($a_d(\lambda)$), and colored dissolved organic matter ($a_{CDOM}(\lambda)$) from shipboard surveys and shore-based sampling in and around Tampa Bay in April-June 2021 (Table 1).

Hu Table 1. Summary of field measurements made by the Optical Oceanography Laboratory in Tampa Bay in April-June 2021.

Sample date	Surface Chl-a (24hr, cold)	Bottom Chl-a (24hr, cold)	Surface Chl-a (20min., hot)	Bottom Chl-a (20min., hot)	Surface absorption	Bottom absorption	Surface underway
04/08/21	11	8	0	0	0	0	-
04/09/21	12	3	1	0	1	0	-
04/12/21	13	7	13	2	13	2	-
04/13/21	2	0	2	0	2	0	-
04/21/21	5	0	0	0	0	0	-
04/29/21	15	10	15	8	15	8	-
05/27/21	15	10	15	9	15	9	-
06/22/21	15	10	20	10	20	10	X
TOTAL:	88	48	66	29	66	29	

Near-surface (~3 m) underway fluorescence was also collected using an Aquatic Laser Fluorescence Analyzer (ALFA; developed by LDEO/WET Labs) aboard the R/V W.T. Hogarth on 22 June 2021. This instrument provides spectral deconvolution analysis of laser-stimulated emission excited at blue and green wavelengths for assessment of chlorophyll-a, phycoerythrin, and CDOM. Raw chlorophyll-a and CDOM fluorescence were calibrated using Chl-a ($r^2=0.88$, $n=13$) and $a_{CDOM}(443)$ ($r^2=0.96$, $n=15$), respectively. All of these samples and data were processed and analyzed as part of this effort.

Surface Chl-a was also used to develop an empirical remote sensing algorithm for generating satellite-derived Chl-a from the Ocean and Land Colour Instrument (OLCI) aboard EUMETSAT's Sentinel-3A and Sentinel-3B spacecrafts. Cloud-free OLCI Chl-a imagery beginning shortly after the Piney Point release event in early-April and continuing on through the red tide event in June-July were examined in relation to shipboard measurements.

Deliverables produced:

- Surface and bottom chlorophyll-a concentrations [Method: 24hr, cold extraction] (April-June 2021; n=136)
- Surface and bottom chlorophyll-a concentrations [Method: 20min., hot extraction] (April-June 2021; n=95)
- Surface and bottom spectral absorption coefficients of phytoplankton, detritus, and CDOM (April-June 2021; n=95)
- Near-surface underway chlorophyll-a, phycoerythrin, and CDOM fluorescence (22 June 2021)
- OLCI/Sentinel-3A,-3B Chl-a imagery (April-July 2021, and April of 2016 - 2020)

Discussion of findings: Surface Chl-a measured within ~2.5 km of Port Manatee was relatively high (up to 272 mg m⁻³) between April 8-13th (**Figure Hu-1**). These results are consistent with reports in this region of a short-lived and localized non-harmful diatom bloom (Beck et al., 2022). Surface Chl-a in surrounding waters at this time was relatively low (<3 mg m⁻³) and remained low through late-May for the entire study area. These values are typical of Chl-a in Middle and Lower Tampa Bay during the dry season (Le et al., 2013). On June 22nd, mean surface Chl-a increased (5.9 ± 3.0 mg m⁻³, n=20) in response to a red tide event.

Bottom Chl-a (not shown) was mostly similar to surface values, indicating a mixed water column. The greatest deviation between near-surface and bottom Chl-a (9.6 and 3.5 mg m⁻³, respectively) occurred on June 22nd at Station 2 (northernmost site) where high *K. brevis* abundance (>10⁶ cells/L) was observed (**Figure Hu-2**).

Measurements of spectral light absorption due to optically significant particulate (phytoplankton and detritus) and dissolved (CDOM) components of water (e.g., **Figures Hu-3-4**) are often used to understand and model the underwater light field and to develop remote sensing algorithms. Phytoplankton absorption spectra is mainly characterized by peaks at ~443nm and 675nm caused by chlorophyll-a. The spectral variability and magnitude of $a_{ph}(\lambda)$ is also strongly influenced by the amount and type of accessory pigments (e.g., chlorophyll-b, chlorophyll-c, carotenoids, and phycobiliproteins) that are present. This varies depending on the taxonomic composition of phytoplankton populations. Compared to $a_{ph}(\lambda)$, the absorption spectra of non-algal detrital material and CDOM are generally featureless, exhibiting exponentially decreasing absorption with increasing wavelength and higher spectral slopes for CDOM than for detritus.

Figure Hu-3 shows the spectral absorption properties for samples collected at the “Piney Shore” site located just north of Port Manatee and the “Piney Source” site located in the Piney Point reservoir. “Piney Shore” Chl-a on April 9th was 272 mg m⁻³ indicative of an extreme bloom. Phytoplankton clearly dominated total non-water absorption ($a_{t-w}(\lambda) = a_{ph}(\lambda) + a_d(\lambda) + a_{CDOM}(\lambda)$) at all wavelengths (**Figure Hu-3a**). The spectral shape of $a_{ph}(\lambda)$ for blue-green wavelengths (~443-550 nm) is consistent with that of chlorophyll-c containing chromophytic algae (e.g., diatoms, dinoflagellates). Absorption shoulders in $a_{ph}(\lambda)$ at ~490nm and $a_d(\lambda)$ at ~475nm, though, indicate that phycoerythrin-containing phytoplankton (e.g. cyanobacteria and cryptophytes) may have also been present.

Four days later on April 13th, Chl-a at the “Piney Shore” site decreased by nearly 7-fold (40 mg m⁻³), causing CDOM to exhibit increased dominance at blue-green wavelengths (**Figure Hu-3b**).

Chl-a at the “Piney Source” location on April 13th was 112 mg m⁻³. The prominent absorption shoulder at 490nm and broad decline in absorption for wavelengths <675nm are consistent with cyanobacteria and chlorophyll-b containing green algae (**Figure Hu-3c**). Detrital absorption was relatively high at this site, indicating higher turbidity.

Overall, absorption of phytoplankton, detritus, and CDOM was generally lower for samples collected on April 12th, April 29th, May 27th, and June 22nd (**Figure Hu-4**). **Figure Hu-5** shows the relative contributions of $a_{ph}(443)$, $a_d(443)$, and $a_{CDOM}(443)$ to $a_{t-w}(443)$ for all surface samples collected as part of this effort. Excluding the “Piney Shore” and “Piney Source” samples, CDOM typically dominated light absorption at 443nm in April and May. This is consistent with previous results for the dry season (November-May) in Middle and Lower Tampa Bay (Le et al., 2013). Increased contributions by phytoplankton and detritus are typical of the wet season (June-October) in this region. However, the red tide on June 22nd led to increased phytoplankton contributions and decreased CDOM contributions only. This is consistent with previous results that showed how *K. brevis* blooms on the West Florida Shelf are associated with a paucity of detrital absorption that is likely caused by reduced grazing pressure and/or lower concentrations of terrestrial-derived inorganic material (Cannizzaro et al., 2008).

Near-surface underway Chl-a on June 22nd (**Figure Hu-6a**) ranged from 1.6 – 32 mg m⁻³ and was relatively low (<3 mg m⁻³) in Lower Tampa Bay south of the Sunshine Skyway Bridge. Increased Chl-a with increased patchiness was observed further north in Middle Tampa Bay where medium and high *K. brevis* abundances were often observed (**Figure Hu-2**). Peak Chl-a (32 mg m⁻³) occurred ~1.4 km southeast of Station 2.

Near-surface underway $a_{CDOM}(443)$ ranged from 0.1 – 0.6 m⁻¹ and decreased steadily with distance south and away from major riverine sources (**Figure Hu-6b**). At the same time, underway salinity measured with the ship’s Sea-bird SBE 21 SeaCAT thermosalinograph increased steadily with distance south (**Figure Hu-6c**). Salinity and $a_{CDOM}(443)$ showed a strong inverse correlation (not shown).

In addition to measuring Chl-a and CDOM fluorescence, the ALFA flow-thru system is also capable of quantifying three spectral types of phycoerythrin (PE1, PE2, and PE3) that are associated with oceanic cyanobacteria, coastal cyanobacteria, and cryptophytes, respectively. Normalizing the fluorescence values for these pigments to chlorophyll-a fluorescence allows for their relative contributions to be calculated in mixed phototrophic populations. **Figure Hu-7** shows that coastal cyanobacteria were prominent throughout most of the study area on June 22nd while cryptophytes were mostly unimportant. Oceanic cyanobacteria showed strong contributions in Lower Tampa Bay as expected given its close proximity to the Gulf of Mexico. Interestingly, contributions of oceanic cyanobacteria were also high inside the red tide patch southeast of Station 2. Yentsch et al. (2008) also documented high cyanobacterial abundance associated with natural red tide populations off Charlotte Harbor. Several studies have suggested that *K. brevis* may graze on *Synechococcus* (cyanobacteria), thus enhancing the range of nutritional substrates available to meet its growth requirements and helping to sustain populations in nutrient-poor waters (Glibert et al., 2009; Jeong et al., 2005).

Satellite-derived Chl-a obtained using a regional algorithm shows the phytoplankton bloom offshore of Port Manatee in early- and mid-April both during and after the Piney Point release (first three rows of **Figure Hu-8**). The short-lived bloom had a maximum size of about 25 km² with Chl-a mostly between 5 - 40 mg m⁻³. This bloom was dominated by diatoms and disappeared by the end of April. Monthly mean OLCI Chl-a in April of previous years (2016-2020) was low (**Figure Hu-9**), indicating that the bloom observed following the Piney Point release event in April 2021 was truly anomalous.

A red tide bloom dominated by *K. brevis* in Middle/Lower Tampa Bay in June-July 2021 and a toxic dinoflagellate bloom dominated by *Pyrodinium bahamense* in Old Tampa Bay in July 2021 were also observed (**Figure Hu-8**). Note that bloom type for all of these bloom events was determined using light microscopy by the FWC Fish and Wildlife Research Institute (FWRI).

Diatoms and dinoflagellates (*K. brevis*, *P. bahamense*) contain major accessory pigments with similar broad, overlapping absorption contributions, resulting in similarly shaped $a_{ph}(\lambda)$ (**Figure Hu-3a, 4d**). Consequently, it is difficult to discriminate between these algal groups using multi-spectral satellite ocean color data (e.g. OLCI) based on $a_{ph}(\lambda)$ alone (Cannizzaro et al., 2008). This is why understanding the spectral absorption (and backscattering) properties of phytoplankton as well as that of non-algal optically active constituents (e.g., CDOM, detritus) is important. Future hyperspectral sensors such as NASA's Plankton, Aerosol, Cloud, ocean Ecosystem (PACE) mission will provide higher resolution spectral information perhaps allowing for the discrimination between harmful and non-harmful blooms.

References

- Beck, M. W., Altieri, A., Angelini, C., Burke, M. C., Chen, J., Chin, D. W., ... & Whalen, J. (2022). Initial estuarine response to inorganic nutrient inputs from a legacy mining facility adjacent to Tampa Bay, Florida. *Marine Pollution Bulletin*, 178, 113598.
- Cannizzaro, J. P., Carder, K. L., Chen, F. R., Heil, C. A., & Vargo, G. A. (2008). A novel technique for detection of the toxic dinoflagellate, *Karenia brevis*, in the Gulf of Mexico from remotely sensed ocean color data. *Continental Shelf Research*, 28(1), 137-158.
- Glibert, P. M., Burkholder, J. M., Kana, T. M., Alexander, J., Skelton, H., & Shilling, C. (2009). Grazing by *Karenia brevis* on *Synechococcus* enhances its growth rate and may help to sustain blooms. *Aquatic Microbial Ecology*, 55(1), 17-30.
- Jeong, H. J., Park, J. Y., Nho, J. H., Park, M. O., Ha, J. H., Seong, K. A., ... & Yih, W. H. (2005). Feeding by red-tide dinoflagellates on the cyanobacterium *Synechococcus*. *Aquatic microbial ecology*, 41(2), 131-143.
- Le, C., Hu, C., English, D., Cannizzaro, J., Chen, Z., Kovach, C., ... & Carder, K. L. (2013). Inherent and apparent optical properties of the complex estuarine waters of Tampa Bay: what controls light?. *Estuarine, Coastal and Shelf Science*, 117, 54-69.
- Yentsch, C. S., Lapointe, B. E., Poulton, N., & Phinney, D. A. (2008). Anatomy of a red tide bloom off the southwest coast of Florida. *Harmful Algae*, 7(6), 817-826.

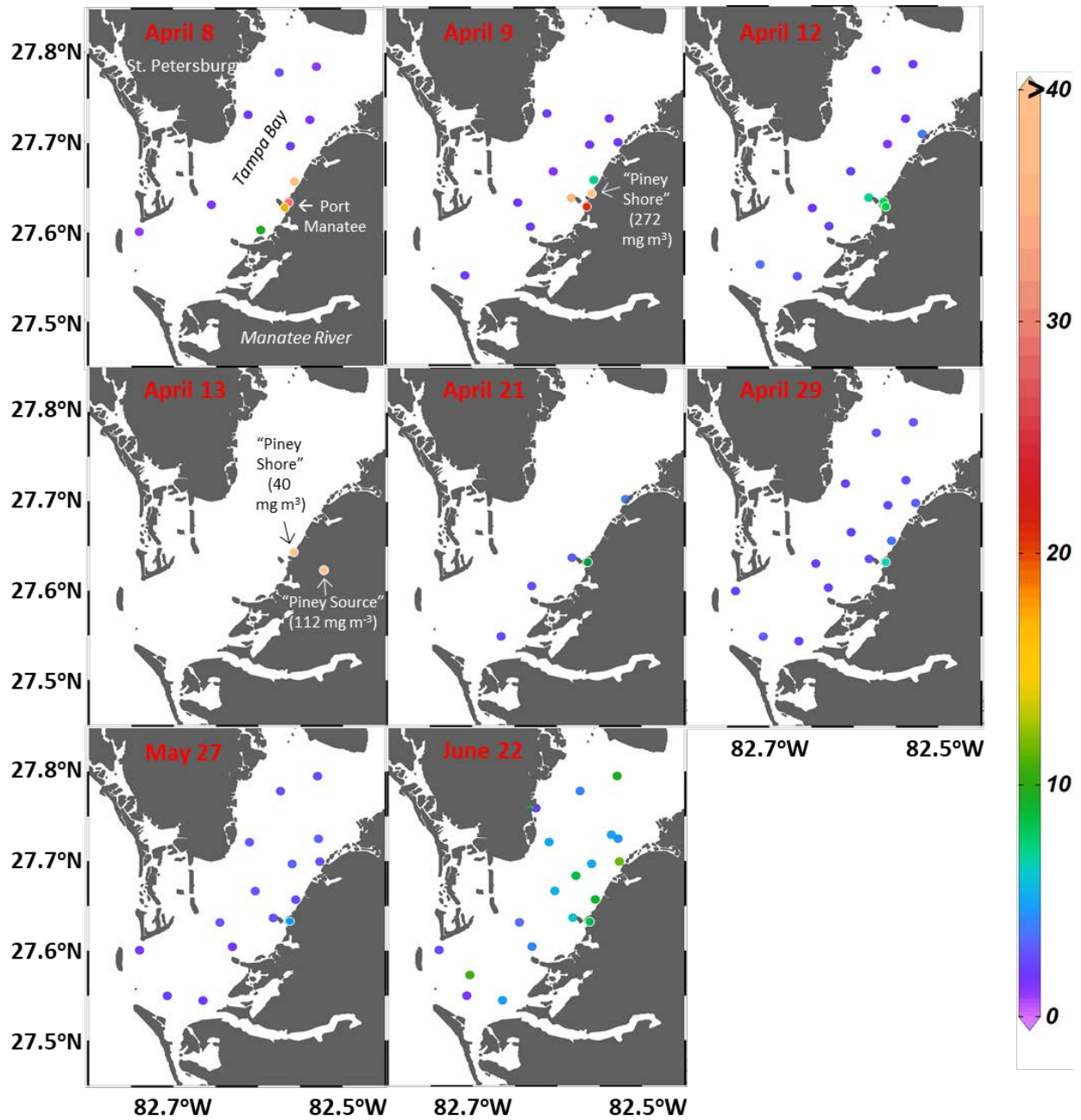


Figure Hu-1. Surface Chl-a (mg m^{-3}) in Tampa Bay in April-June 2021.

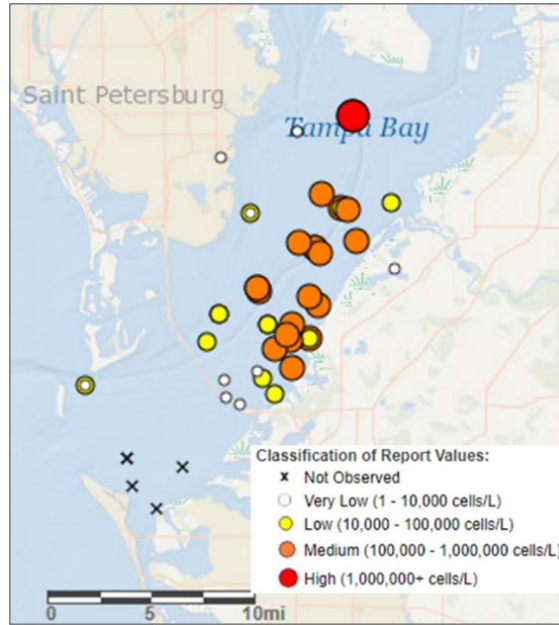


Figure Hu-2. *K. brevis* abundance (cells/L) in Tampa Bay reported by the FWC Fish and Wildlife Research Institute (FWRI) on June 22, 2021. [Source: NOAA HABSOS (<https://habsos.noaa.gov/>)]

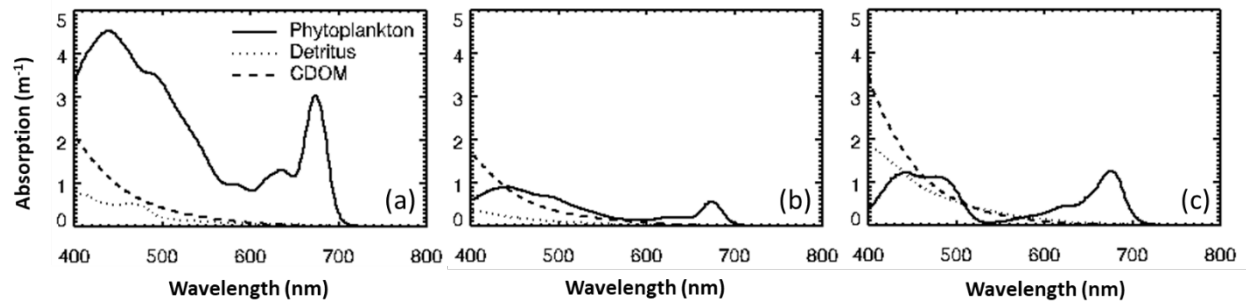


Figure Hu-3. Absorption spectra of phytoplankton (solid line), non-algal detrital material (dotted line), and CDOM (dashed line) at “Piney Shore” on (a) April 9, 2021 and (b) April 13, 2021 and (c) “Piney Source” on April 13, 2021. See **Figure Hu-1** for map of station locations.

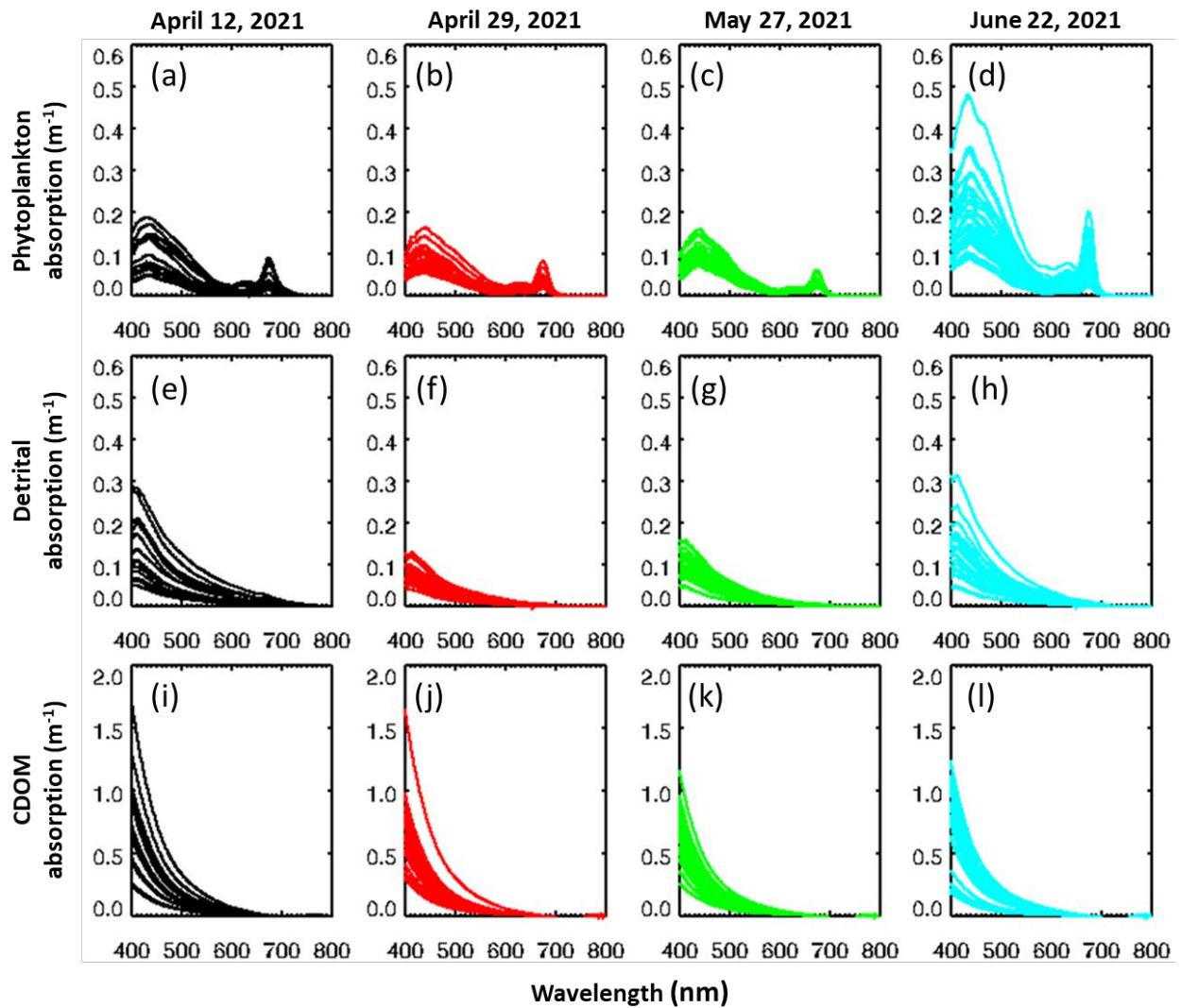


Figure Hu-4. Near-surface and bottom absorption spectra of (a-d) phytoplankton, (e-h) non-algal detrital material, and (i-l) CDOM in Tampa Bay in April-June 2021. Note the change in y-axis scaling for CDOM absorption.

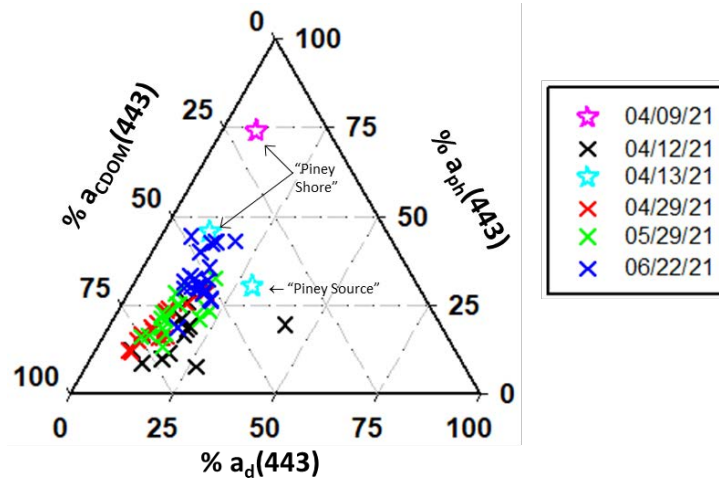


Figure Hu-5. Percentage contribution of absorption by detrital particles, phytoplankton, and CDOM to total non-water absorption at 443nm for surface waters collected in Tampa Bay in April-June 2021.

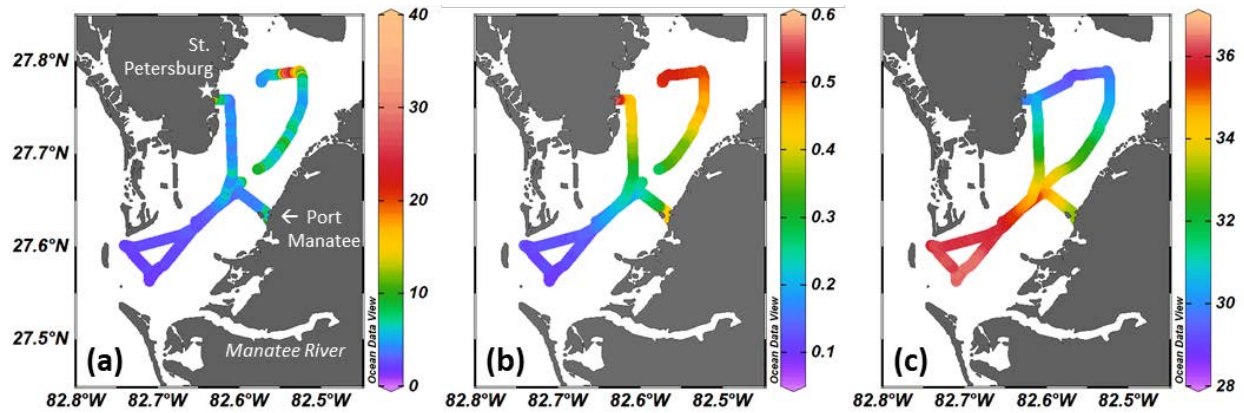


Figure Hu-6. Near-surface underway (a) Chl-*a* ($mg\ m^{-3}$), (b) $a_{CDOM}(443)$ (m^{-1}), and (c) salinity (ppt) in Tampa Bay on June 22, 2021.

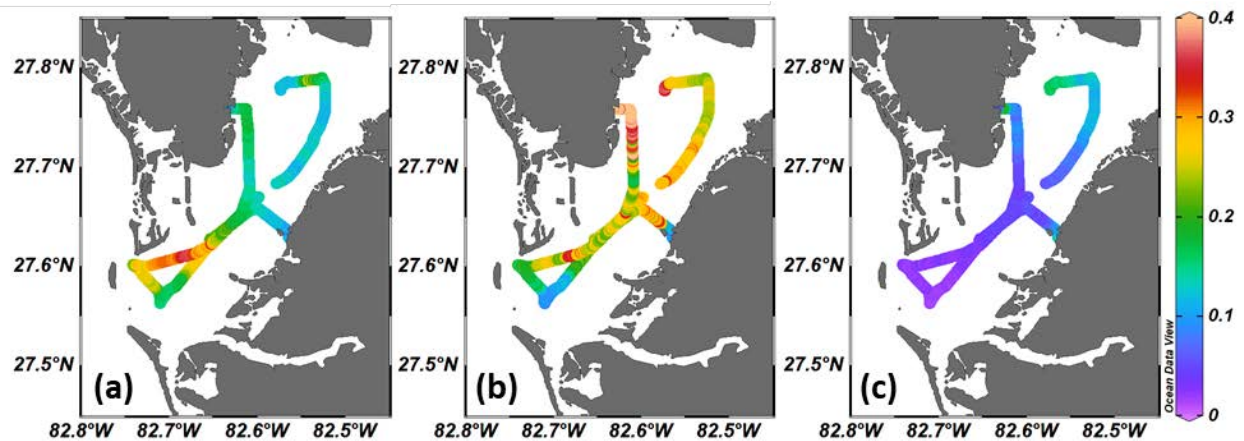


Figure Hu-7. Near-surface underway (a) F_{PE1}/F_{chl_a} , (b) F_{PE2}/F_{chl_a} , and (c) F_{PE3}/F_{chl_a} in Tampa Bay on June 22, 2021. [Units: dimensionless]

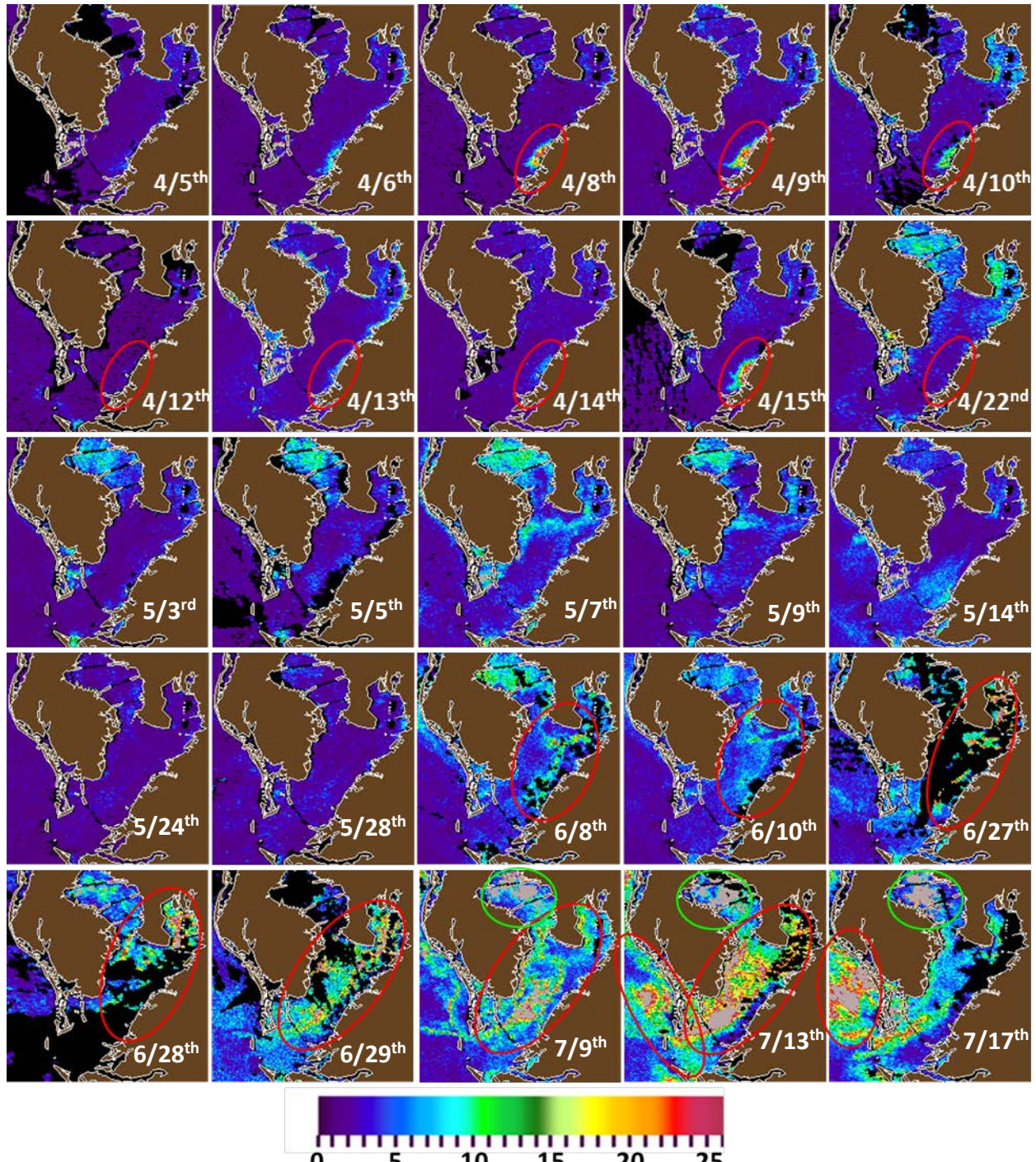


Figure Hu-8. Daily OLCI Chl-a (mg m^{-3}) in Tampa Bay in April-July 2021. The red circles in April point to a non-harmful bloom dominated by diatoms that directly resulted from the Piney Point release event. The red circles in June and July point to a red tide bloom dominated by *K. brevis* in Middle/Lower Tampa Bay. The green circles in July point to a *P. bahamense* bloom in Old Tampa Bay.

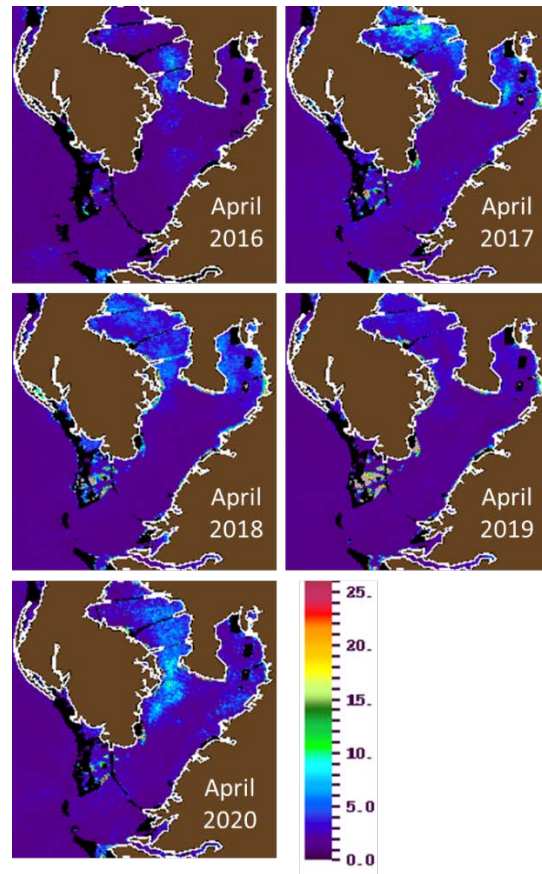


Figure Hu-9. Monthly mean OLCI Chl-a (mg m^{-3}) in Tampa Bay for April in 2016-2020. These maps show background levels of Chl-a $< 3 \text{ mg m}^{-3}$ in the vicinity of the Piney Point discharge location (Port of Manatee), in contrast to the post-discharge bloom (Chl-a $> 5 \text{ mg m}^{-3}$) in April 2021 (**Fig. Hu-8**).

VII. Steven Murawski, Sherryl Gilbert, Ethan Goddard, Isabel Romero, Patrick Schwing, Devon Firesinger, Kylee Rullo

Contaminants (organic), phosphorus, ¹³C, ¹⁵N

Fish

Total budget: \$62,070

Activities during this period:

1. Small Boat Sampling off Port Manatee – collection methods

Expeditions to collect samples of potential pollution emanating from the release of water from the Piney Point phosphate processing retention ponds were conducted on April 7 and 17, 2021. On April 7th, the expedition was crewed by Drs. Patrick Schwing and Rebekka Larson from Eckerd College and Dr. Steven Murawski from the USF College of Marine Science. Sampling occurred on Eckerd's 24' CapeHorn that is operated and maintained through Eckerd's waterfront program. The regime consisted of two inshore to offshore transects consisting of five sampling stations. The first transect started inside of Port Manatee and ended in about 30' water depths offshore. A second, parallel transect was sampled starting in Bishop's Bay, just south of Port Manatee. At each station, a profile of salinity, temperature and depth was obtained. Additionally, large volumes of surface water were obtained, and a sediment grab sample was taken. A representative sample of fishes in the region was also obtained just off Port Manatee. On April 17th, an expedition to collect additional fish samples was launched from the R/V Misty Dawn off Port Manatee at the day marker for the channel. The combination of demersals and pelagics was targeted to show if there is site accumulation and if it radiates with more mobile species (mackerels).

Two additional collections were made opportunistically from other studies to gain insight on the baseline conditions (pre Piney Point) and the recovery conditions (post Piney Point). Fish samples were collected in the same region, adjacent to Port Manatee, on August 29, 2020 associated with a Tampa Bay Estuary Program project to look at PFAS concentrations in fish and sediments in Tampa Bay. On April 2nd 2022, additional fish samples were collected in the same region with funding from another study to determine if any potential contaminations diminished to baseline levels. Note that "pre" and "post" collection was not funded by this study. Table 1 is a full catalog of specimens that were analyzed.

The samples obtained complemented those taken simultaneously from the R/V Weatherbird II on April 7th. When appropriate, similar analyses were performed on fish, sediments and water to determine the extent of contamination. The sediment analyses occurred on a separate contract with Eckerd College as well as the radionuclide analyses for the fish samples.

For all fish collections, the fish were placed in a cooler and processed with IACUC methods. For each fish, standard length, total length, and fork length (where applicable) were measured to the nearest 0.5 cm. Total weight was recorded to the nearest 0.001 kg. Muscle samples, whole livers, and whole gills were removed and placed into combusted glass jars and vials. The samples were refrozen before being freeze-dried.

Due to budgetary constraints, all of the fish were not analyzed for this study. Priority was given to those species that were collected for all time points to minimize any variability due to species-specific lifestyle and physiology. A table of species, biometrics, matrix to be analyzed (gill, liver or muscle) and analysis is provided here in worksheet (1).

2. Analysis of semi-volatile organic chemicals (SVOCs)

Samples were kept frozen until freeze-dried at the Marine Environmental Chemistry Laboratory (MECL, College of Marine Science, University of South Florida). Approximately 50-100 µg of

freeze-dried and homogenized muscle and liver samples were extracted using an Accelerated Solvent Extraction system (ASE 200®, Dionex) under high temperature (100°C) and pressure (1500 psi) with hexane:dichloromethane (8:2 v:v). We followed modified EPA methods and QA/QC protocols (8270D, 8015C). Targeted compounds included polycyclic aromatic hydrocarbons (PAHs; 2-6 ring including alkylated homologs, 66 total PAHs), organochlorinated pesticides (OCPs; 36), polychlorinated biphenyls (PCBs; 32), and oxidized-PAHs (34 total oxidized-PAHs). Deuterated and non-deuterated surrogate standards were added before extraction for PAHs (acenaphthene-d10, benz[a]anthracene d12, benzo[a]pyrene d12, dibenz[a,h]anthracene d14, fluoranthene d10, and phenanthrene d10; ISM-750-1, Ultra Scientific-Agilent, Santa Clara, CA, USA), oxidized-PAHs (2-naphthol d8, 1-nitronaphthalene d7, and 9-fluorenone d8; D-5648, D-5797, D-5442, CDN Isotopes, Pointe-Claire, QC, Canada), and PCBs and OCPs (tetrachloro-m-xylene; Cat# 32027, Restek, Bellefonte, PA, USA; and biphenyl d10; Cat# 72058, Absolute Standards, Hamden, CT, USA). Reference standards include SRM 2779 Gulf of Mexico Crude Oil (NIST, Gaithersburg, MD, USA), PAH standard mix (US-106-N-1, Agilent, Santa Clara, CA, USA), M-508.1-X1 and M-508.1-X2 (Accustandard, New Haven, CT, USA), oxidized-PAH reference standards (anthrone 319899, xanthone X600, 9,10-phenanthrenequinone 275034, 1-naphthol N1000, 2-naphthol 185507, 9-hydroxyfluorene H31204, 2-naphthaldehyde N206, 9-fluorenone F1506, 1,4-naphthoquinone 152757, 1-nitronaphthalene 103594, and 9-hydroxyphenanthrene 21128 from Sigma Aldrich, St. Louis, MO, USA; and 9-nitrophenanthrene R-020N from Accustandard, New Haven, CT, USA); PCB Congener Mix #6 (C-CSA-06, Accustandard, New Haven, CT, USA).

For extraction in the ASE, we applied a one-step extraction and clean up procedure using a predetermined packing of the extraction cells (Romero et al., 2018, Romero et al. 2020) using a 6 ml extraction cell with glass fiber filter (pre-combusted at 450°C for 4 h), 5g silica gel (high purity grade, 100–200 mesh, pore size 30A, Sigma Aldrich, USA; pre-combusted at 450°C for 4 h, and deactivated 2%), and sand (pre-combusted at 450°C for 4 h). Organic extracts were concentrated to ~2 ml in a RapidVap (LABONCO RapidVap® Vertex™ 73200 series) and further concentrated to about 150 µl by gently blowing with a nitrogen stream. Two extraction control blanks were included with each set of samples (17 samples).

SVOC compounds were quantified using GC/MS/MS (Agilent 7680B gas chromatograph coupled with an Agilent 7010 triple quadrupole mass spectrometer) in multiple reaction monitoring mode (MRM) to target multiple chemical fractions in one-run-step. Molecular ion masses for hydrocarbon compounds were selected from previous studies (Romero et al., 2015, 2018; Sørensen et al., 2016; Adhikari et al., 2017). All samples were analyzed in splitless injections, inlet temperature of 295°C, constant flow rate of 1 ml/min, and a MS detector temperature of 250°C using a Rxi-5sil chromatographic column. The GC oven temperature program was 60°C for 2 min, 60°C to 200°C at a rate of 8°C/min, 200°C to 300°C at a rate of 4°C/min and held for 4 min, and 300°C to 325°C at a rate of 10°C/min and held for 5 min. Source electron energy was operated at 70 eV, and argon was used as the collision gas at 1 mTorr pressure. For accuracy and precision of analyses we included laboratory and analytical blanks, tuned MS/MS to PFTBA (perfluorotributylamine) daily, checked samples with a standard reference material (NIST 2779) daily, and reanalyzed sample batches when replicated standards exceeded ±30% of relative standard deviation (RSD), and/or when recoveries were low. Recovery ranged within QA/QC criteria of 50–130% for all compounds, except for propachlor, simazine, atrazine, metribuzin, alachlor, metolachlor and cyanazine (with concentrations reported as semi-quantitative). PAH concentrations are reported as recovery

corrected. Each analyte was identified using certified standards (Chiron S-4083-K-T, Chiron S-4406-200-T, NIST 2779) and performance was checked using a 5-point calibration curve (0.04, 0.08, 0.31, 1.0 ppm). Quantitative determination of compounds was conducted using response factors (RFs) calculated from the certified standard NIST2779. SVOC compounds are expressed as dry weight concentrations.

3. Radionuclide Analysis

According to a measurement in 2019, the Piney Point southern holding pond effluent had concentrations of total nitrogen and phosphorus three orders magnitude higher than Tampa Bay waters (Beck et al., 2022). In addition to increased nutrients, other contaminants and radioisotopes were also present at concentrations higher than Tampa Bay waters (Beck et al., 2022). Short-lived radioisotope activities were measured in various fish tissues (gills, liver, gall bladder) to assess uptake and potential vectors into the food web associated with the effluent. The most commonly used short-lived radioisotopes include excess ^{234}Th and ^{210}Pb , ^{137}Cs , ^{226}Ra , ^{228}Ra , and ^7Be (Swarzenski 2014; Holmes 1998; Appleby 2001). Short-lived radioisotopes were analyzed by gamma spectrometry on Series HPGe (high-purity Germanium) Coaxial Planar Photon Detectors for total ^{210}Pb (46.5 keV), ^{214}Pb (295 keV and 351 keV), ^{214}Bi (609 keV), ^{234}Th (63 keV) ^{137}Cs (661 keV), and ^7Be (477). Activities were reported as disintegrations per minute per gram of tissue (dpm/g) using methodology described by Brooks et al. (2015). Data were corrected for counting time and detector efficiency, as well as for the fraction of the total radioisotope measured yielding activity in dpm g⁻¹ (disintegrations per minute per gram).

Detector efficiencies (limit of detection) were all <3% of the activities measured, determined by similar methods to Kitto et al. (1991). Efficiency calibrations were based on analyzing 12 varying masses (1-50g) of the IAEA-414 standard. By relating the counts measured at variable masses to the known activity of the standard, self-absorption is also included in the efficiency calibrations (Hussain et al., 1996). The Cutshall method (Cutshall et al., 1983) was used on select samples, and results show that the self-absorption and variability is negligible and within detection error. The mean activity of the ^{214}Pb (295 Kev), ^{214}Pb (351 Kev), and ^{214}Bi (609 Kev) was used as a proxy for ^{226}Ra activity.

4. Stable Isotope Methods

Nitrogen and carbon isotope and bulk composition were measured by CF-EA-irms (Continuous Flow Elemental Analyzer Isotope Ratio Mass Spectrometry) at the University of South Florida College of Marine Science Marine Environmental Chemistry Laboratory using commonly accepted procedures (Werner et al 1999). Isotope compositions were measured on a ThermoFinnigan Delta+XL IRMS, are reported in per mil (‰) notation and are scaled to VPDB (d13C) and AT-Air (d15N). Secondary reference materials (NIST 8574 d13C = +37.63 ± 0.10 ‰, d15N = +47.57 ± 0.22 ‰, N = 9.52%, C = 40.81%, C:N (molar) = 5.0; NIST 8573 d13C = -26.39 ± 0.09‰, d15N = -4.52 ± 0.12‰ N = 9.52%, C = 40.81%, C:N (molar) = 5.0) were used to normalize raw measurements to the VPDB (d13C) and AT-Air (d15N) scales (Werner et al. 2002, Qi et al. 2002, Coplen et al 2006) and to calibrate elemental N, C and C:N. Measurement uncertainties, expressed as ±1 standard deviation of n=10 measurements of a laboratory reference material (NIST1577b d13C = -21.69 ± 0.14‰, d15N = 7.83 ± 0.16‰, %N = 9.95 ± 0.48%, %C = 48.04 ± 0.71%, C:N (molar) = 5.63 ± 0.27) were ±0.08‰ for d13C ±0.14‰ for d15N, ±2.44 %RSD for %N, ±2.74 %RSD for %C, and ±0.68 %RSD for C:N.

5. Trace Metal Methods

Samples were digested following Ashoka et al. (2009). Briefly, 0.1-0.2mg dry tissue was placed in a 15ml trace-metal clean centrifuge tube with 1.5ml trace-metal grade nitric acid, 1.5ml ultra-pure water and 1.0ml trace-metal grade hydrogen peroxide. Samples were sealed and placed in a 900W microwave for 7 minutes at 30% power followed by a 10-minute cool down. This was repeated two additional times prior to dilution with 11 ml of ultra-pure water. A 1.0ml aliquot of the sample digest was transferred to a second 15ml trace-metal clean centrifuge tube and diluted with 4.0 ml 2% trace-metal grade nitric acid with a 1.0 ppb Y internal standard prior to analysis. Six digest blanks and six control samples (NIST 1577b) were included in the digestion procedure.

Elemental concentrations were measured with a Thermo ElementXR High-Resolution-ICP-MS using a 100 μ l/min PFA nebulizer, cyclonic spray chamber and quartz torch. A 5-point signal-to-concentration calibration was established with a laboratory multi-element calibration standard gravimetrically prepared from SPEX-Certiprep single-element standards. Acquisition was performed in Medium Resolution (R=4250) and normalized to the Yttrium internal standard prior to blank and dilution correction. Elemental concentrations are reported in μ g/g (AL, Mn, Fe, Ni, Cu, Zn, Cd, Pb), ng/g (Co, V) and percent (P). Digestion yields (% recovery) and measurement uncertainty (%RSD) based on n=6 NIST1577b control standards were: Al 79% recovery, 112% RSD; P: 81% recovery; 21% RSD; V: 66% recovery; 17% RSD; Mn: 87% recovery; 5% RSD; Fe: 85% recovery; 7% RSD; Co:74 % recovery; 9% RSD; Cu: 67% recovery; 23% RSD; Zn: 82% recovery; 8% RSD; Cd: 84% recovery; 4% RSD; Pb 56% recovery; 31% RSD.

Deliverables produced:

We produced pseudo time-series of target organic compounds, trace metals, stable isotope and radionuclide concentrations at sites near the Piney Point effluent. Concentrations were assessed in three tissues to determine potential time of exposure as well as exposure vector. The pathways were through the water, sediment, or diet. The tissues that were analyzed were gill, muscle and liver. Due to budget constraints, all of the tissues for all of the fish were not analyzed.

Discussion of findings:

All organic compounds measured show an increase in concentrations over the sampling period, peaking in the post-Piney Point samples in April of 2022 (Figures 1-4). The only exception to this is the ratio of high molecular weight to low molecular weight compounds indicating fewer volatile compounds in April of 2021 during the spill. Overall concentrations were approximately three times higher in liver tissue than muscle tissue.

Radionuclide concentrations in all fish tissue show an increase during the Piney Point collection periods from pre-Piney Point specimens with the most significant increase occurring in the gill tissue (Figure 5). The tissue samples that were analyzed from April of 2022 exhibited concentrations that were below the detectable limits of the instrument. We note here that the fish tissue samples analyzed for the specimens collected in April 2021 were under another contract with Eckerd College. We present them here for context with other analytical data.

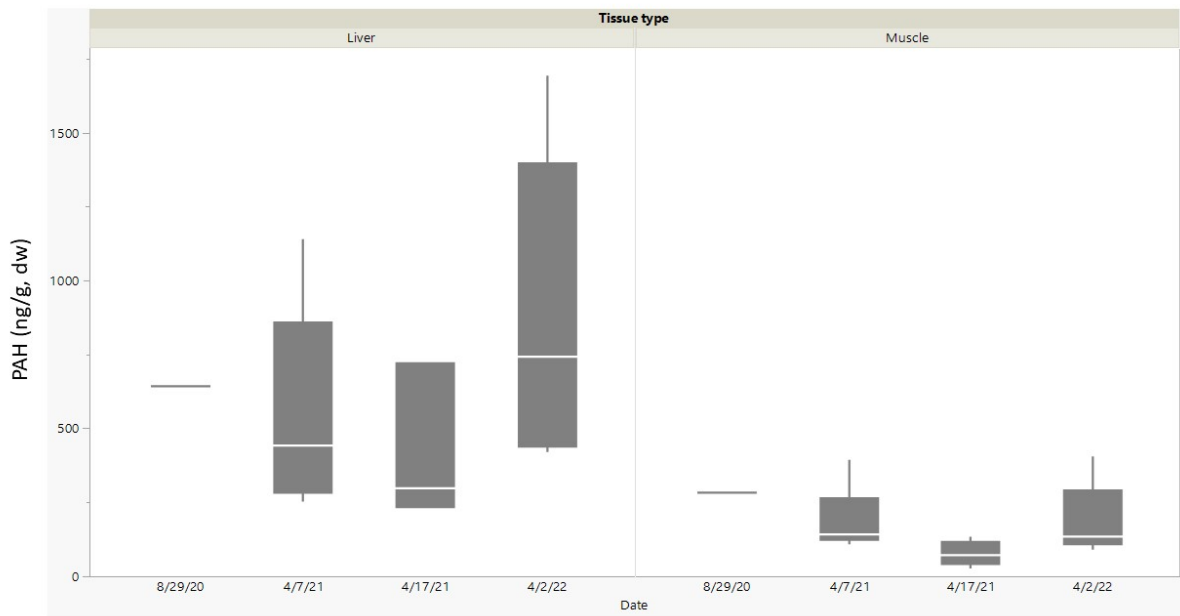
Carbon and nitrogen isotope concentrations in fish liver and muscle did not vary significantly over the sampling period (Figures 6-7). However, the concentration of isotopic nitrogen in muscle was greater than the concentration in liver.

Trace metals in fish liver and muscle varied significantly over the sampling period with a significant increase in copper concentrations during the Piney Point sampling period (Figures 8-10). Cadmium concentrations in liver increased in April of 2022, however, no significant difference was observed in muscle. Lead concentrations in liver and muscle were elevated in April of 2021 showing a decline in April of 2022. Zinc concentrations in liver and muscle did not show significant variations over the sampling period. Nickel and vanadium concentrations showed similar trends with no significant differences in liver concentrations but an increase in muscle concentrations in April of 2021 and a subsequent decline in April of 2022.

Murawski Table 1. Biometrics of fish specimens collected for study.

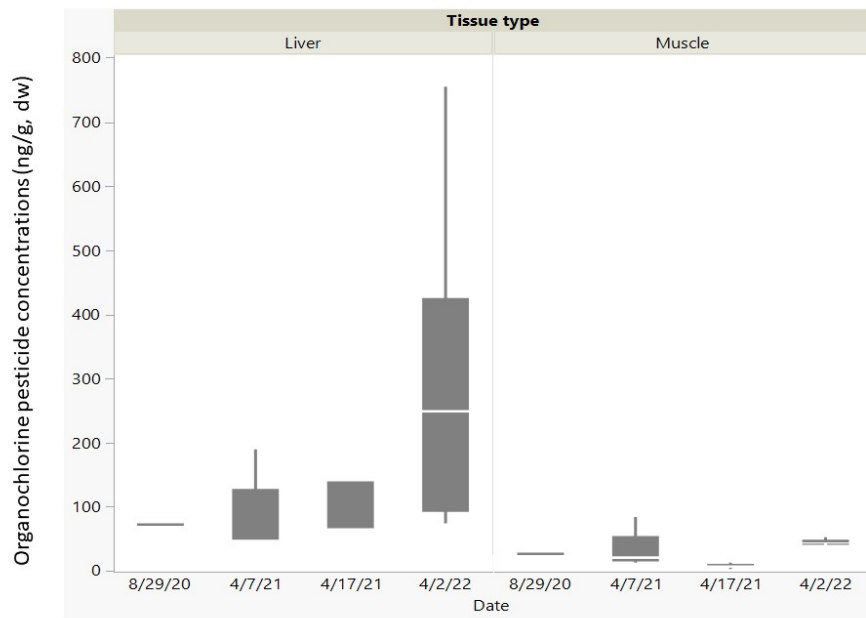
Location	Common Name	Date Collected	Standard Length (cm)	Fork Length (cm)	Total Length (cm)	Ttl Wt (kg)	Latitude (DD)	Longitude (DD)
Pre Piney Point (from previous project)								
Port Manatee	Thread Herring	8/29/2020	14	15.5	18.5	0.054	27.6476	-82.5967
Hillsborough Bay	Thread Herring	8/29/2020	14.5	16	19.5	0.06	27.9107	-82.4407
Lower Tampa Bay	Thread Herring	8/29/2020	14	15.5	19	0.06	27.6191	-82.6539
Lower Tampa Bay	Thread Herring	8/29/2020	15	17	20	0.07	27.6191	-82.6539
Port Manatee	Atlantic Bumper	8/29/2020	14	16.5	20	0.066	27.6476	-82.5967
Port Manatee	Mangrove Snapper	8/29/2020	14	-	18.5	0.092	27.6476	-82.5967
Piney Point First Sampling								
Piney Point	Gray Snapper	4/7/2021	17.5		21.5	0.154	27.6475	-82.5965
Piney Point	Gray Snapper	4/7/2021	16.5		20.2	0.13	27.6475	-82.5965
Piney Point	Gray Snapper	4/7/2021	16.5		20	0.124	27.6475	-82.5965
Piney Point	Gulf Toadfish	4/7/2021	18		20.4	0.174	27.6475	-82.5965
Piney Point	Pinfish	4/7/2021	13.5	16	18	0.084	27.6475	-82.5965
Piney Point	Blue Runner	4/7/2021	18	21	25.5	0.178	27.6475	-82.5965
Piney Point	Black Sea Bass	4/7/2021	13.5		17	0.096	27.6475	-82.5965
Piney Point Second Sampling								
Piney Point	Spanish Mackerel	4/17/2021	38.5	42.5	48	0.572	27.6475	-82.5965
Piney Point	Spanish Mackerel	4/17/2021	37.5	41	48	0.59	27.6475	-82.5965
Piney Point	Spanish Mackerel	4/17/2021	37	41	48	0.578	27.6475	-82.5965
Piney Point	Southern Flounder	4/17/2021	23		30	0.284	27.6475	-82.5965
Piney Point	Ladyfish	4/17/2021	44	48.5	57	1.068	27.6475	-82.5965
Piney Point	Ladyfish	4/17/2021	37	40.5	46	0.526	27.6475	-82.5965
Piney Point	Least Puffer	4/17/2021	21		24	0.288	27.6475	-82.5965
Piney Point	Crevalle Jack	4/17/2021	24	28	34	0.446	27.6475	-82.5965
Post Piney Point								
Port Manatee	Ladyfish	4/2/2022	38	42	50	0.562	27.6477	-82.5967
Port Manatee	Ladyfish	4/2/2022	40	44	51.5	0.688	27.6477	-82.5967
Port Manatee	Spanish Mackerel	4/2/2022	43	48.5	55.5	0.886	27.6477	-82.5967
Port Manatee	Lizardfish	4/2/2022	20	21.5	23	0.07	27.6477	-82.5967
Port Manatee	Leatherjacket #1	4/2/2022	19.5	22	25	0.092	27.6477	-82.5967
Port Manatee	Leatherjacket #2	4/2/2022	20.5	23.5	26	0.11	27.6477	-82.5967
Port Manatee	Leatherjacket #3	4/2/2022	19.5	22	24.5	0.084	27.6477	-82.5967
Port Manatee	Leatherjacket #4	4/2/2022	22.5	25	28.5	0.114	27.6477	-82.5967
Port Manatee	Leatherjackets	4/2/2022	17	19	21.5	0.052	27.6477	-82.5967
Port Manatee	Leatherjackets	4/2/2022	17.5	20	22	0.058	27.6477	-82.5967
Port Manatee	Leatherjackets	4/2/2022	16	17.5	19.5	0.04	27.6477	-82.5967
Port Manatee	Leatherjackets	4/2/2022	17.5	19.5	22.5	0.054	27.6477	-82.5967
Port Manatee	Leatherjackets	4/2/2022	21	23	26	0.096	27.6477	-82.5967

Total PAHs in Fish



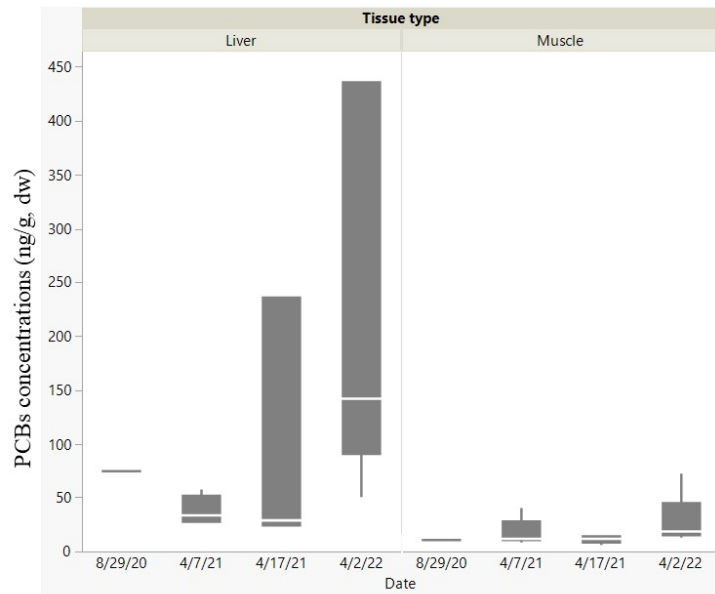
Murawski Figure 1. Total PAH in fish

Total Organochlorine Pesticides in Fish



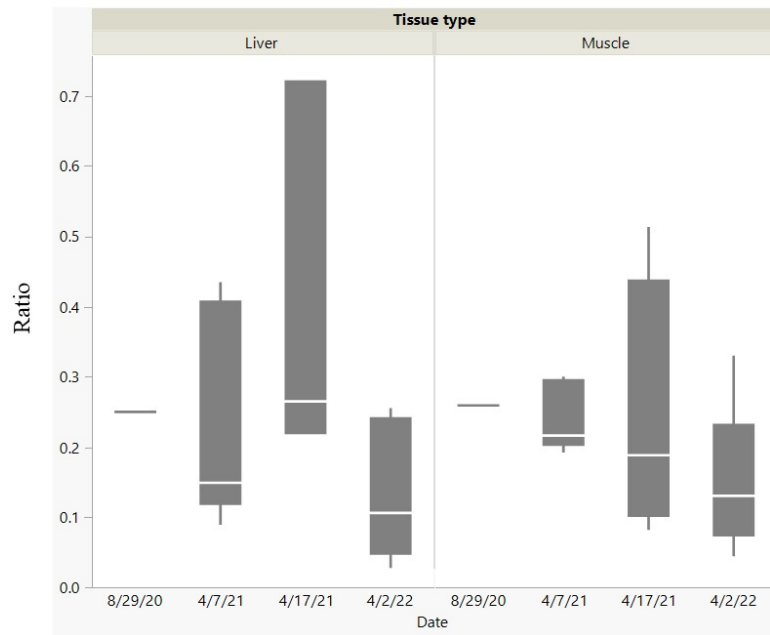
Murawski Figure 2. Total Organochlorine pesticides in fish

Polychlorinated Biphenyls in Fish



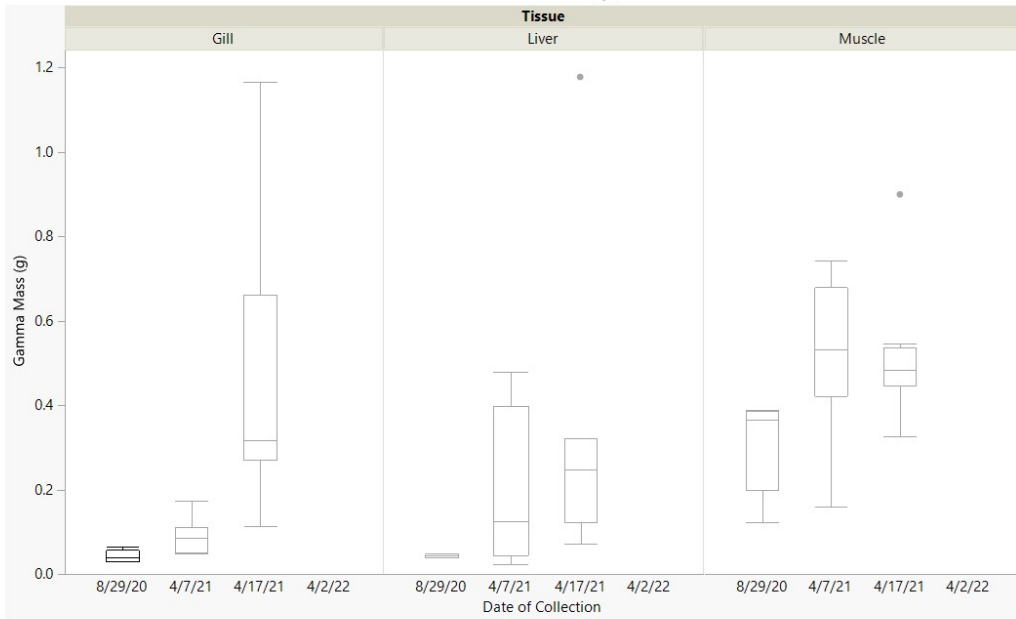
Murawski Figure 3. Polychlorinated biphenyls in fish

HMW/LMW PAHs in Fish



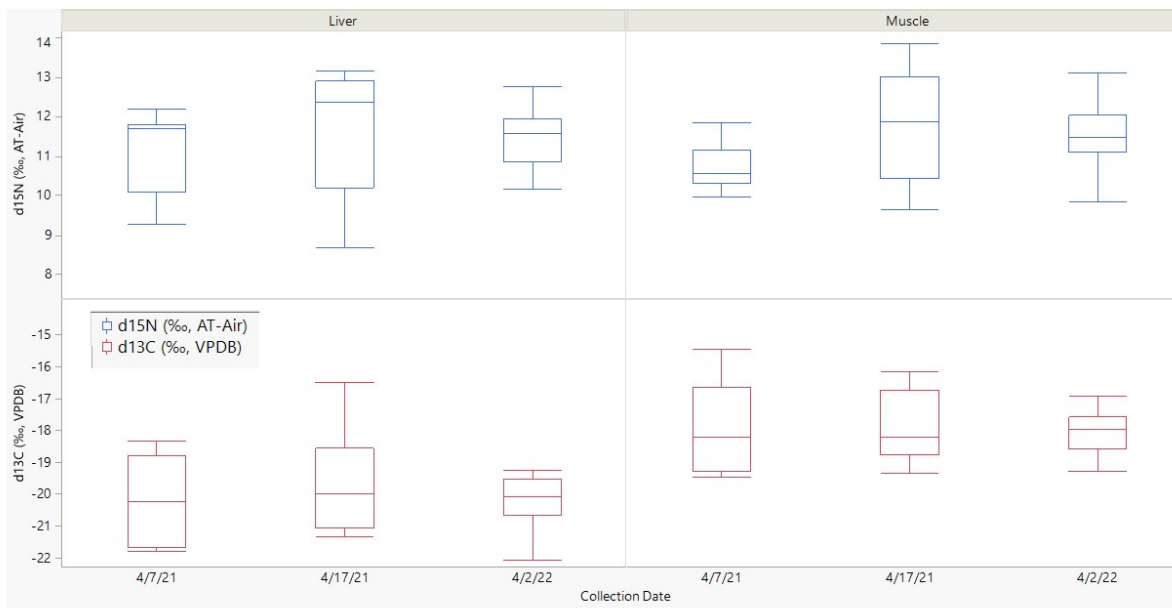
Murawski Figure 4. PAH ratios in fish

Gamma Mass (g) in Fish

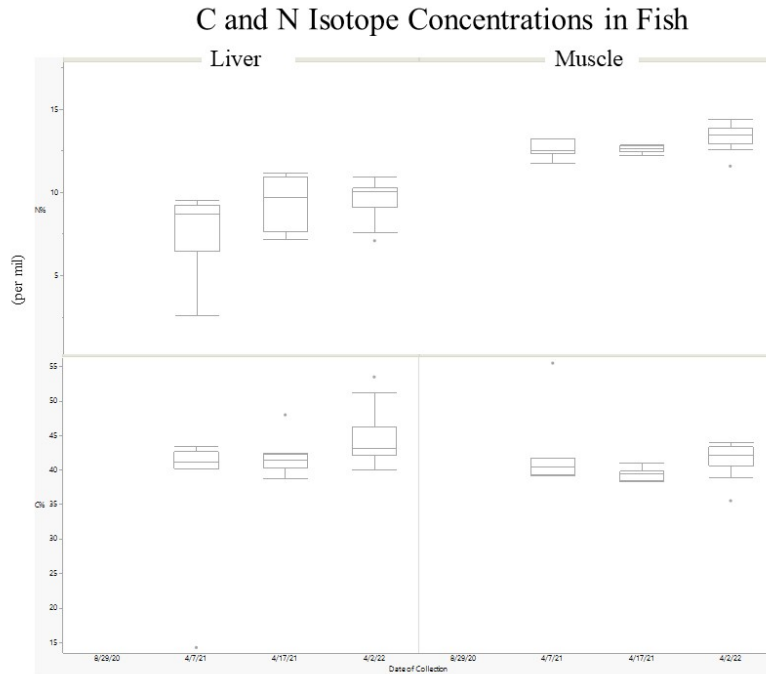


Murawski Figure 5. Radionuclide concentrations by tissue in all fish

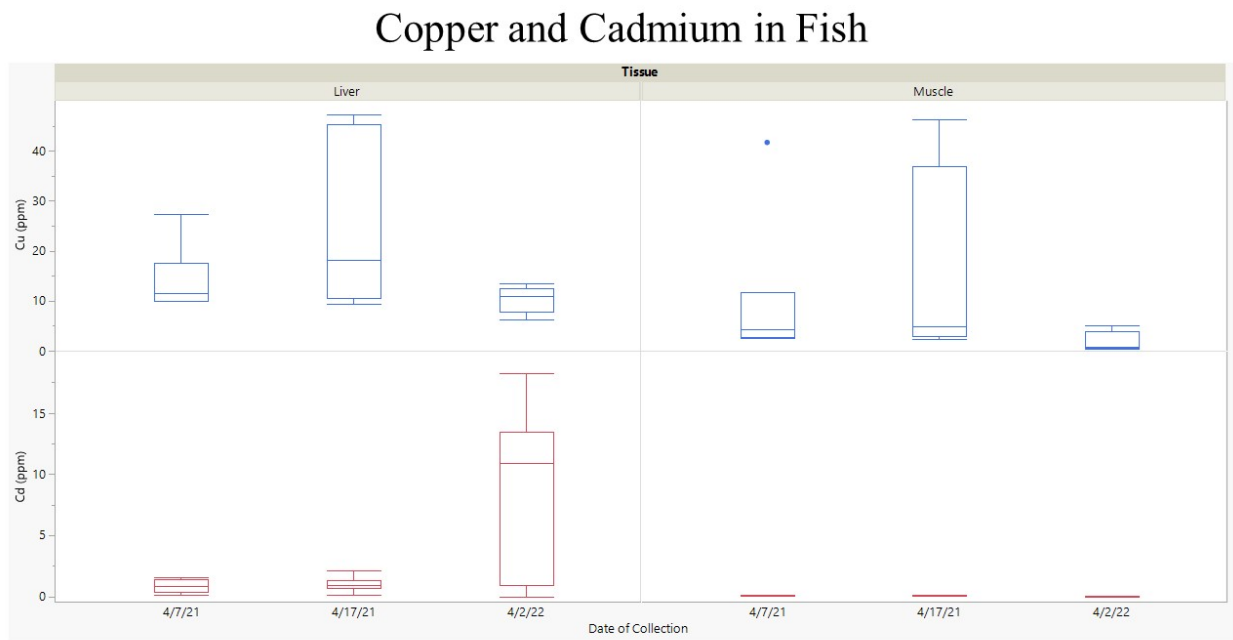
Delta 15N and delta 13C in Fish



Murawski Figure 6. Stable isotope ratios for N and C liver and muscle from all fish.

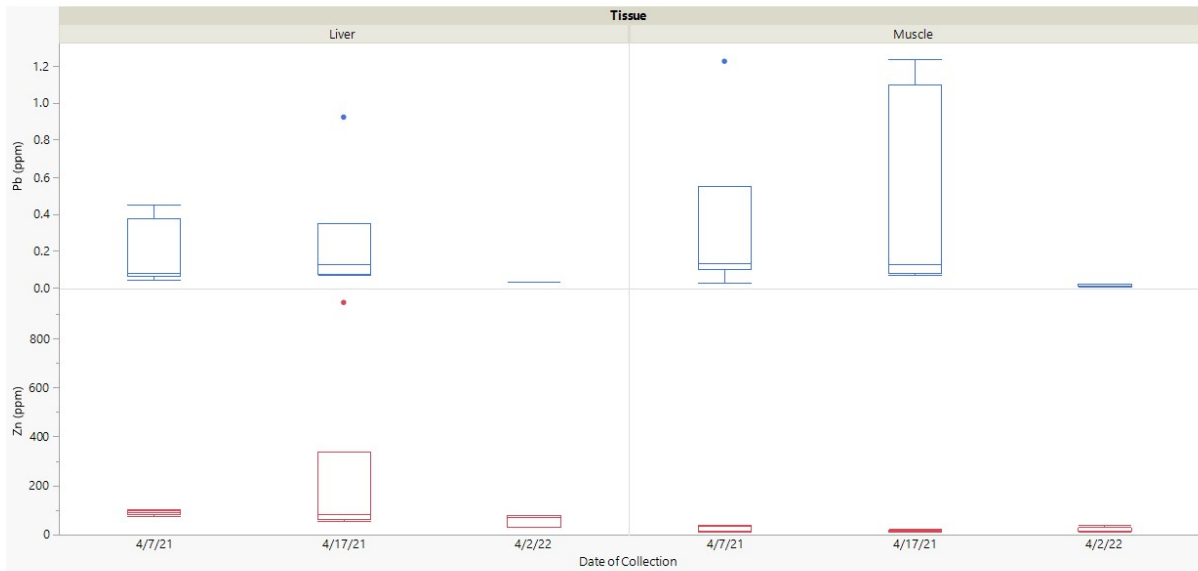


Murawski Figure 7. N and C concentrations in fish liver and muscle from all specimens.



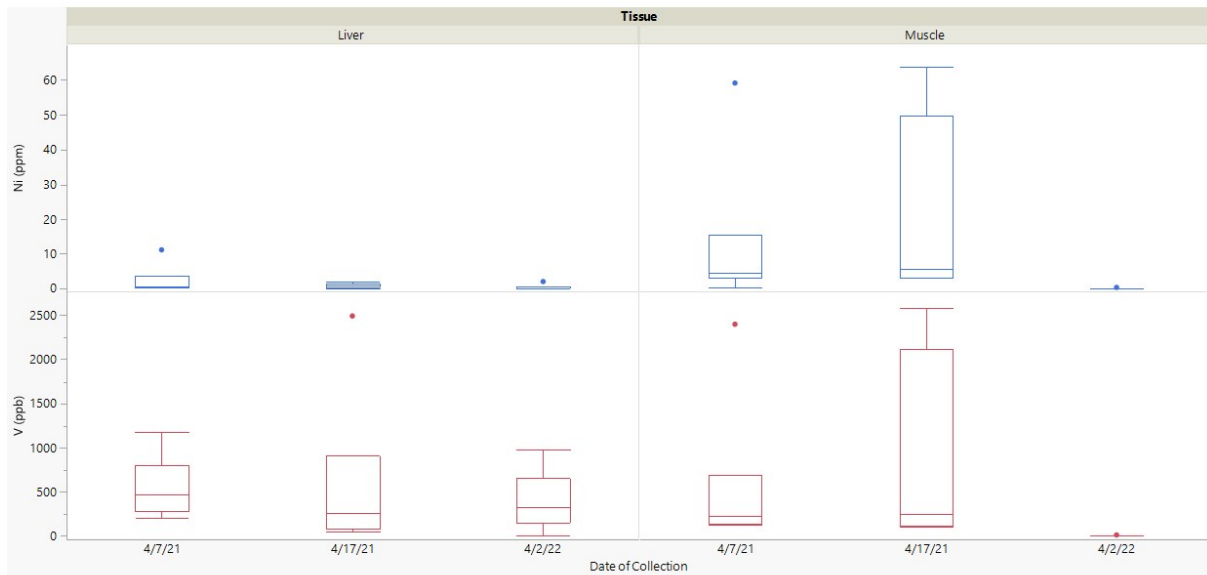
Murawski Figure 8. Trace metals (copper and cadmium) fish liver and muscle from all specimens.

Lead and Zinc in Fish



Murawski Figure 9. Trace metals (lead and zinc) fish liver and muscle from all specimens.

Nickel and Vanadium in Fish



Murawski Figure 10. Trace metals (nickel and vanadium) fish liver and muscle from all specimens.

References:

- Adhikari, P., Wong, R., and Overton, E. (2017). Application of enhanced gas chromatography/triple quadrupole mass spectrometry for monitoring petroleum weathering and forensic source fingerprinting in samples impacted by the Deepwater Horizon oil spill. *Chemosphere* 184, 939–950. doi:10.1016/j.chemosphere.2017.06.077.
- Appleby, P. G. (2001) Chronostratigraphic Techniques in Recent Sediments, Ch 9 In: Tracking Environmental Change Using Lake Sediments Volume 1. Editor Last WM, Smol JP. Kluwer Academic Publishers, The Netherlands.
- Ashoka, S., B.M. Peake, G. Bremner, K.J. Hageman, M.R. Reid. (2009). Comparison of digestion methods for ICP-MS determination of trace elements in fish tissues. *Anal. Chim. Acta*, 653 (2) (2009), pp. 191-199. 10.1016/j.aca.2009.09.025
- Beck, M. W., Altieri, A., Angelini, C., Burke, M. C., Chen, J., Chin, D. W., Gardiner, J., Hu, C., Hubbard, K. A., Liu, Y., Lopez, C., Medina, M., Morrison, E., Philips, E. J., Raulerson, G. E., Sclaro, S., Sherwood, E. T., Tomasko, D., Weisberg, R. H., & Whalen, J. (2022). Initial estuarine response to inorganic nutrient inputs from a legacy mining facility adjacent to Tampa Bay, Florida. *Marine Pollution Bulletin*, 178(February), 113598. <https://doi.org/10.1016/j.marpolbul.2022.113598>
- Brooks GR, Larson RA, Schwing PT, Romero I, Moore C, Reichart GJ, Jilbert T, Chanton J P, Hastings DW, Overholt WA, Marks KP, Kostka JE, Holmes CW, Hollander D (2015) Sedimentation Pulse in the NE Gulf of Mexico Following the 2010 DWH Blowout. *PLOSone* 10(7): 1-24.
- Coplen, T.B., Brand, W.A., Gehre, M., Gröning, M., Meijer, H.A.J., Toman, B. and Verkouteren, R.M. (2006), New Guidelines for $\delta^{13}\text{C}$ Measurements. *Analytical Chemistry* 2006 78 (7), 2439-2441 DOI: 10.1021/ac052027c
- Cutshall, N.H.; Larsen, I.L.; Olsen, C.R. Direct analysis of ^{210}Pb in sediment samples: self-absorption corrections. *Nuc. Inst. and Meth.*, 1983, 206: 309–312.
- Diercks, A.R., Romero, I.C., Larson, R.A., Schwing, P., Harris, A., Bosman, S., Chanton, J.P. and Brooks, G. (2021) Resuspension, Redistribution, and Deposition of Oil-Residues to Offshore Depocenters After the Deepwater Horizon Oil Spill. *Frontiers in Marine Science* 8.
- Holmes CW (1998) Short-lived Isotopic Chronometers – A Means of Measuring Decadal Sedimentary Dynamics. U.S. Geological Survey, Dept. of the Interior. Fact Sheet FS-073-98.
- Hussain N.; Kim G.; Church T.M.; Carey W. A simplified technique for gamma-spectrometric analysis of ^{210}Pb in sediment samples. *Appl. Radiat. Isot.*, 1996, 47: 473–477.
- Kitto, M.E. Determination of photon self-absorption corrections for soil samples, *Appl. Radiat. Isot.*, 1991, 42, 835-839.
- Romero, I.C., Judkins, H. and Vecchione, M. (2020) Temporal Variability of Polycyclic Aromatic Hydrocarbons in Deep-Sea Cephalopods of the Northern Gulf of Mexico. *Frontiers in Marine Science* 7.
- Romero, I. C., Sutton, T., Carr, B., Quintana-Rizzo, E., Ross, S. W., Hollander, D. J., et al. (2018). Decadal Assessment of Polycyclic Aromatic Hydrocarbons in Mesopelagic Fishes from the Gulf of Mexico Reveals Exposure to Oil-Derived Sources. *Environmental Science & Technology*. doi:10.1021/acs.est.8b02243.
- Romero, I. C., Schwing, P. T., Brooks, G. R., Larson, R. A., Hastings, D. W., Ellis, G., et al. (2015). Hydrocarbons in Deep-Sea Sediments following the 2010 Deepwater Horizon Blowout in the Northeast Gulf of Mexico. *PLOS ONE* 10, e0128371. doi:10.1371/journal.pone.0128371.

Sørensen, L., Meier, S., and Mjøs, S. A. (2016). Application of gas chromatography/tandem mass spectrometry to determine a wide range of petrogenic alkylated polycyclic aromatic hydrocarbons in biotic samples. *Rapid Communications in Mass Spectrometry* 30, 2052–2058. doi:10.1002/rcm.7688.

Swarzenski PW (2014) 210Pb Dating, In: *Encyclopedia of Scientific Dating Methods*. Springer Science and Business Media, Dordrecht, doi: 10.1007/978-94-007-6326-5_236-1.

Supplemental Information:



Port Manatee Sampling Location



Dr. Steven Murawski at Piney Point location for sample collection.



Drs. Rebekka Larson and Patrick Schwing sampling off Port Manatee, April 7, 2021.



Patrick Schwing sampling water chemistry in Port Manatee



Representative fishes sampled off Port Manatee, April 7, 2021



Representative fishes sampled off Port Manatee, April 17. 2021



R/V Weatherbird II sampling off Port Manatee on April 7, 2021.

VIII. Isabel Romero

Contaminants (165 organic molecules), elemental composition (%C, %N, ¹³ C, ¹⁵ N)	Sediments
Contaminants (165 organic molecules), elemental composition (%C, %N, ¹³ C, ¹⁵ N)	Zooplankton

Total budget: \$87,016

Activities during this period: The Biogeochemistry Group studied the chemical composition of zooplankton and sediment samples collected between 4/12/21 to 6/22/21. Zooplankton were selected as bioindicators of environmental conditions for this study because they play a key role in ecosystem functioning and are important entry points for contaminants such as SVOCs (semi-volatile organic chemicals), nutrients and trace metals into the food web. Sediments were studied because they are repository systems of water-column events, including contaminated organic matter. In particular, SVOCs are of interest because most are produced through anthropogenic processes, are toxic, ubiquitous, and persistent in the environment, and can pose a significant risk to organisms. A total of 29 zooplankton samples for 146 SVOCs (polycyclic aromatic hydrocarbons-PAHs, oxidized-PAHs organochlorinated pesticides-OCPs, and polychlorinated biphenyls-PCBs), elemental composition (d13C, d15N, %C, %N, %P), and trace metals (Fe, Cu, Co, Cd, Ni, Mn, Zn, Pb) were analyzed. Also, a total of 24 sediment samples were analyzed for 179 SVOCs (PAHs, oxidized-PAHs, OCPs, PCBs, aliphatics, and fecal sterols) and elemental composition (d13C, d15N, %C, %N).

In each cruise, zooplankton samples were collected using a ~4.5 m², 1 mm mesh Neuston net. Samples were rinsed with DI water and kept frozen until freeze-dried at the Marine Environmental Chemistry Laboratory (MECL, College of Marine Science, University of South Florida). Collected sediment samples were also freeze-dried before analyses.

Analysis of SVOCs:

Approximately 20-100 mg of freeze-dried and homogenized samples were extracted using an Accelerated Solvent Extraction system (ASE 200®, Dionex) under high temperature (100°C) and pressure (1500 psi) with hexane:dichloromethane (9:1 v:v). Deuterated and non-deuterated surrogate standards were obtained for PAHs (acenaphthene-d10, benz[a]anthracene d12, benzo[a]pyrene d12, dibenz[a,h]anthracene d14, fluoranthene d10, and phenanthrene d10; ISM-750-1, Ultra Scientific-Agilent, Santa Clara, CA, USA), oxidized-PAHs (2-naphthol d8, 1-nitronaphthalene d7, and 9-fluorenone d8; D-5648, D-5797, D-5442, CDN Isotopes, Pointe-Claire, QC, Canada), PCBs and OCPs (tetrachloro-m-xylene; Cat# 32027, Restek, Bellafonte, PA, USA; and biphenyl d10; Cat# 72058, Absolute Standards, Hamden, CT, USA), and aliphatics (*n*-pentacosane d32, D-3915, CDN Isotopes, Pointe-Claire, QC, Canada; tetracosane d50, IST-730-1, Ultra Scientific-Agilent, Santa Clara, CA, USA; *n*-dotriacontane d66, D-0973, CDN Isotopes, Pointe-Claire, QC, Canada).

For extraction in the ASE, we applied a one-step extraction and clean up procedure using a predetermined packing of the extraction cells (Kim et al., 2003; Choi et al., 2014; Romero et al., 2018) using a 6 ml extraction cell with glass fiber filter (pre-combusted at 450°C for 4 h), 5g silica gel (high purity grade, 100–200 mesh, pore size 30A, Sigma Aldrich, USA; pre-combusted at 450°C for 4 h, and deactivated 2%), and sand (pre-combusted at 450°C for 4 h). Organic extracts were concentrated to ~2 ml in a RapidVap (LABONCO RapidVap® Vertex™ 73200 series) and further concentrated to about 150 µl by gently blowing with a nitrogen stream. Two extraction control blanks were included with each set of samples (17 samples).

We followed modified EPA methods and QA/QC protocols (8270D, 8015C). Targeted compounds included polycyclic aromatic hydrocarbons (PAHs; 2-6 ring including alkylated homologs, 66 total PAHs), organochlorinated pesticides (OCPs; 36), polychlorinated biphenyls (PCBs; 32), biomarkers (3 fecal sterols), aliphatic hydrocarbons (C10-C37 *n*-alkanes and isoprenoid alkanes, 30 total aliphatics), and oxidized-PAHs (34 total oxidized-PAHs). SVOC compounds were quantified using GC/MS/MS (Agilent 7680B gas chromatograph coupled with an Agilent 7010 triple quadrupole mass spectrometer) in multiple reaction monitoring mode (MRM) to target multiple chemical fractions in one-run-step. Molecular ion masses for hydrocarbon compounds were selected from previous studies (Romero et al., 2015, 2018; Sørensen et al., 2016; Adhikari et al., 2017). All samples were analyzed in splitless injections, inlet temperature of 295°C, constant flow rate of 1 ml/min, and a MS detector temperature of 250°C using a Rxi-5sil chromatographic column. The GC oven temperature program was 60°C for 2 min, 60°C to 200°C at a rate of 8°C/min, 200°C to 300°C at a rate of 4°C/min and held for 4 min, and 300°C to 325°C at a rate of 10°C/min and held for 5 min. Source electron energy was operated at 70 eV, and argon was used as the collision gas at 1 mTorr pressure.

For accuracy and precision of analyses we included laboratory and analytical blanks, tuned MS/MS to PFTBA (perfluorotributylamine) daily, checked samples with a standard reference material (NIST 2779) daily, and reanalyzed sample batches when replicated standards exceeded $\pm 30\%$ of relative standard deviation (RSD), and/or when recoveries were low. Recovery ranged within QA/QC criteria of 50–130%, except for OCPs such as propachlor, simazine, atrazine, metribuzin, alachlor, metolachlor and cyanazine (with concentrations reported as semi-quantitative). Concentrations are reported as recovery corrected. Each analyte was identified using certified standards and performance was checked using a 5-point calibration curve. Quantitative determination of compounds was conducted using response factors (RFs) calculated from the certified standards. SVOC compounds are expressed as dry weight concentrations. Reference standards include SRM 2779 Gulf of Mexico Crude Oil (NIST, Gaithersburg, MD, USA), PAH standard mix (US-106-N-1, Agilent, Santa Clara, CA, USA), M-508.1-X1 and M-508.1-X2 (Accustandard, New Haven, CT, USA), oxidized-PAH standards (anthrone 319899, xanthone X600, 9,10-phenanthrenequinone 275034, 1-naphthol N1000, 2-naphthol 185507, 9-hydroxyfluorene H31204, 2-naphthaldehyde N206, 9-fluorenone F1506, 1,4-naphthoquinone 152757, 1-nitronaphthalene 103594, and 9-hydroxyphenanthrene 21128 from Sigma Aldrich, St. Louis, MO, USA; and 9-nitrophenanthrene R-020N from Accustandard, New Haven, CT, USA); PCB Congener Mix #6 (C-CSA-06, Accustandard, New Haven, CT, USA), and fecal sterol standards (epi-coprostanol C2882, and cholestanol 47129, Sigma Aldrich, St. Louis, MO, USA, and coprostanol/cholesterol, 92266, Absolute Standards, Hamden, CT, USA).

Elemental Analysis:

Nitrogen and carbon isotope and bulk composition were measured by CF-EA-IRMS (Continuous Flow Elemental Analyzer Isotope Ratio Mass Spectrometry) at the University of South Florida College of Marine Science Marine Environmental Chemistry Laboratory using commonly accepted procedures (Werner et al 1999). Isotope compositions were measured on a ThermoFinnigan Delta+XL IRMS, are reported in per mil (‰) notation and are scaled to VPDB (d13C) and AT-Air (d15N). Secondary reference materials (NIST 8574 d13C = +37.63 \pm 0.10‰, d15N = +47.57 \pm 0.22 ‰, N = 9.52%, C = 40.81%, C:N (molar) = 5.0; NIST 8573 d13C = -26.39 \pm 0.09‰, d15N = -4.52 \pm 0.12‰ N = 9.52%, C = 40.81%, C:N (molar) = 5.0) were used to normalize raw measurements to the VPDB (d13C) and AT-Air (d15N) scales (Werner et al

2002, Qi et al 2002, Coplen et al 2006) and to calibrate elemental N, C and C:N. Measurement uncertainties, expressed as ± 1 standard deviation of $n=12$ measurements of a laboratory reference material (NIST2702 $d_{13}C = -24.49 \pm 0.09\text{‰}$, $d_{15}N = 5.95 \pm 0.25\text{‰}$, $\%N = 0.26 \pm 0.06\%$, $\%C = 3.11 \pm 0.01\%$, C:N (molar) = 13.84 ± 0.53) were $\pm 0.15\text{‰}$ for $d_{13}C \pm 0.22\text{‰}$ for $d_{15}N$, $\pm 2.87\%$ RSD for $\%N$, $\pm 3.02\%$ RSD for $\%C$, and $\pm 4.50\%$ RSD for C:N.

Trace Metal Analysis:

Samples were digested following Ashoka et al (2009) for trace metal analysis. Briefly, 0.1-0.2 mg dry tissue was placed in a 15ml trace-metal clean centrifuge tube with 1.5 ml trace-metal grade nitric acid, 1.5ml ultra-pure water and 1.0ml trace-metal grade hydrogen peroxide. Samples were sealed and placed in a 900W microwave for 7 minutes at 30% power followed by a 10 minute cool-down. This was repeated two additional times prior to dilution with 11 ml of ultra-pure water. A 1.0 ml aliquot of the sample digest was transferred to a second 15 ml trace-metal clean centrifuge tube and diluted with 4.0 ml 2% trace-metal grade nitric acid with a 1.0 ppb Y internal standard prior to analysis. Six digest blanks and six control samples (NIST 1577b) were included in the digestion procedure.

Elemental concentrations were measured with a Thermo ElementXR High-Resolution-ICP-MS using a 100 μ l/min PFA nebulizer, cyclonic spray chamber and quartz torch. A 5-point signal-to-concentration calibration was established with a laboratory multi-element calibration standard gravimetrically prepared from SPEX-Certiprep single-element standards. Acquisition was performed in Medium Resolution ($R=4250$) and normalized to the Yttrium internal standard prior to blank and dilution correction. Elemental concentrations are reported in μ g/g (AL, Mn, Fe, Ni, Cu, Zn, Cd, Pb), ng/g (Co, V) and percent (P). Digestion yields (% recovery) and measurement uncertainty (%RSD) based on $n=6$ NIST1577b control standards were: Al 79% recovery, 112% RSD; P: 81% recovery; 21% RSD; V: 66% recovery; 17% RSD; Mn: 87% recovery; 5% RSD; Fe: 85% recovery; 7% RSD; Co: 74 % recovery; 9% RSD; Cu: 67% recovery; 23% RSD; Zn: 82% recovery; 8% RSD; Cd: 84% recovery; 4% RSD; Pb 56% recovery; 31% RSD.

Deliverables produced:

- SVOC concentrations in zooplankton samples collected from surface waters (April 12, 2021; 5 stations; 148 analytes: OCPs, PAHs, Oxidized-PAHs, PCBs; **Table Romero-1**)
- Elemental composition in zooplankton samples collected from surface waters (April 12, 2021; 5 stations)
- Trace metals concentrations in zooplankton samples collected from surface waters (April 12, 2021; 3 stations)
- SVOC concentrations in sediment samples (April 7, 2021; 6 stations; 181 analytes: OCPs, PAHs, Oxidized-PAHs, PCBs, aliphatics, and fecal-sterols; **Table Romero-1**)
- Elemental composition in sediment samples (April 7, 2021; 6 stations)
- SVOC concentrations in zooplankton samples collected from surface waters (April 29, 2021; 9 stations; 148 analytes: OCPs, PAHs, Oxidized-PAHs, PCBs; **Table Romero-1**)
- Elemental composition in zooplankton samples collected from surface waters (April 29, 2021; 9 stations)
- Trace metals concentrations in zooplankton samples collected from surface waters (April 29, 2021; 8 stations)

- SVOC concentrations in sediment samples (April 28, 2021; 6 stations; 181 analytes: OCPs, PAHs, Oxidized-PAHs, PCBs, aliphatics, and fecal-sterols; **Table Romero-1**)
- Elemental composition in sediment samples (April 28, 2021; 6 stations)
- SVOC concentrations in zooplankton samples collected from surface waters (May 27, 2021; 8 stations; 148 analytes: OCPs, PAHs, Oxidized-PAHs, PCBs; **Table Romero-1**)
- Elemental composition in zooplankton samples collected from surface waters (May 27, 2021; 7 stations)
- Trace metals concentrations in zooplankton samples collected from surface waters (May 27, 2021; 4 stations)
- SVOC concentrations in zooplankton samples collected from surface waters (June 22, 2021; 7 stations; 148 analytes: OCPs, PAHs, Oxidized-PAHs, PCBs; **Table Romero-1**)
- Elemental composition in zooplankton samples collected from surface waters (June 22, 2021; 7 stations)
- Trace metals concentrations in zooplankton samples collected from surface waters (June 22, 2021; 6 stations)
- SVOC concentrations in sediment samples (June 18, 2021; 12 stations; 181 analytes: OCPs, PAHs, Oxidized-PAHs, PCBs, aliphatics, and fecal-sterols; **Table Romero-1**)
- Elemental composition in sediment samples (June 18, 2021; 12 stations)

Table Romero-1. List of SVOCs (semi-volatile organic compounds) analyzed

Compound groups		
OCPs (N=36):	PAHs (N=46):	Oxidized-PAHs (N=34):
Alachlor	Naphthalene	1,4-naphthoquinone (+untargeted)
Aldrin	Acenaphthylene	1-naphthaldehyde (+untargeted)
Dieldrin	Acenaphthene	2-naphthaldehyde
Endrin	Fluorene	1-hydroxynaphthalene (+untargeted)
Endrin aldehyde	Dibenzothiophene	2-hydroxynaphthalene
Atrazine	Phenanthrene	1-nitronaphthalene (+untargeted)
a-HCH	Anthracene	2-nitronaphthalene
b-HCH	Fluoranthene	9-fluorenone (+untargeted)
g-HCH	Pyrene	9,10-anthrone (+untargeted)
d-HCH	Retene	2-nitrofluorene (+untargeted)
Chlorobenzilate	Benz[a]anthracene	9-xanthone (+untargeted)
Chloroneb	Chrysene	9-nitroanthracene (+untargeted)
Chlorothalonil	Benzo[b]fluoranthene	9-nitrophenanthrene (+untargeted)
g-Chlordane	Benzo[k]fluoranthene	2,3-hydroxyphenanthrene (+untargeted)
a-Chlordane	Benzo(e)pyrene	4,9-hydroxyphenanthrene
Cyanazine	Benzo[a]pyrene	9,10-phenanthroquinone (+untargeted)
DCPA	Perylene	3-nitrofluoranthene (+untargeted)
DDE	Benzo[g,h,i]perylene	1-nitropyrene (+untargeted)
DDD	Indeno[1,2,3]pyrene	6-nitrochrysene (+untargeted)
DDT	Dibenz[a,h]anthracene	6-nitrobenzo(a)pyrene (+untargeted)
Endosulfan I	C1-C4 naphthalene	PCBs (N=32):
Endosulfan II	C1-C3 fluorene	Dichlorobiphenyls
Endosulfan sulfate	C1-C4 dibenzothiophene	Trichlorobiphenyls
Etridiazole	C1-C4 phenanthrene-anthracene	Tetrachlorobiphenyls
Heptachlor	C1-C4 fluoranthene-pyrene	Pentachlorobiphenyls
Heptachlor epoxide	C1-C4 benz[a]anthracene-chrysene	Hexachlorobiphenyls
Hexachlorobenzene	C1-C3 benzopyrene-perylene	Heptachlorobiphenyls
Hexachlorocyclopentadiene	Aliphatics (N = 30):	Fecal Sterols (N=3):
Methoxychlor	<i>n</i> C10 - <i>n</i> C37	Coprostanol/epi-coprostanol
Metolachlor	Pristane	Cholestanol
Metribuzin	Phytane	Cholesterol
Propachlor		

Discussion of findings:**Zooplankton**

The concentration of all SVOCs and specific compound groups (PAHs, oxidized-PAHs, OCPs, and PCBs) determined in the zooplankton samples during this study (four cruises: 4/12/21, 4/29/21, 5/27/21, and 6/22/21) are shown in **Figure Romero-1**. All compound groups, except PCBs, showed a similar trend over time, with a spike in concentration observed on 4/29/21 relative to 4/12/21. Specifically, a 3-, 5-, and 14-fold increase in OCPs, Oxidized-PAHs, and PAHs, respectively, were found between 4/12/21 and 4/29/21. PCBs showed a small change of about 1.3-fold increase between 4/12/21 and 4/29/21. The temporal trend in the concentration of

SVOCs (**Figure Romero-1**) suggests an episodic contamination event. This observed trend is supported by the temporal change in lipid normalized concentrations (**Figure Romero-2**), some compounds (**Figure Romero-3, -4, -5, -6**), and specific compound ratios (**Figure Romero-7**). For example, since 4/29/21, HMW PAHs (4-6 ring PAHs), banned pesticides, and Di- and Tri-PCBs (all banned since 1980) increased in concentrations (**Figure Romero-7**), indicating a larger input from industrial operations in the studied area. Overall, the average concentrations observed on 4/29/21 (**Table Romero-2, Figure Romero-1, Figure Romero-2**) for PAHs and OCPs (specifically current-use pesticides or others such as Endosulfan II) are in the same range found in other contaminated areas (West et al. 2011, Balmer et al. 2019, Zebral et al. 2021).

Table Romero-2. Average concentrations (\pm SE) for SVOCs and compound groups for each sampling date. Concentrations shown as ng/g, dw (dry weight normalized concentrations).

	Sampling date			
	4/12/21	4/29/21	5/27/21	6/22/21
No. stations analyzed	5	9	7	7
SVOCs (ng/g, dw)	1890.6 \pm 1440.6	11017.0 \pm 6294.4	12129.6 \pm 5416.7	27882.9 \pm 22636.0
PAHs (ng/g, dw)	258 \pm 69.7	3666 \pm 2943.1	1090 \pm 292.1	777 \pm 203.8
Oxidized-PAHs (ng/g, dw)	1586.0 \pm 1384.5	7235.0 \pm 3838.6	10940.0 \pm 5242.1	27033.0 \pm 22687.1
OCPs (ng/g, dw)	36.6 \pm 4.4	103.1 \pm 34.2	92.0 \pm 22.2	58.6 \pm 11.0
PCBs (ng/g, dw)	9.26 \pm 1.3	11.76 \pm 3.5	6.39 \pm 4.0	14.03 \pm 7.1

The delay observed in detecting higher concentrations of SVOCs in the zooplankton samples until 4/29/21 and not shortly after the release of stack water from the Piney Point facility (March 30th to April 9th, 2021) may be due to multiple factors such as exposure pathway (ingestion of food and/or absorption from the surrounding water), bioaccumulation rate, water circulation, and chemical properties of the compounds analyzed. We found that the bioaccumulation of SVOCs in zooplankton followed a spatial and temporal pattern similar to the water circulation hindcast developed for this study (<http://ocgweb.marine.usf.edu/~liu/Tracer/>). Specifically, the temporal trends of SVOCs were different among the three areas studied in Tampa Bay (Area 1: sites # 5 and 6, closest to Piney Point; Area 2: sites #1, 2, 3, 4, and 10, north of Piney Point; and Area 3: sites 7, 8, and 9, south of Piney Point) (**Figure Romero-8**). Higher SVOC concentrations were observed on 4/12/21 at Area 1, 4/29/21 at Area 2, and 6/27/21 and 6/22/21 at Area 3. Decreasing concentrations over time were observed in Area 2, while SVOC concentrations increased in Area 3, indicating SVOCs reached Area 2 towards the end of April and then reached Area 3 at the end of May and continued accumulating SVOCs towards the end of June (**Figure Romero-8**).

Altogether, the spatial and temporal variability of SVOCs in zooplankton followed the TBCOM simulated surface tracer concentration (**Figure Weisberg-7**).

The intrinsic chemical properties of the compounds analyzed further explained the temporal trends observed and the high variability among compounds. The octanol-water partitioning coefficient (log Kow) ranges from 1.7 to 7.7 in the compounds analyzed (**Figure Romero-9**). The relative concentration of compounds based on the log Kow coefficients also varied among the sampling dates (**Figure Romero-10**). A spike in the relative concentration of compounds with log Kow >4 was observed on 4/29/21, which decreased later, probably by sinking onto the seafloor due to their high affinity to bind with sediments. Compounds with log Kow <3 have a higher solubility and were observed to persist in the environment longer and probably beyond the sampling period of this study (**Figure Romero-11**). Therefore, based on the log Kow of

compounds, zooplankton were exposed to different SVOCs over the period covered in this study (see **Figure Romero-12**, as an example).

Additionally, SVOCs degradation products detected in zooplankton samples also denoted an episodic contamination event, indicating zooplankton were exposed to highly toxic products during this study (**Figure Romero-13**). Due to the increasing concentrations of degradation products observed over time, zooplankton were likely exposed to degradation products beyond the time period covered in this study. Both insecticides and degradation products targeted in this study (**Table Romero-1**) showed a spike in concentration on 4/29/21, but only insecticides decreased by 6/22/21 (**Figure Romero-13**). For PAHs, their oxidation products (oxidized-PAHs) showed an increase in concentration on 5/27/21 that continued to 6/22/21, indicating in situ degradation of SVOCs compounds, in particular for PAHs (**Figure Romero-13**). This was observed mostly for nitro-PAHs (**Figure Romero-11**) as products of PAH photooxidation. The temporal trend of elemental nutrients measured in zooplankton also suggests an episodic contamination event on 4/29/21 characterized by higher C:N and N:P ratios (**Figure Romero-14**). A temporal trend of increasing $\delta^{15}\text{N}$ values during the study period indicates more recycled nutrients in the environment (**Figure Romero-14**). In contrast, trace metal concentrations have different temporal trends than those observed for SVOCs (**Figure Romero-15**).

Altogether, results suggest the phosphate mining wastewater and marine dredge water from the Piney Point facility released into Tampa Bay is likely to be the source of the increased concentrations of SVOCs observed in zooplankton during the studied period.

Sediments

The concentration of all SVOCs and specific compound groups (PAHs, oxidized-PAHs, OCPs, and PCBs) measured in the sediment samples collected during this study (three cruises: 4/07/21, 4/28/21, and 6/18/21) are shown in **Figure Romero-16**. Compared to concentration values measured in zooplankton, SVOC concentrations in sediments were low and without a clear temporal trend (**Figure Romero-16**). Also, SVOC compound ratios and elemental nutrients measured in sediments did not have a clear temporal pattern (**Figure Romero-17**, **Figure Romero-18**).

In addition, naturally occurring SCVOCs were measured in sediments, such as aliphatics and fecal sterols, as indicators of carbon sources and sewage inputs to the marine environment. A temporal change in the concentration of aliphatics was not observed (**Figure Romero-19**). However, the composition of the organic matter settled on the seafloor showed a slight change towards the end of the study, with higher relative amounts of degraded (lower phyto/microbial ratio) marine inputs (higher marine ratio) (**Figure Romero-19**). In contrast, total fecal sterols and specific compounds measured in sediments showed a temporal trend similar to the SVOC concentrations detected in zooplankton, with a spike in concentration on 4/28/21 (**Figure Romero-20**). Even though the concentrations of fecal sterols were low, the temporal patterns observed indicate an episodic event during the studied period.

References:

Adhikari, P., Wong, R., and Overton, E. 2017. Application of enhanced gas chromatography/triple quadrupole mass spectrometry for monitoring petroleum weathering and forensic source fingerprinting in samples impacted by the Deepwater Horizon oil spill. *Chemosphere* 184, 939–950. doi:10.1016/j.chemosphere.2017.06.077.

- Ashoka, S., B.M. Peake, G. Bremner, K.J. Hageman, M.R. Reid. 2009. Comparison of digestion methods for ICP-MS determination of trace elements in fish tissues. *Anal. Chim. Acta*, 653 (2), pp. 191-199. 10.1016/j.aca.2009.09.025.
- Balmer et al., J.E. Balmer, A.D. Morris, H. Hung, L. Jantunen, K. Vorkamp, F. Riget, M. Evans, M. Houde, D.C.G. Muir. 2019. Levels and trends of current-use pesticides (CUPs) in the arctic: an updated review, 2010–2018. *Emerging Contaminants*, 5, pp. 70-88, 10.1016/j.emcon.2019.02.002.
- Coplen, T.B., Brand, W.A., Gehre, M., Gröning, M., Meijer, H.A.J., Toman, B. and Verkouteren, R.M. 2006. New Guidelines for $\delta^{13}\text{C}$ Measurements. *Analytical Chemistry* 2006 78 (7), 2439-2441 DOI: 10.1021/ac052027c.
- Diercks, A.R., Romero, I.C., Larson, R.A., Schwing, P., Harris, A., Bosman, S., Chanton, J.P. and Brooks, G. 2021. Resuspension, Redistribution, and Deposition of Oil-Residues to Offshore Depocenters After the Deepwater Horizon Oil Spill. *Frontiers in Marine Science*, <https://doi.org/10.3389/fmars.2021.630183>.
- Qi, H., Coplen, T. B., Geilmann, H., Brand, W. A. and Böhlke, J. K. 2003. Two new organic reference materials for $\delta^{13}\text{C}$ and $\delta^{15}\text{N}$ measurements and a new value for the $\delta^{13}\text{C}$ of NBS 22 oil. *Rapid Commun. Mass Spectrom.*, 17: 2483–2487. doi:10.1002/rcm.1219.
- Romero, I. C., Schwing, P. T., Brooks, G. R., Larson, R. A., Hastings, D. W., Ellis, G., et al. 2015. Hydrocarbons in Deep-Sea Sediments following the 2010 Deepwater Horizon Blowout in the Northeast Gulf of Mexico. *PLOS ONE* 10, e0128371. doi:10.1371/journal.pone.0128371.
- Romero, I. C., Sutton, T., Carr, B., Quintana-Rizzo, E., Ross, S. W., Hollander, D. J., et al. 2018. Decadal Assessment of Polycyclic Aromatic Hydrocarbons in Mesopelagic Fishes from the Gulf of Mexico Reveals Exposure to Oil-Derived Sources. *Environmental Science & Technology*. doi:10.1021/acs.est.8b02243.
- Romero, I.C., Judkins, H. and Vecchione, M. 2020. Temporal Variability of Polycyclic Aromatic Hydrocarbons in Deep-Sea Cephalopods of the Northern Gulf of Mexico. *Front. Mar. Sci.* 7:54; doi: 10.3389/fmars.2020.00054.
- Sørensen, L., Meier, S., and Mjøs, S. A. 2016. Application of gas chromatography/tandem mass spectrometry to determine a wide range of petrogenic alkylated polycyclic aromatic hydrocarbons in biotic samples. *Rapid Communications in Mass Spectrometry* 30, 2052–2058. doi:10.1002/rcm.7688.
- Werner, R. A. and Brand, W. A. 2001. Referencing strategies and techniques in stable isotope ratio analysis. *Rapid Commun. Mass Spectrom.*, 15: 501–519. doi:10.1002/rcm.258.
- Werner, R. A., Bruch, B. A. and Brand, W. A. 1999. ConFlo III – an interface for high precision $\delta^{13}\text{C}$ and $\delta^{15}\text{N}$ analysis with an extended dynamic range. *Rapid Commun. Mass Spectrom.*, 13: 1237–1241. doi:10.1002/(SICI)1097-0231(19990715)13:13<1237::AID-RCM633>3.0.CO;2-C.
- West, J. E., Lanksbury, J., and O'Neill, S. M. 2011. Control of toxic chemicals in Puget Sound phase 3: Persistent organic pollutants in marine plankton from Puget Sound.; Publication no. 11-10-002; Washington Department of Ecology: Olympia, WA.
- Zebral, Y.D., B.D.P. Righi, I.S. Abou Anni, A.L.V. Escarrone, M. Roza, C.E.D. Vieira, et al. 2021. Pollution levels and biomarker responses in zooplankton from three hydrographic regions of southern Brazil: an integrated approach for water quality monitoring. *J. Environ. Chem. Eng.*, 9 (5) Article 106180.

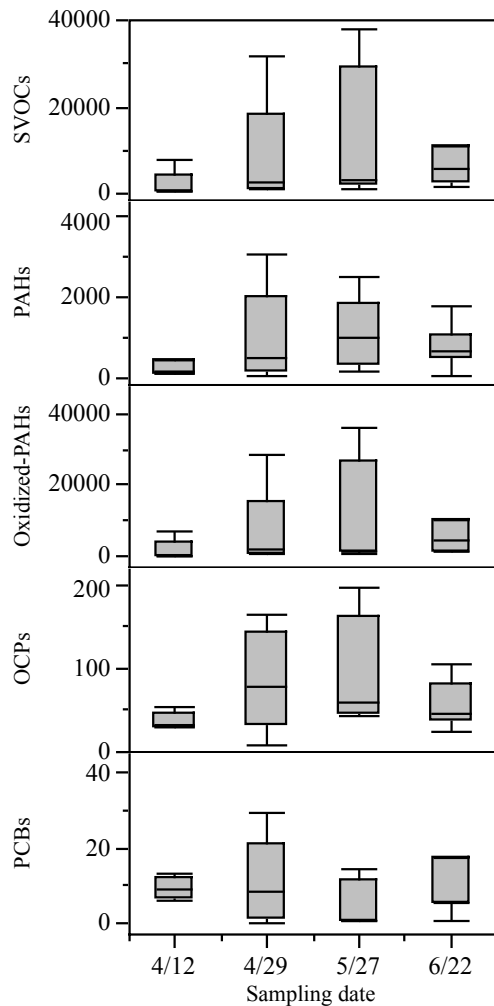


Figure Romero-1. Temporal assessment of semi-volatile organic compounds (SVOCs) and specific compound groups in zooplankton samples collected in Tampa Bay. Concentrations shown as ng/g, dw (dry weight normalized concentrations). PAHs: 2-6 ring polycyclic aromatic hydrocarbons; oxidized-PAHs: oxy-, nitro-, and hydroxy-PAHs (only targeted compounds); OCPs: organochlorinated pesticides such as insecticides, fungicides, and herbicides; and PCBs: 2-7 polychlorinated biphenyls. Graph shows shaded boxes as the interquartile ranges, with horizontal lines indicating median values and whiskers representing the 10th and 90th percentiles.

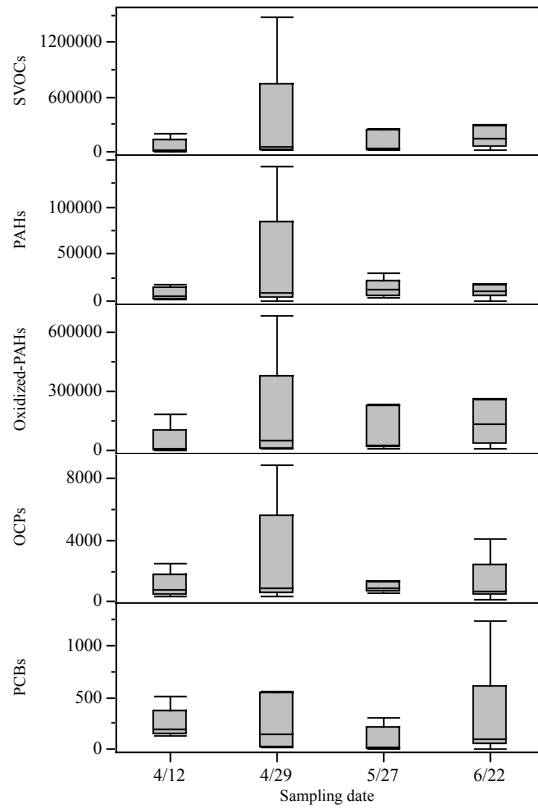


Figure Romero-2. Temporal assessment of semi-volatile organic compounds (SVOCs) and specific compound groups in zooplankton samples collected in Tampa Bay. Concentrations shown as ng/g, lw (lipid normalized concentrations). PAHs: 2-6 ring polycyclic aromatic hydrocarbons; oxidized-PAHs: oxy-, nitro-, and hydroxy-PAHs (only targeted compounds); OCPs: organochlorinated pesticides such as insecticides, fungicides, and herbicides; and PCBs: 2-7 polychlorinated biphenyls. Graph shows shaded boxes as the interquartile ranges, with horizontal lines indicating median values and whiskers representing the 10th and 90th percentiles.

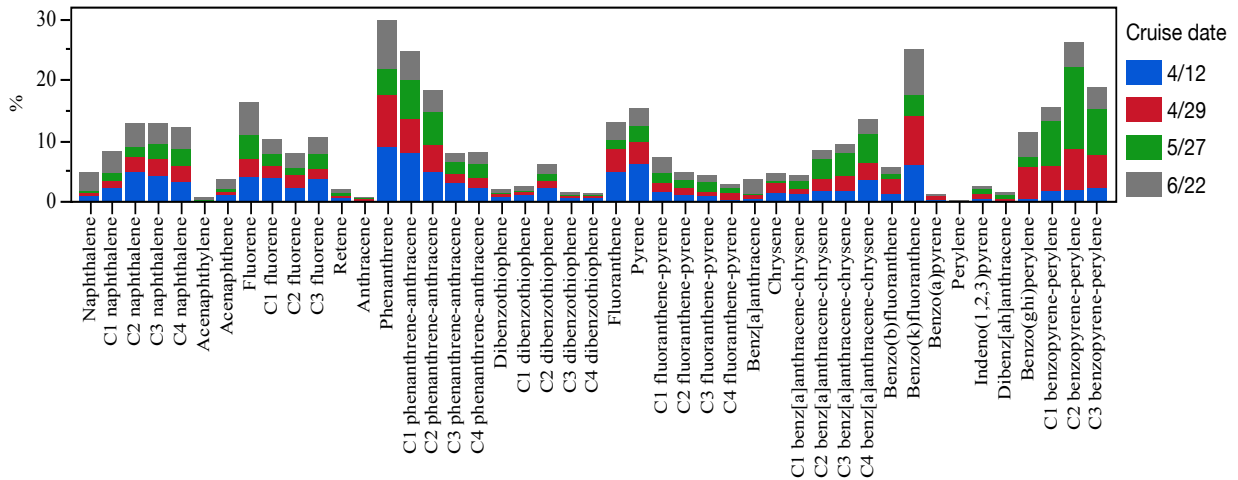


Figure Romero-3. Relative abundance of PAHs (polycyclic aromatic hydrocarbons) in zooplankton samples shown by cruise date. Cruise dates: 4/12/21, 4/29/21, 5/27/21, 6/22/21.

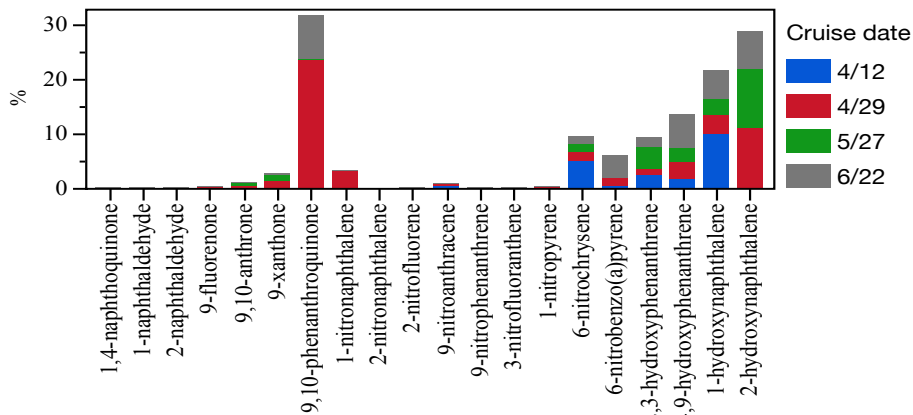


Figure Romero-4. Relative abundance of Oxidized-PAHs (targeted compounds) in zooplankton samples shown by cruise date. Cruise dates: 4/12/21, 4/29/21, 5/27/21, 6/22/21.

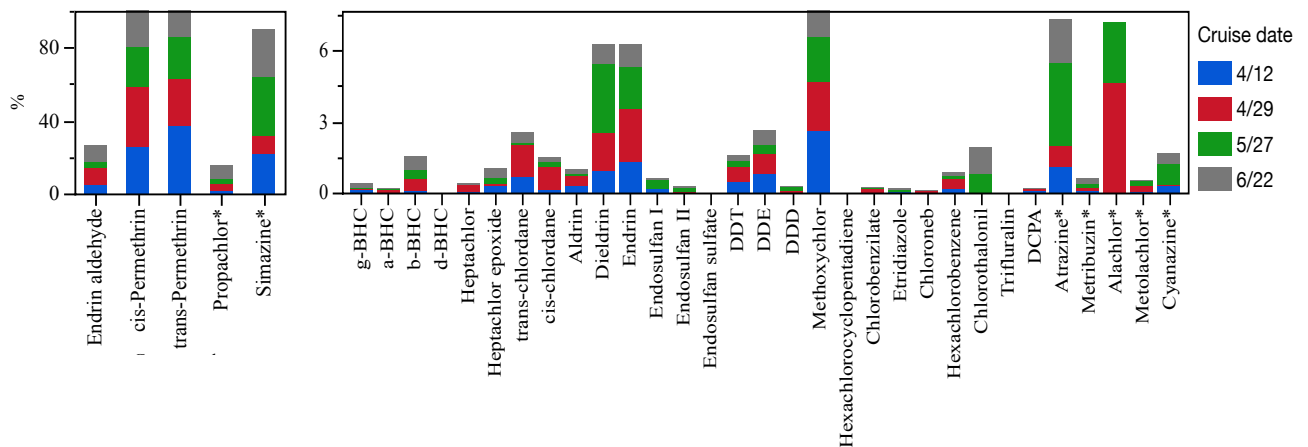


Figure Romero-5. Relative abundance of pesticides in zooplankton samples shown by cruise date. Cruise dates: 4/12/21, 4/29/21, 5/27/21, 6/22/21.

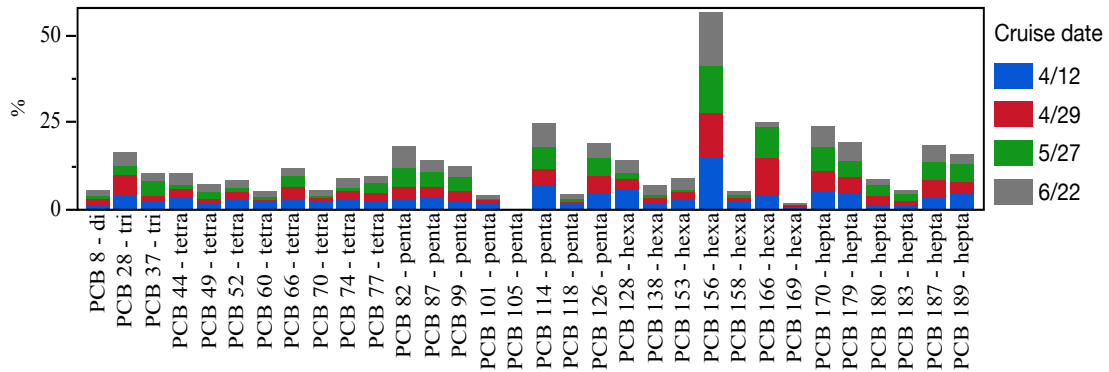


Figure Romero-6. Relative abundance of PCBs in zooplankton samples shown by cruise date. Cruise dates: 4/12/21, 4/29/21, 5/27/21, 6/22/21.

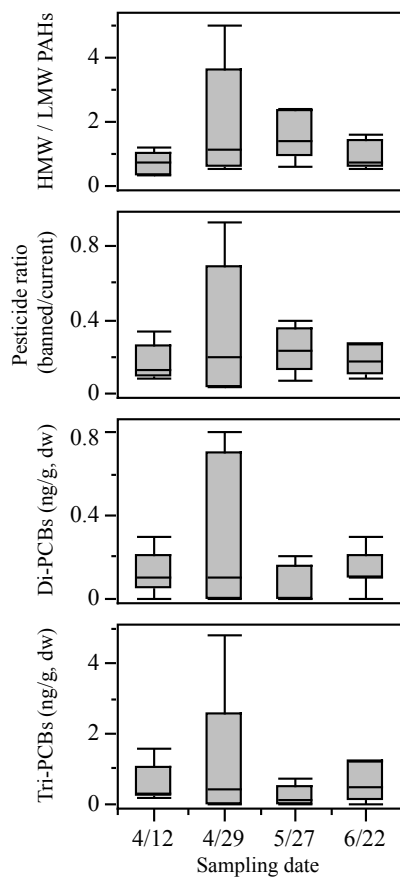


Figure Romero-7. Temporal variation of geochemical indicators of environmental change in zooplankton samples collected in Tampa Bay. HMW/LMW PAHs: 2-3 ring PAHs/4-6 ring PAHs; banned pesticides: Heptachlor, cis- and trans-Chlordane, Aldrin, Dieldrin, Endrin, Endosulfan I and II, DTT, Hexachlorocyclopentadiene, Chlorobenzilate, and Hexachlorobenzene; current-use pesticides: g-BHC, Methoxychlor, cis- and trans-Permethrin, Etridiazole, Chloroneb, Chlorothalonil, Trifluralin, DCPA, Propachlor, Simazine, Atrazine, Metribuzin, Alachlor, Metolachlor, and Cyanazine. Graph shows shaded boxes as the interquartile ranges, with horizontal lines indicating median values and whiskers representing the 10th and 90th percentiles.

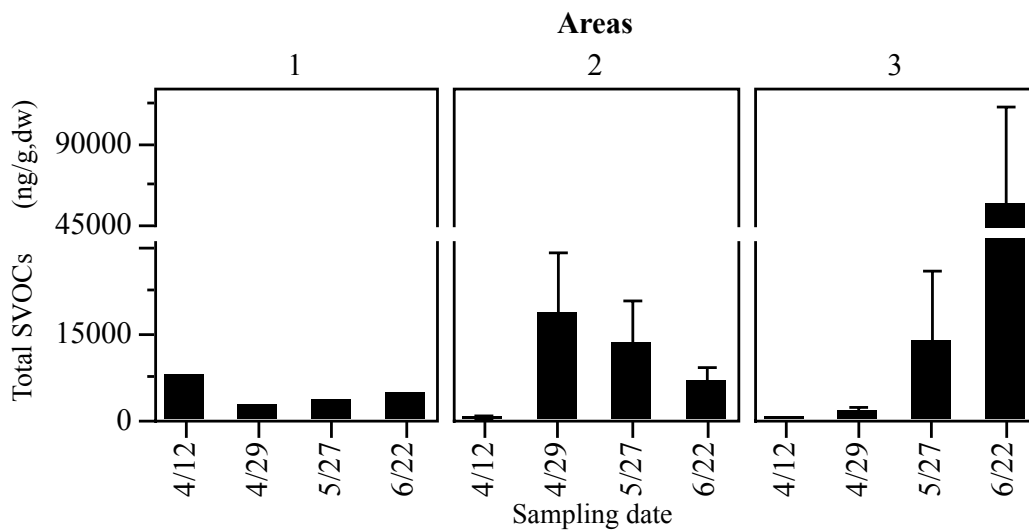


Figure Romero-8. Temporal changes of semi-volatile organic compounds (SVOCs) in zooplankton samples by sampling areas in Tampa Bay. Area 1: sites # 5 and 6, closest to Piney Point; Area 2: sites #1, 2, 3, 4, and 10, north of Piney Point; and Area 3: sites 7, 8, and 9, south of Piney. Data are shown as mean \pm SE.

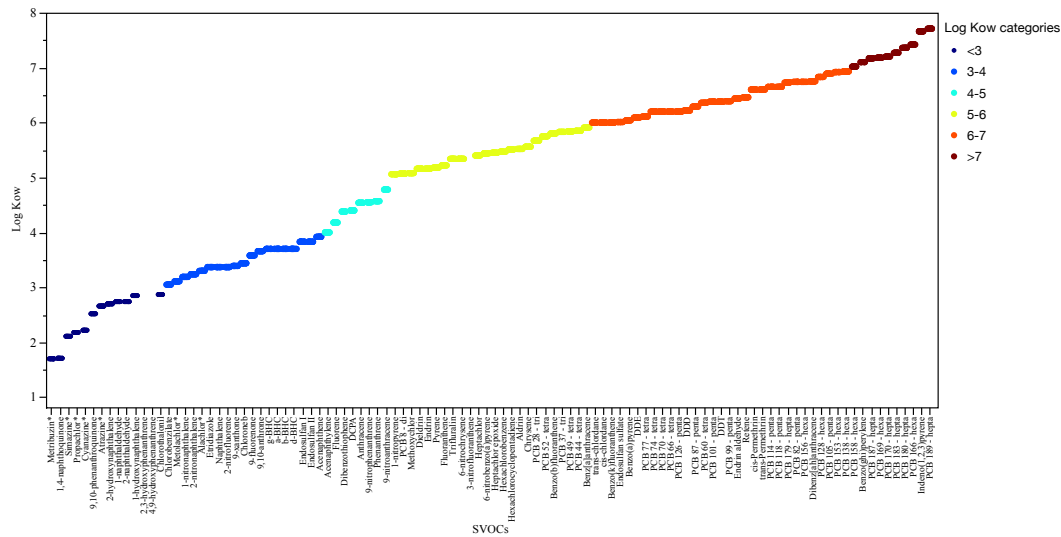


Figure Romero-9.
Log Kow for all

compounds analyzed in the zooplankton samples collected in Tampa Bay.

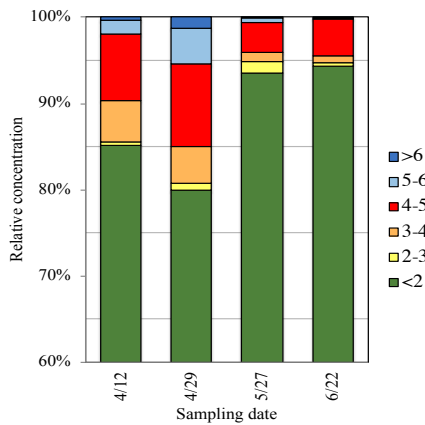


Figure Romero-10. Relative concentration (%) of SVOCs by their log Kow in each sampling date. SVOCs include: PAHs (2-6 rings), oxidized-PAHs (oxy-, nitro-, and hydroxy-PAHs), OCPs (insecticides, fungicides, and herbicides), and PCBs (2-7 polychlorinated biphenyls).

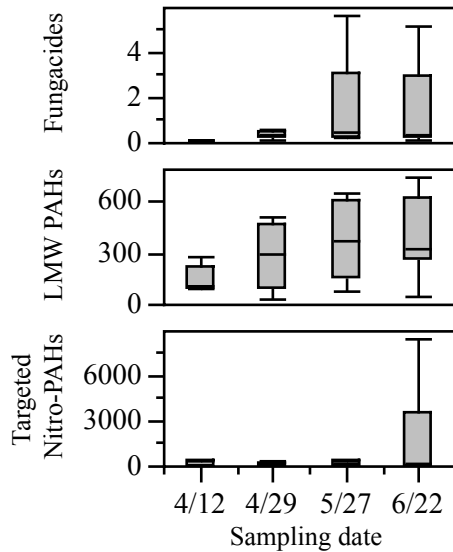


Figure Romero-11. Temporal variation of fungicides, LMW PAHs, and nitro-PAHs in zooplankton samples collected in Tampa Bay. Fungicides: Etridiazole, Chloroneb, Hexachlorobenzene, Chlorothalonil; LMW PAHs: 2-3 rings; nitro-PAHs (only targeted): 1-nitronaphthalene, 2-nitronaphthalene, 9-nitroanthracene, 9-nitrophenanthrene, 3-nitrofluoranthene, 1-nitropyrene, 6-nitrochrysene, 6-nitrobenzo(a)pyrene. Graph shows shaded boxes as the interquartile ranges, with horizontal lines indicating median values and whiskers representing the 10th and 90th percentiles.

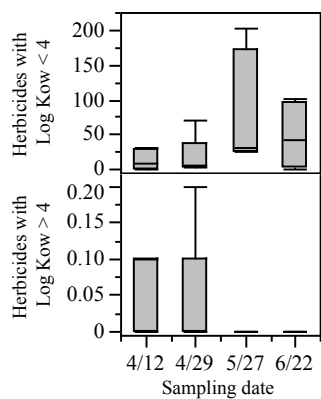


Figure Romero-12. Temporal variation of herbicides with log Kow <4 (Chlorothalonil, Etridiazole, Chloroneb) and >4 (Hexachlorobenzene) in zooplankton samples collected in Tampa Bay. Graph shows shaded boxes as the interquartile ranges, with horizontal lines indicating median values and whiskers representing the 10th and 90th percentiles.

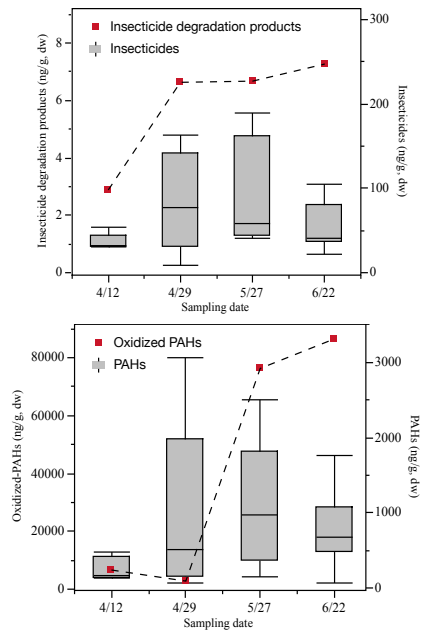


Figure Romero-13. Temporal variability of insecticides and PAHs, and some of their degradation products. Insecticide degradation products: a-BHC, b-BHC, d-BHC, Heptachlor epoxide, Endrin aldehyde, Endosulfan sulfate, DDE, and DDD. PAH degradation products: oxidized-PAHs (oxy-, nitro-, and hydroxy-PAHs). Graph shows shaded boxes as the interquartile ranges, with horizontal lines indicating median values and whiskers representing the 10th and 90th percentiles.

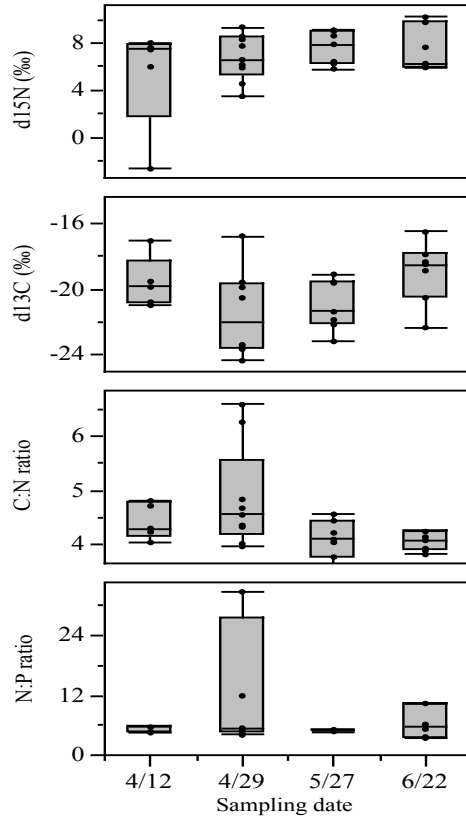


Figure Romero-14. Temporal variability of elemental nutrients in zooplankton samples collected in Tampa Bay. Graph shows shaded boxes as the interquartile ranges, with horizontal lines indicating median values and whiskers representing the 10th and 90th percentiles.

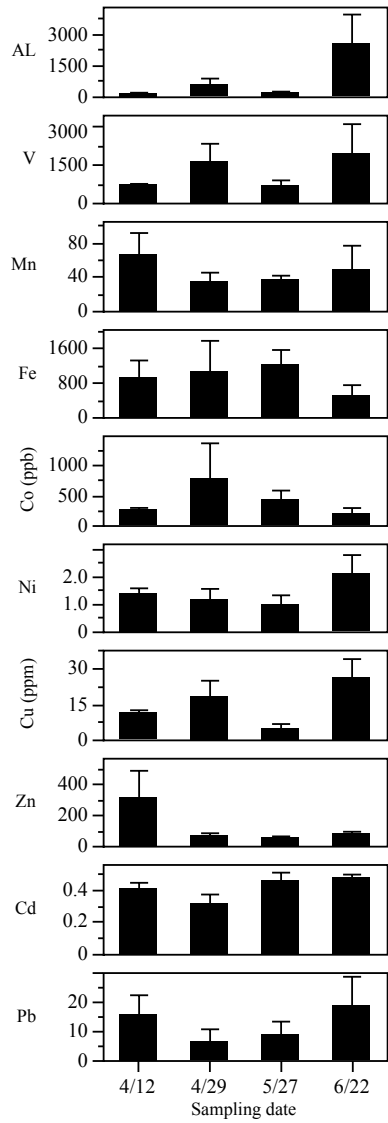


Figure Romero-15. Temporal variability of trace metals measured in zooplankton samples collected in Tampa Bay. Data are shown as mean \pm SE.

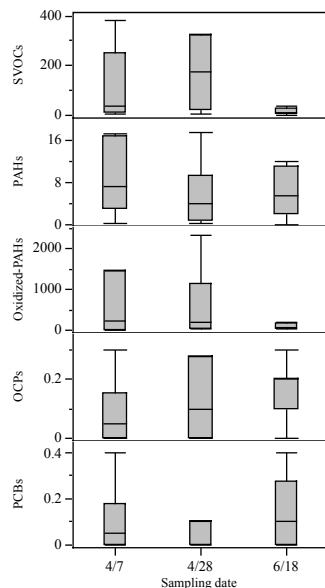


Figure Romero-16. Temporal assessment of semi-volatile organic compounds (SVOCs) and specific compound groups in sediment samples collected in Tampa Bay. Concentrations shown as ng/g, dw (dry weight normalized concentrations). PAHs: 2-6 ring polycyclic aromatic hydrocarbons; oxidized-PAHs: oxy-, nitro-, and hydroxy-PAHs (only targeted compounds); OCPs: organochlorinated pesticides such as insecticides, fungicides, and herbicides; and PCBs: 2-7 polychlorinated biphenyls. Graph shows shaded boxes as the interquartile ranges, with horizontal lines indicating median values and whiskers representing the 10th and 90th percentiles.

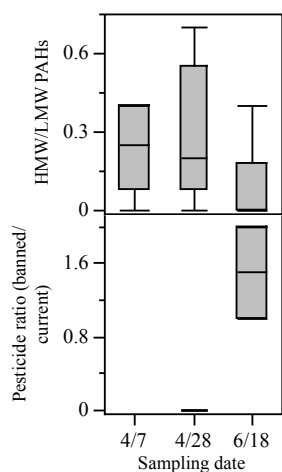


Figure Romero-17. Temporal variation of geochemical indicators of environmental change in sediment samples collected in Tampa Bay. HMW/LMW PAHs: 2-3 ring PAHs/4-6 ring PAHs; banned pesticides: Heptachlor, cis- and trans-Chlordane, Aldrin, Dieldrin, Endrin, Endosulfan I and II, DTT, Hexachlorocyclopentadiene, Chlorobenzilate, and Hexachlorobenzene; current-use pesticides: g-BHC, Methoxychlor, cis- and trans-Permethrin, Etridiazole, Chloroneb,

Chlorothalonil, Trifluralin, DCPA, Propachlor, Simazine, Atrazine, Metribuzin, Alachlor, Metolachlor, and Cyanazine. Graph shows shaded boxes as the interquartile ranges, with horizontal lines indicating median values and whiskers representing the 10th and 90th percentiles.

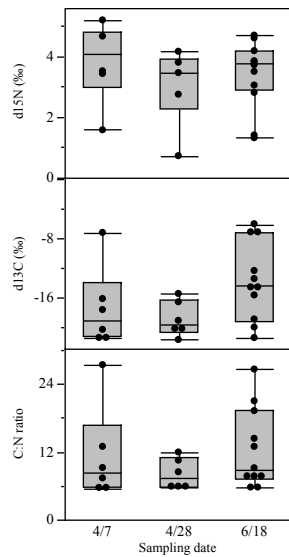


Figure Romero-18. Temporal variability of elemental nutrients in sediment samples collected in Tampa Bay. Graph shows shaded boxes as the interquartile ranges, with horizontal lines indicating median values and whiskers representing the 10th and 90th percentiles.

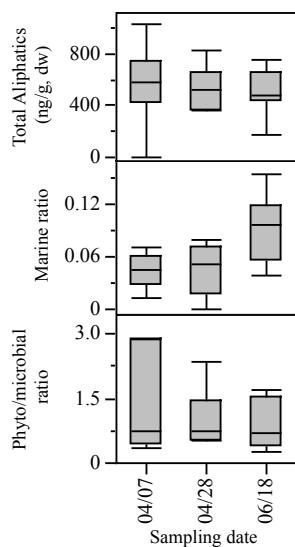


Figure Romero-19. Temporal assessment of aliphatics and ratios in sediment samples collected in Tampa Bay. Concentrations shown as ng/g, dw (dry weight normalized concentrations). Marine ratio: *n*-alkanes (C15,17,19)/(C9-32); phyto/microbial ratio: *n*-alkanes

(C15,17,19)/(C14,16,18). Graph shows shaded boxes as the interquartile ranges, with horizontal lines indicating median values and whiskers representing the 10th and 90th percentiles.

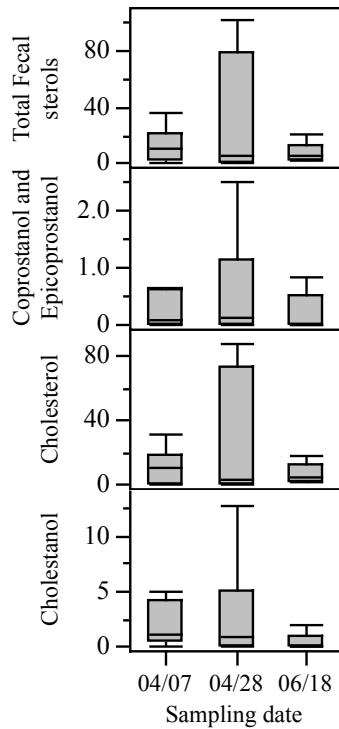


Figure Romero-20. Temporal assessment of fecal sterols and specific compounds in sediment samples collected in Tampa Bay. Concentrations shown as ng/g, dw (dry weight normalized concentrations). Graph shows shaded boxes as the interquartile ranges, with horizontal lines indicating median values and whiskers representing the 10th and 90th percentiles.

IX. Yonggang Liu, and Robert H. Weisberg

Hindcast models of discharge mixing and distribution, calibration of in situ sensor data

Total budget: \$75,000

Activities during this period:

The Ocean Circulation Lab performed realistic hindcast simulation of the circulation in the Tampa Bay and vicinity during the time period of March 30 – July 31, 2021. The Tampa Bay Coastal Ocean Model (TBCOM, Chen et al., 2018) was forced by NOAA NCEP winds and heat fluxes, and nested within the West Florida Coastal Ocean Model (WFCOM, Zheng and Weisberg, 2012) for tides, velocity, temperature and salinity at the open boundary. Both WFCOM and TBCOM are applications of unstructured grid Finite Volume Community Ocean Model (FVCOM), developed by University of Massachusetts Dartmouth (Chen et al., 2003). The TBCOM development was funded by the Pinellas County RESTORE Act Program, and continued with support by the College of Marine Science, University of South Florida, and other agencies, e.g., NOAA/IOOS through SECOORA, and NOAA COMIT.

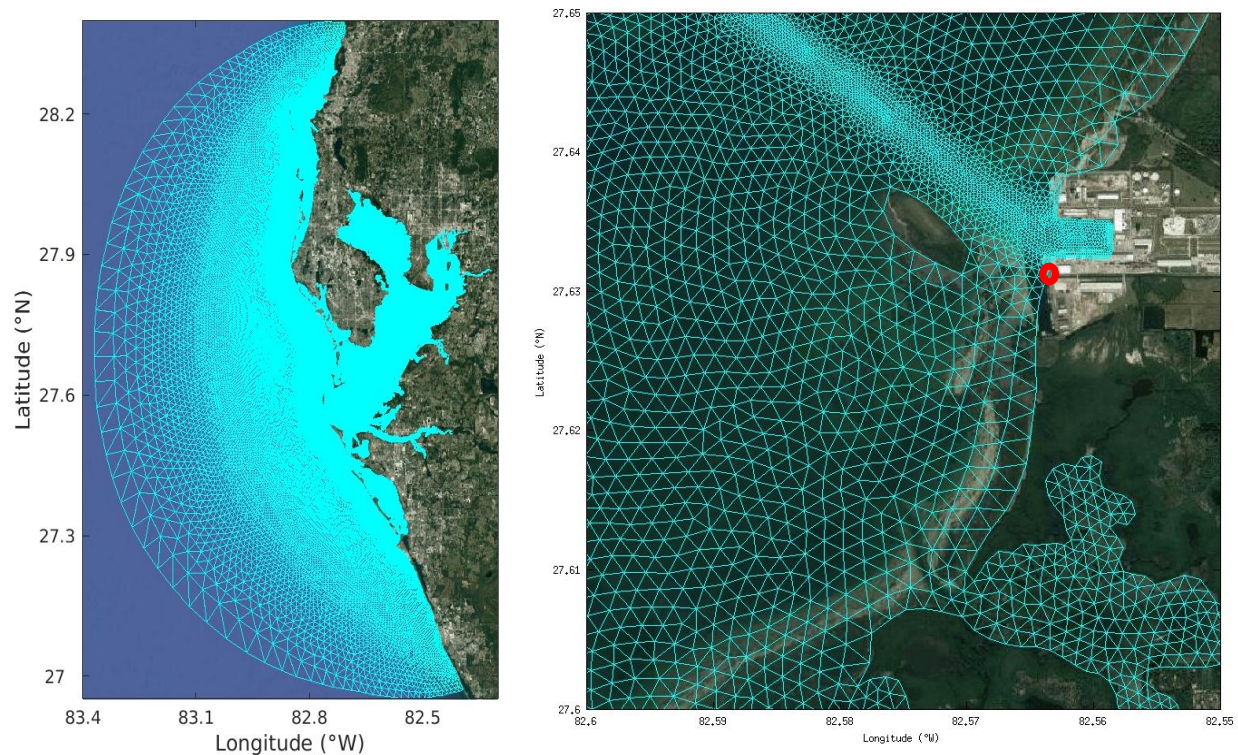


Figure Weisberg-1. Tampa Bay Coastal Ocean Model (TBCOM) grid (left) and a zoomed-in view of the grid near the discharge site (right).

Figure Weisberg-1 shows the entire TBCOM domain with the unstructured grid. TBCOM domain covers Tampa Bay, Sarasota Bay, the Intra-Coastal Water Way, and all of the inlets connecting these water bodies with the adjacent Gulf of Mexico. The model resolution increases from open boundary to the bay, with the highest resolution of up to 20 m in the ship channel areas (**Fig. Weisberg-1**). TBCOM was tested for veracity using in situ observations during the

extreme event of hurricane Irma in 2017 (Chen et al. 2018). The model was also diagnosed for momentum balances in a comprehensive dynamical analysis (Chen et al., 2019). Automated TBCOM circulation nowcast/forecast has been in operation since 2017 (<http://ocgweb.marine.usf.edu/~tbm/>). A short-term red tide tracking product has also been set up as a collaboration between the USF Ocean Circulation Lab and the Florida Wildlife Commission (FWC) and the Florida Wildlife Research Institute (FWRI), and the daily updated red tide product is publicly available online at <http://ocgweb.marine.usf.edu/tbm/hab/>.

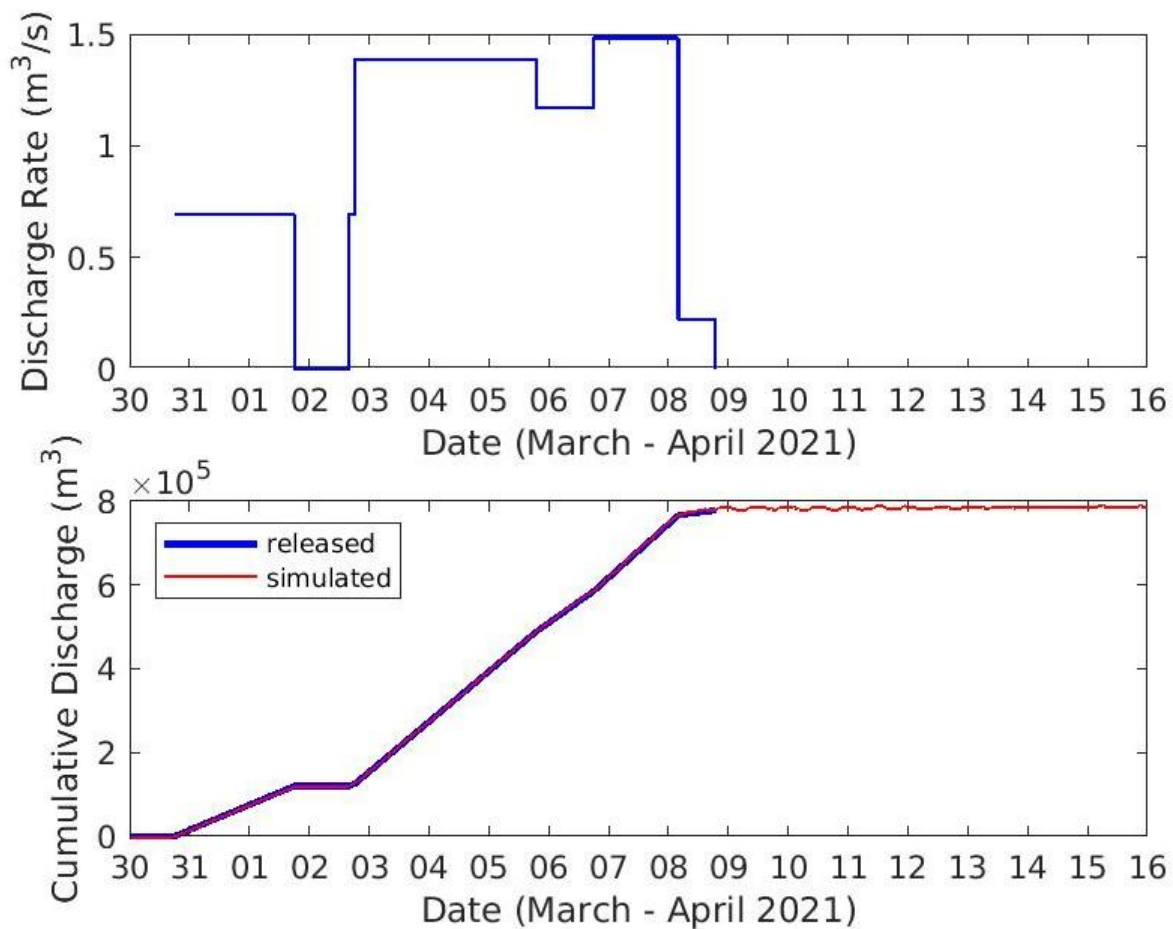


Figure Weisberg-2. Timeline of the Piney Point discharge rate (top) and cumulative discharge (released vs. model simulated total tracer mass).

FVCOM includes a dye module that simulates tracer concentration variations by advection and diffusion. The tracer serves as a virtual marker of the water mass in the model domain. It is transported from one place to another by advection and diluted through mixing with ambient water. The dye module conserves tracer mass by using a flux calculation of second-order accuracy to avoid numerical tracer loss (Chen et al., 2008). Several applications exist in the literature. As examples, Weisberg (2011) adopted it for simulating the flushing of a residential channel under the action of tides and winds. Lai et al. (2013) used it in tracking the radionuclide that flowed out of the Fukushima nuclear power plant. Zhu et al. (2015) applied it in a study of

the flushing processes in the Tampa Bay. Weisberg et al. (2016) employed the virtual tracer for examining the transport of the Deepwater Horizon hydrocarbons to the WFS. Recently, Liu et al. (2022) used it to examine the termination process of the 2018 red tide event. Here we use the FVCOM tracer module to study the Piney Point wastewater had been spread out within the Tampa Bay and flushed out of the bay over time.

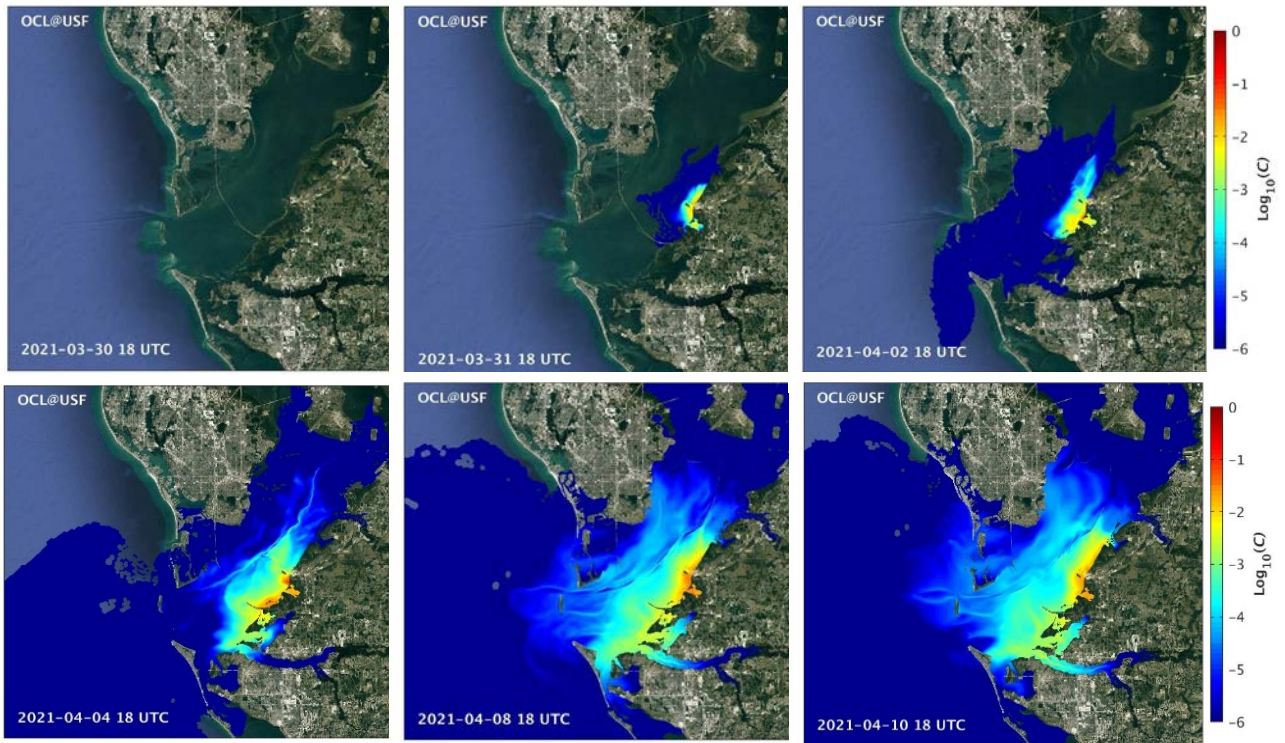


Figure Weisberg-3. Evolution of the Piney Point effluent plume during the initial days as shown by instantaneous snapshots of the surface tracer concentration simulated by the TBCOM tracer model.

The tracer module was implemented online with the TBCOM circulation model hindcast. Tracer was released on the node nearest to the end of the ditch where wastewater was discharged into Tampa Bay. Time series of realistic wastewater discharge rate during the Piney Point event were used in the tracer model (**Figure Weisberg-2**, top panel), which was similar to the daily nowcast/forecast but now more consistent in time. Discharge started at 20:00 UTC on 3/30/2021 at a rate of 11k GPM ($0.694 \text{ m}^3/\text{s}$). It stopped at 18:00 UTC on 4/1 and restarted at a rate of 22k GPM at 18:00 UTC on 4/2, with small variations. It finally ended at 19:00 UTC on 4/8/2021. The total wastewater discharge was $\sim 800,000 \text{ m}^3$. The comparison of cumulative discharge between the released and the model simulated demonstrates the perfect conservation of the total tracer mass in the model domain (**Figure Weisberg-2**, bottom panel).

In early April 2021, USF Ocean Circulation Lab also deployed three bottom mounts to monitor the time series of water quality at three locations to the south of the Piney Point near Port Manatee, under the Sunshine Skyway Bridge, and near the Manatee River mouth in the lower

Tampa Bay, respectively (**Figure Weisberg-4**). We used the water quality sensors from In Situ, Inc., model Aqua Troll 600 (**Figure Weisberg-5**). They are a type of low-cost water quality sensors. The locations of the three moorings are:

PP1: 27° 38.2096'N, 82° 34.9099'W
PP2: 27° 36.2771'N, 82° 37.8091'W
PP3: 27° 32.6733'N, 82° 39.8951'W

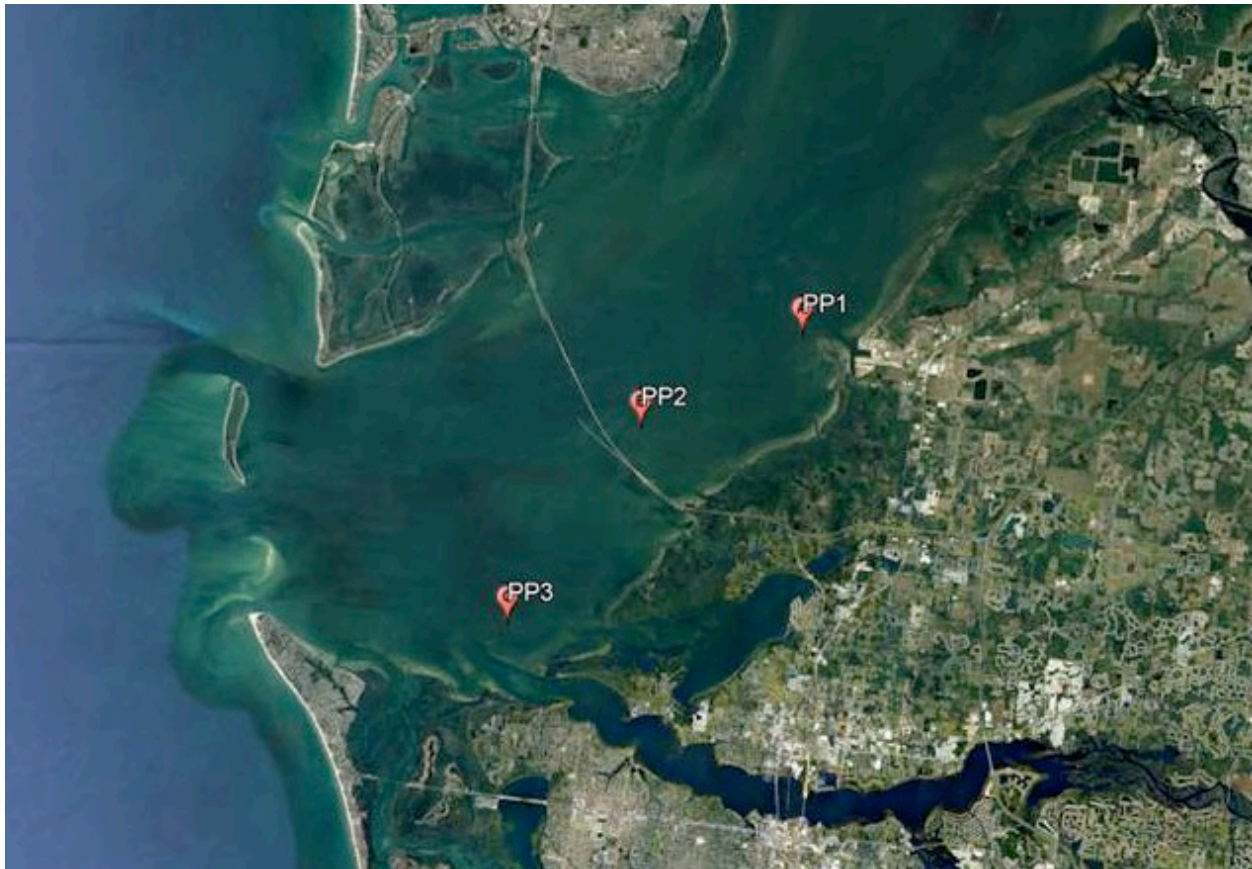


Figure Weisberg-4. Locations of the water quality bottom mount stations deployed during the Piney Point event.



Figure Weisberg-5. Images of the three water quality bottom mounts.

Effort has been made to calibrate and quality control the time series data, even recognizing that useable data may be of short duration. Due to heavy biofouling, only the first week of the data are considered acceptable and submitted along this report. Time series of water quality data (Chl-a, dissolved O₂, T & S) are shown in **Figure Weisberg-6**.

There were Chlorophyll-a concentration peaks at PP1 around April 8, 2021 (after a week's discharge). The Chl-a peaks at PP2 are lower than those at PP1 and lags in several hours. High Chl-a peaks at PP3 started even later around April 8, 2021, and continued to be much higher than those of the two northern sites.

Dissolved oxygen was much higher in PP1 than the other two stations during April 7 – 9, 2021, a week after the discharge started. However, the dissolved oxygen gradually decreased in the next three days (April 10 – 12, 2021). Decreasing trends are seen from both PP2 and PP3 dissolved oxygen records.

Water temperature records are consistent among the three stations, showing daily fluctuations and an increasing trend due to seasonal heating in April in this region. There is not obvious differences in near bottom temperature between the three stations.

Salinity records exhibit daily variations that may be associated with tidal fluctuations. The increase of salinity during April 9 – 10, 2021 may be related to the weather event – more

seawater were transported into and mixed with bay water. There was an overall decrease trend of salinity during this week (April 7 – 14, 2021).

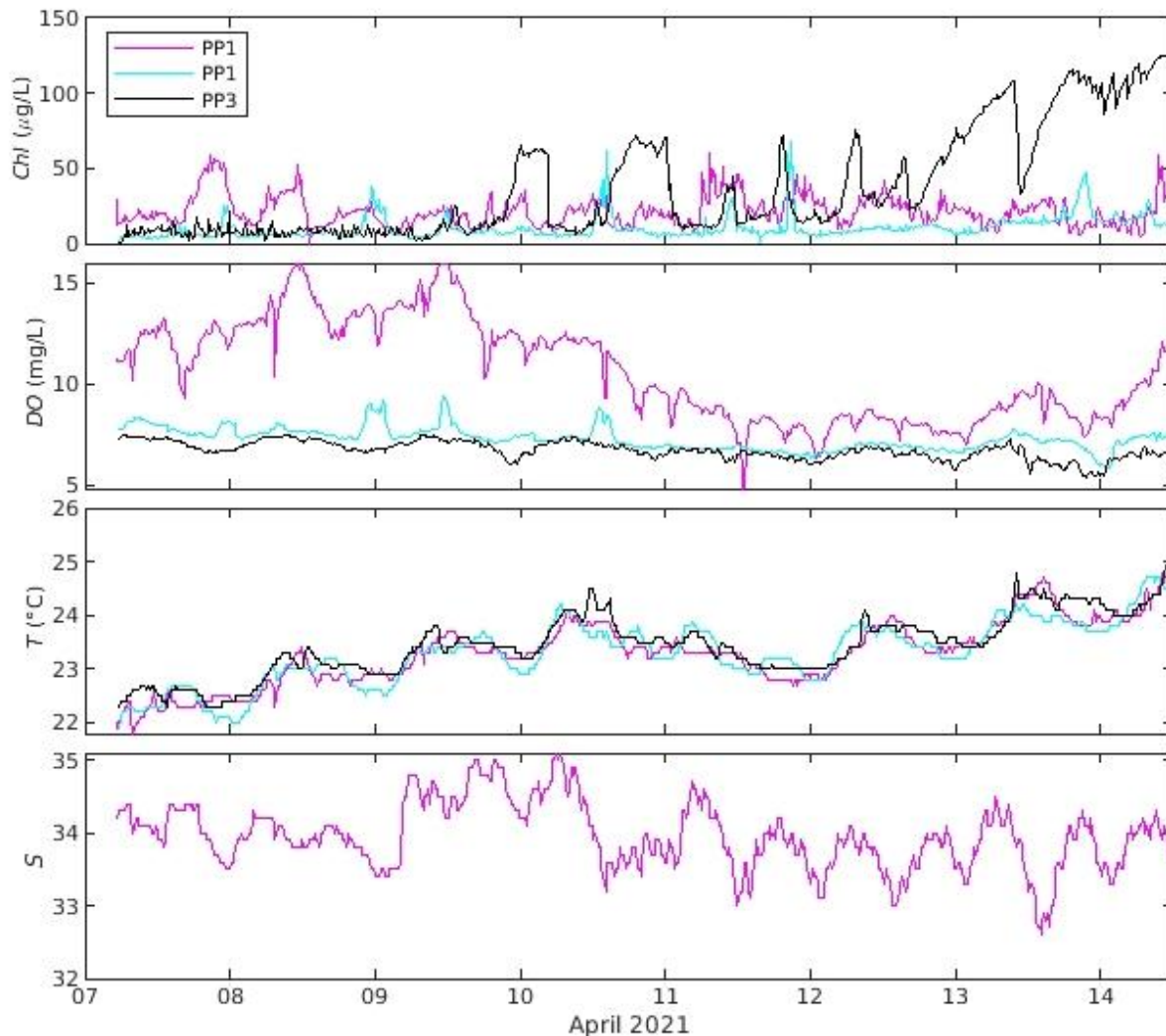


Figure Weisberg-6. Time series of water quality data chlorophyll-a (Chl-a), dissolved oxygen (DO), temperature (T), and salinity (S) collected from the three bottom mounts, PP1, PP2, and PP3.

Deliverables produced:

- TBCOM hindcast simulated surface velocity in MATLAB format (u and v components, March 30 to July 31, 2021)
- TBCOM hindcast tracer concentration at surface level in MATLAB format (March 30 to July 31, 2021)
- Maps of model simulated surface tracer concentration displayed as animation (gif file) showing the evolution of the effluent plume

- Time series of water quality data (Chl-a, dissolved O₂, T & S) collected at the three bottom mounts deployed to south of the Piney Point in early April 2021
- Peer-reviewed publication in *Marine Pollution Bulletin* (Beck et al., 2022):
- AGU 2021 Fall Meeting presentation with published abstract (Liu et al., 2021a)
- CERF 2021 Virtual Meeting presentation with published abstract (Liu et al., 2021b)

Discussion of findings:

The initial tracer concentration was normalized to be 1. Due to advection and mixing, the tracer concentration was quickly reduced by two orders of magnitude or more as the plume spread out (**Figure Weisberg-3**). Highest tracer concentrations hugged the southeastern shore of Tampa Bay during the first week. Lower concentrations gradually permeated to the entire bay, as the tracer was slowly flushed out of the bay. The tracer concentration slowly decreased over time after the effluent plume spread away from the near-field of the discharge site (**Figure Weisberg-7**).

The effluent plume was influenced by tides, winds, rivers and the adjacent Gulf of Mexico. It initially tended southwestward before tending northward and across the bay; it did not affect the Little Manatee site (to the northeast) until a week after the discharge ended. Given the rapid temporal and spatial variations in tracer concentration by tidal currents, especially in the deeper channels, caution must be used in interpreting the results from discrete water samples.

The modeled plume evolution had served as principal guidance for coordinating environmental monitoring by state, local and academic personnel. This hindcast simulation results will also provide a basis for multidisciplinary studies.

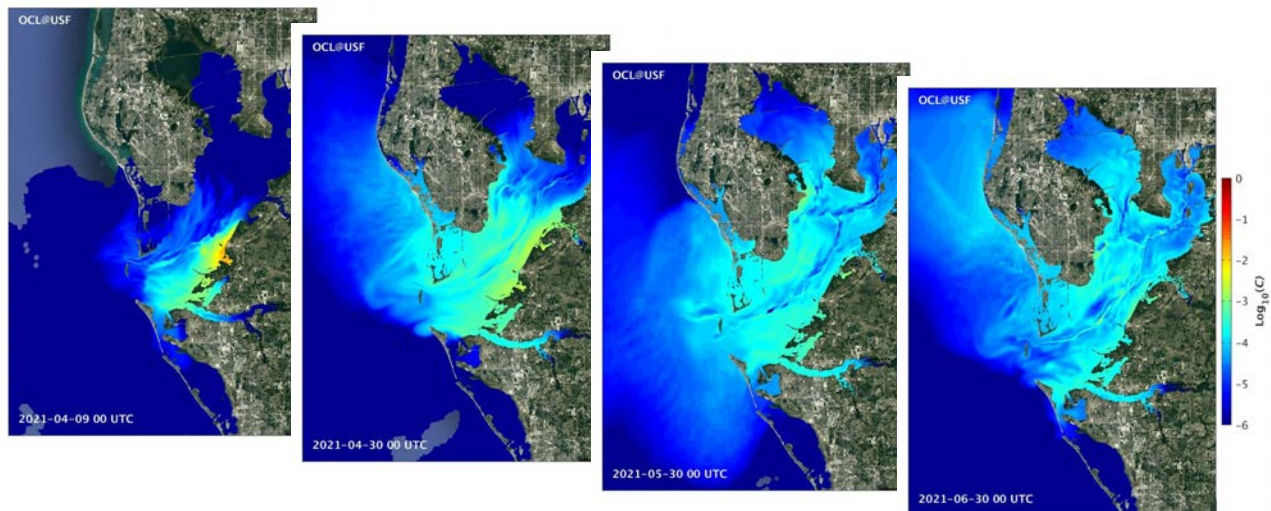


Figure Weisberg-7. Snapshots of TBCOM simulated surface tracer concentration during April – June 2021 showing the spread of the plume and the tracer concentration decay.

These initial findings were presented in the American Geophysical Union (AGU) 2021 Meeting Fall Meeting (Liu et al., 2021a) and the Coastal and Estuarine Research Federation (CERF) 2021 Virtual Meeting (Liu et al., (2021b) with published abstracts. The Piney Point effluent tracer modeling has been mentioned in a peer-reviewed publication in *Marine Pollution Bulletin* (Beck et al., 2022).

The chlorophyll sensor on PP1 may have a problem beyond just biofouling. It might have a small leak or a wiring issue. The PP1 chlorophyll data were corrected by normalizing to FDEP Station #3. However, users should be cautious in using PP1 chlorophyll data in the future. PP2 and PP3 chlorophyll data were not changed.

Continued efforts are needed to analyze the rest of the data and figure out how much of the data can be considered as valid record. It seems that biofouling was a serious issue for water quality time series observation in Tampa Bay. We should purchase more water quality sensors so that frequent cleaning and swapping can be made in the future. Realizing the problems associated with the sensors, we learned that more reliable water quality sensors should be purchased for future observations. Also, real-time transfer/delivery of water quality data is essential for timely monitoring the performance of the sensors as well as water quality conditions in the bay.

News report:

- [Hustle and flow: USF studies how water moves in Tampa Bay](#) (*Tampa Bay Times*, 05/19/2022)
- [It won't take the perfect storm to wreak havoc across Tampa Bay](#) (*Tampa Bay Times*, 01/27/2022)
- [Red tide in Sarasota and Manatee remains patchy. Could a new bloom be on the way?](#) (*Herald-Tribune*, 10/22/2021)
- [Red Tide is still floating out there and could return. But when?](#) (*Tampa Bay Times*, 8/27/2021)
- [No, there isn't 'scientific consensus' on red tide impact from Piney Point](#) (WTSP Tampa Bay 10, 7/26/2021)

References:

- Beck, M., Altieri, A., Angelini, C., Burke, M.C., Chen, J., Chin, D.W., Gardiner, J., Hu, C., Hubbard, K.A., Liu, Y., Lopez, C., Medina, M., Morrison, E., Philips, E.J., Raulerson, G.E., Scolaro, S., Sherwood, E.T., Tomasko, D., Weisberg, R.H., Whalen, J. (2022), [Initial estuarine response to inorganic nutrient inputs from a legacy mining facility adjacent to Tampa Bay, Florida](#), *Marine Pollution Bulletin*, 178, 113598, doi:10.1016/j.marpolbul.2022.113598
- Chen, C. S., Liu, H., & Beardsley, R. C. (2003), An unstructured, finite-volume, three-dimensional, primitive equation ocean model: Application to coastal ocean and estuaries. *J. Atmos. Oceanic Technol.* 20(1), 159–186
- Chen, C.S., Xu, Q., Houghton, R., & Beardsley, R.C. (2008), A model-dye comparison experiment in the tidal mixing front zone on the southern flank of Georges Bank. *J. Geophys. Res.* 113, C02005, doi:10.1029/2007jc004106

- Chen, J., Weisberg, R.H., Liu, Y., Zheng, L. (2018), [The Tampa Bay Coastal Ocean Circulation Model performance for Hurricane Irma](#), *MTS Journal*, 52(3), 33-42, doi:10.4031/MTSJ.52.3.6
- Chen, J., Weisberg, R.H., Liu, Y., Zheng, L., Zhu, J. (2019), [On the momentum balance of Tampa Bay](#), *Journal of Geophysical Research Oceans*, 124, 4492-4510, doi:10.1029/2018JC014890
- Lai, Z., Chen, C., Beardsley, R., Lin, H., Ji, R., Sasaki, J., & Lin J. (2013), Initial spread of ^{137}Cs from the Fukushima Dai-ichi Nuclear Power Plant over the Japan continental shelf: a study using high-resolution, global-coastal nested ocean model. *Biogeosciences* 10, 5439–5449.
- Liu, Y., Weisberg, R.H., Zheng, L., Heil, C.A., Hubbard, K.A. (2022), [Termination of the 2018 Florida red tide event: A tracer model perspective](#), *Estuarine, Coastal and Shelf Science*, 272, 107901, doi:10.1016/j.ecss.2022.107901
- Liu, Y., Weisberg, R.H., Zheng, L., Sun, Y., Chen, J. (2021a), Nowcast/Forecast of the Tampa Bay, Piney Point Effluent Plume: A Rapid Response, Abstract (Os35b-1036) Presented at AGU Fall Meeting, December, 2021 (2021) New Orleans, Louisiana
- Liu, Y., Weisberg, R.H., Zheng, L., Sun, Y., Chen, J. (2021b), Nowcast/Forecast of the Tampa Bay, Piney Point Effluent Plume: A Rapid Response, Coastal and Estuarine Research Federation (CERF) 2021 Virtual Meeting, November 2021
- Weisberg, R.H. (2011), Coastal ocean pollution, water quality and ecology: a commentary. *Mar. Technol. Soc. J.* 45 (2), 35-42.
- Weisberg, R.H., Zheng, L., Liu, Y., Murawski, S., Hu, C., & Paul, J. (2016), Did Deepwater Horizon hydrocarbons transit to the west Florida continental shelf? *Deep Sea Res. II*, 129, 259-272, doi:10.1016/j.dsr2.2014.02.002.
- Zheng, L.Y., and R.H. Weisberg (2012), Modeling the west Florida coastal ocean by downscaling from the deep ocean, across the continental shelf and into the estuaries, *Ocean Modell.*, 48, 10-29, doi:10.1016/j.ocemod.2012.02.002.
- Zhu, J., Weisberg, R.H., Zheng, L., & Han, S. (2015), On the flushing of Tampa Bay. *Estuaries and Coasts* 38, 118-131, doi:10.1007/s12237-014-9793-6.